A distributed, predictive secondary control for voltage and frequency regulation, economic dispatch and imbalance sharing in isolated microgrids

Alex Dario Navas Fonseca

Thesis submitted to the University of Nottingham
for the degree of Doctor of Philosophy

June 2022

To the memory of my grandfathers Alonso and Humberto, you will always be in my heart.
To my wife, Verónica, the most important person in my life, thanks for your constant support and encouragement in difficult times and for always being by my side.
To my parents, Marco and Mónica, for their unconditional love and support during my whole life.
To my brother Daniel and my sister Sheyla, I love you both with all my heart.

Abstract

Microgrids (MGs) are the cornerstone for a new model of electrical generation and distribution based on renewable resources. However, managing the operation of an MG is a challenging and complex task due to the characteristics of the various types of renewable sources and interactions between different types of generating equipment. In this context, some of the most pressing problems in MGs are associated with guaranteeing a cost-effective operation and the quality of the supply. Therefore, new and more reliable control strategies need to be developed for the management of microgrids. Distributed model predictive control (DMPC) is one of the best solutions for MGs as it can model complex systems and simultaneously address multiple objectives.

Traditionally MGs have been controlled via a three-level hierarchical structure, where each level operates at a different time scale. The primary control level is the fastest and aims to maintain the stability of the MG and ensures correct power sharing. The secondary control level restores the variables modified by the primary control level. The tertiary control level is the slowest and aims for economic dispatch (i.e., aiming for the lowest monetary cost of generated energy) of the MG and correct coordination with the main grid. However, isolated MGs are prone to fast changes in generation and demand whilst having a slow time response at the tertiary control level. The latest research suggests that this control should be performed on a time-scale comparable to that used at the secondary control level. In addition, as the power references sent by the tertiary control level tend to be updated with a slower sample time, the power limits of distributed generators (DGs) can be exceeded.

Therefore, this thesis focuses on the application of DMPC schemes for the secondary control level for *ac* MGs and hybrid *ac/dc* microgrids (H-MGs - composed of an *ac* sub-MG and a *dc* sub-MG connected through interlinking converters (ILCs)). The main characteristics of the proposed methodologies are the use of novel multi-objective cost functions and prediction models that correctly represent the main dynamics of the DGs and the ILCs (in the case of H-MGs) in the formulation. Three control strategies are proposed that fulfil the main task of the secondary control level (i.e. restoring frequency and voltage). These strategies are able to restore the frequency and voltage to nominal values or within secure bands. The first proposed strategy considers the economic dispatch of DGs in a balanced *ac* MG. The second strategy achieves the economic dispatch of *ac* DGs, *dc* DGs and manages the power transference of ILCs based on an economic criterion in H-MGs. The third strategy manages the sharing of phase imbalance in an unbalanced *ac* MG. All the proposed strategies include important operating constraints, e.g., power limits due to convertor ratings.

Extensive experimental, real-time simulation and simulation studies validate the proposed DMPC schemes for the most common operating scenarios in MGs, namely, load changes, robustness in the presence of changes in microgrid structure (i.e., disconnection and reconnection of DGs and ILCs (in H-MGs)), and communication link failures and communication delays. Finally, the controllers' scalability has been investigated, and comparative studies have also been performed to highlight the advantages of the proposed schemes over other reported distributed schemes.

Acknowledgements

List of Abbreviations

ADL — Active damping loop.

APF — Active power filter.

BESS — Battery energy storage system.

CSI — Current source inverter.

DAPI — Distributed averaging proportional integral.

DER — Distributed energy resources.

DG — Distributed generator.

DMPC — Distributed model predictive control.

ESS — Energy storage systems.

EV — Electric vehicle.

FCS-MPC — Finite control set model predictive control.

FPGA — Field-programmable gate array.

H-MG — Hybrid ac/dc Microgrid.

ICC — incremental cost consensus

LC — Inductive capacitive filter.

MAS — Multi-agent system

MIMO — Multiple input - multiple output.

MG — Microgrid.

MPC — Model predictive control.

PE — Power electronics.

PI   Proportional integral.

PLL   Phase locked loop .

PR   Proportional resonant.

PV   Photovoltaic panels .

PVUR   Phase voltage unbalance rate index.

PWM   Pulse-width modulation.

QP   Quadratic programming.

QSG   Quadrature signal generator.

RH   Rolling Horizon.

RT   Real time.

RTT   Real time target.

SISO   Single input - single output.

SOC   State of charge.

VSC   Voltage source converter.

WT   Wind turbine.

List of Symbols

x={a,b,c}	Phases of the MG.
Q_{ix}	Per-phase reactive power of DG_i.
Q_i	Three-phase reactive power of DG_i.
V_{ix}	Per-phase voltages at the output of DG_i.
V_i	Average voltage at the output of DG_i.
V_{iabc}	DG_i output voltage in the natural reference frame.
N	Number of DGs.
L_i	Coupling inductor.
B_i	Nominal admittance.
ω_i	Angular speed at the output of DG_i.
θ_i	Phase angle at the output of DG_i.
$\hat{V}_{ix}^B$	Per-phase estimated voltages at the coupling point.
$\hat{V}_i^B$	Average estimated voltage at the coupling point.
$\hat{\omega}_i^B$	Angular frequency at the coupling point.
$\hat{\theta}_i^B$	Phase angle at the coupling point.
$\delta\theta_i$	Phase angle deviation of DG_i.
$\Delta\omega_{s,i}$	Frequency control action variation.
$\Delta V_{s,ix}$	Per-phase voltage control action variations.
$\omega_{s,i}$	Frequency control action.
$V_{s,ix}$	Per-phase voltage control actions.
ω_0	Nominal frequency.

$M_{p\omega,i}$ Active droop slope.

P_i Three-phase active power contribution of DG_i.

V_0 Nominal voltage.

$M_{qv,i}$ Reactive droop slope.

A Adjacency matrix.

a_{ij} Communication term between DGs.

τ_{ij} Communication delay.

$\hat{\tau}_{ij}$ Estimated communication delay.

N_y Prediction horizon.

N_u Control horizon.

λ Weighting parameter in the cost function.

$S_{i\,max}$ Maximum apparent power of DG_i.

$\omega_{aux,i}$ Auxiliary optimisation variable for frequency.

$V_{aux,i}$ Auxiliary optimisation variable for voltage.

T_{sec} Predictive controller sample time.

$\overline{\omega}_i$ Local average frequency approximation.

ω_{max} Maximum limit for the local average frequency approximation.

ω_{min} Minimum limit for the local average frequency approximation.

$\overline{V}_i$ Local MG average voltage approximation.

V_{max} Maximum limit for the local average voltage approximation.

V_{min} Minimum limit for the Local average voltage approximation.

$\mathbb{X}_{p,i}$ Predicted variables optimisation vector.

$\mathbb{X}_{\Delta,i}$ Predicted control action sequence vector.

Contents

3 DMPC scheme for frequency regulation and active power dispatch in *ac* microgrids   44

4 DMPC scheme for frequency and voltage regulation within bands and the economic dispatch of active and reactive power for hybrid *ac/dc* microgrids 70

List of Tables

List of Figures

Chapter 1

Introduction

1.1 Research motivation

The way energy is generated around the world is going through significant changes to cope with global warming and cut CO2 emissions. Governments and societies are setting stringent environmental goals for this purpose. For instance, during the COP26, the objective of "NET ZERO" was accorded [1]. Due to the advances in technology development and power electronics, currently, it is cheaper to generate electricity from renewables than fossil fuels. The United Kingdom (UK) is leading the energy transition from contaminating generation sources to more environmentally friendly generation by integrating massively distributed generation mainly based on renewable resources. Currently, renewables account for 43% of the UK's domestic power generation [2]. Moreover, the UK has set the ambitious target to run 100% on renewables by 2035. Similarly, Chile is the leading country in Latin America in the adoption of generation based on renewable resources. Currently, 36.5 % of generation comes from renewables [3]. Moreover, during 2022, 86% of the total installed and to be installed generation capacity correspond to solar or wind energy [4]. It is worth noting that Chile has the best solar ration in the world due to its privileged location. In this context, the study of microgrids (MGs) is essential, as MGs allow the integration and management of traditional and renewable

generation sources, such as wind and photovoltaic.

An MG is defined as "A group of interconnected loads and distributed energy resources (DER) that acts as a single controllable entity with respect to the main grid" [5]. MGs can operate in grid-connected mode and isolated mode. In grid-connected mode, frequency and voltage are fixed by the main grid. In contrast, the isolated mode of operation poses a more complex scenario because the number of available assets is limited, and the MG has to take care of everything by itself [6]. Nevertheless, isolated MGs are one of the most attractive options to bring electricity to communities not connected to the national grid.

In MGs, the generation resources are local, and transmission power losses are reduced [7]. MGs mainly operate at the distribution level with low voltage levels, and can incorporate renewables with energy storage systems (ESS) and *ac* and *dc* loads [7]. Smart loads, such as electric vehicles (EV), can also be managed within an MG. To manage the generators and loads in MGs, efficient and reliable control strategies need to be developed. In recent years, there has been an extensive research effort to improve the management of MGs and enhance their capabilities [8, 9]. Distributed model predictive control (DMPC) has been proposed as a prominent solution for MGs management; it is able to coordinate the MGs' assets to achieve several global objectives simultaneously. According to their specific electrical distribution structure, MGs can be classified as *ac* [10], *dc* [11] and hybrid *ac/dc* MGs (H-MGs) [10]. Both *ac* and *dc* MGs can comprise renewable-based generators, such as wind turbines (WT) and photovoltaic panels (PV), as well as non-renewable-based generators, such as diesel generators. Renewable-based generators tend to be connected through power converters to the distribution network. On the other hand, H-MGs can reduce unnecessary conversion stages and increase the power capacity and the reliability of the entire MG [12]. An H-MG comprises an *ac* sub-MG and a *dc* sub-MG connected through interlinking converters (ILCs). In principle, the MGs described can operate connected to the main grid or in an isolated mode

of operation [10].

To ensure the proliferation of MGs, there are still some pressing issues related to their control and operation. Currently, there is an ongoing effort to ensure that MGs are secure, reliable, and operate cost effectively.. Moreover, as MGs are low voltage networks, they inherently have unbalance between their three phases [13]. These unbalances are the result of asymmetrical impedances per phase and the constant turning on or off of single-phase loads. Unbalanced loads can cause a reduction in the efficiency of grid assets and may affect the stability of the MG [14]. A detailed discussion of the principles and state-of-the-art of MG's control is presented in Chapter 2.

1.2   Problem statement

Microgrids are driving the integration of distributed generation (DG) units, and transforming the traditional centralised power grid. MGs (including H-MGs) inherit the three-level hierarchical control structure of traditional power systems. The primary control level compensates for load changes by quickly changing voltage and frequency deviations to maintain the MG's stability (droop control), while the main task of the secondary level is to then slowly restore the aforementioned variables to their nominal values [15]. The tertiary level is typically in charge of the economic dispatch of generation (usually based on cost and availability) and the coordination of neighbouring MGs [15]. The economic dispatch of an MG consists of minimising the total generation cost of satisfying the power demand. To achieve this goal, the output power of generators must be determined in order to satisfy demand at the lowest cost while maintaining the generation equipment's operating constraints [16, 17]. However, latest research for *dc* MGs [18, 19], *ac* MGs [16, 17, 20] and H-MGs [21, 22] has shown that the economic dispatch of DGs should be accomplished on a timescale that is consistent with the secondary control level due to the vulnerability of isolated MGs to rapid fluctuations in generation and demand.

However, another pressing problem that affects the power quality of an MG is the presence of unbalances, as MGs operate at low and medium voltage levels, i.e. distribution level [23, 24]. Unbalances can be compensated (mitigated) through additional hardware or shared among the DGs that compose the MG. For the first option, active power filters (APFs) can be employed; however, this option is effective only when the issue is concentrated at a specific node. The second approach is a more viable option where the DGs' controllers have the ability to share the imbalances by using their available capacity.

As explained before, the compensation of imbalance can be achieved using APFs to compensate for unbalanced currents or unbalanced voltages at specific points of the MG [25, 26]. However, APFs are not attractive in MGs since they constitute additional hardware and higher costs. A more cost-effective solution is to embed imbalance compensation capabilities into the control schemes of DG units that are already available in the MG [27–29]. Control schemes to improve the sharing of unbalanced powers between the DGs of MGs are mainly based on droop control and use virtual impedance loops. Virtual impedances are used to change the dynamic of the power converter using loss-less software implemented impedances. This means that negative sequence (and zero sequence for four-wire MGs) impedances are implemented to control the sharing of imbalance between the DGs. The magnitude of these virtual impedances is controlled via decentralised control schemes in [30–32], meaning that there is no coordination between the DG units (each DG works autonomously based on variables measured locally). However, better performance could be achieved via coordination between DG units (e.g. using centralised and distributed approaches).

In this sense, the magnitude of the negative sequence impedances is calculated in a coordinated way by a secondary centralised controller in [33–36], while in [37–39] secondary distributed controllers, based on consensus algorithms, are implemented. It is important to note that the sharing of imbalance can only be achieved by increasing the voltage imbalance at the output of the DG

unit. Therefore, a control strategy should share unbalanced powers and, at the same time, regulate the maximum unbalanced voltage at the DGs to fulfil the maximum values stated in the IEEE standard 1547-2018 [40]. The main parameters established by this standard for MGs are presented in Appendix E. Focusing on the secondary level, there are three types of control architectures: centralised, decentralised, and distributed [41]. Centralised controllers require communication between all the DGs and ILCs (which is impractical for large systems), presenting a high computational burden and a single-point-of-failure [10, 41]. On the other hand, decentralised controllers only handle local information, and allow limited coordination between DGs and ILCs [10]. Conversely, distributed schemes present a more compelling solution, achieving global objectives via coordination of DGs by considering only information from communicating neighbouring DGs [10, 41, 42], thus enhancing the robustness in the presence of changes in microgrid structure.

Most distributed control proposals at the secondary level are based on proportional-integral (PI) controllers [16–19, 43]. Furthermore, most approaches in the literature assume fixed operational set-points for voltage and frequency and do not take advantage of the flexibility associated with the secure operational bands defined in the IEEE standard 1547-2018 [40], which suggests that DGs can operate normally as long as the frequency and the voltage are within 1% and 5% of their nominal values, respectively. Furthermore, in the case of H-MGs, existing approaches are designed independently for either *ac* sub-MGs [16, 17, 44] or *dc* sub-MGs [18, 19], without accounting for the specific aspects of H-MGs themselves. It is worth noting that all the aforementioned works assume that frequency and voltages must be set to fixed nominal values, giving up flexibility in the microgrid control system. Also, being based on PI controllers, it is difficult to achieve multiple objectives and cope with operation constraints [45, 46].

Due to the limitations of PI controllers at the secondary control level for MG and H-MG applications, DMPC has attracted the attention of the MG com-

munity. DMPC is based on a model of a local system and the prediction of its behaviour over a prediction horizon. Each local controller computes a control sequence based on its local measurements, and information received from neighbouring controllers [47], reducing the computational burden. The information is updated, and the process is repeated at each sample time (rolling horizon). The rolling horizon property provides robustness against communication delays [20, 46, 48]. DMPC can model complex multi-variable systems, control multiple objectives, and handle hard and soft constraints [45, 46, 48]. For the operation of MGs, DMPC can manage DGs and ILCs (for H-MGs). DMPC can include equipment power rating limits (hard constraint) and regulate variables such as frequency and voltages within secure bands (soft constraints) instead of specific values. Thus, making the MG operation more flexible. For these reasons, DMPC is one of the most prominent solutions for managing MGs.

Based on the motivation described above, this thesis proposes three control strategies at the secondary level to address the main tasks of the secondary control level (restoring frequency and voltage). These strategies are able to restore the frequency and voltage to nominal values, or within secure bands that comply with IEEE standard 1547-2018 [40]. Moreover, the proposed strategies include complementary objectives in their formulation depending on the type of MG studied. For instance, the first proposed strategy considers the economic dispatch of DGs in balanced *ac* MGs. The second strategy achieves the economic dispatch of *ac* DGs, *dc* DGs and manages the power transference of ILCs based on an economic criterion in H-MGs. Finally, the last proposed strategy is able to manage imbalance sharing in unbalanced *ac* MGs while the maximum unbalanced voltage at the DGs output is regulated to fulfil the maximum values stated in the IEEE standard 1547-2018 [40].

Local prediction models based on droop control and power transference equations are developed for the proposed strategies. Moreover, multiobjective cost functions are formulated to address global objectives via information sharing

while important operational constraints, such as equipment power rating, are met. As a result, all the proposed strategies, tested by simulation and experiment, are robust in the presence of changes in microgrid structure and against communication issues. Moreover, they present a low computational burden.

1.3   Hypotheses

The hypotheses that support this thesis are described as follows:

(i) Distributed model predictive control strategies can be designed and implemented at the secondary control level to tackle the main issues of MGs, which are the regulation of frequency and voltage, economic dispatch, and phase imbalance sharing. These strategies can include a detailed mathematical model of the dynamic of the DGs to solve the aforementioned issues.

(ii) It is possible to achieve economic dispatch, and restoration of voltage and frequency in *ac* MGs at the secondary control level through distributed predictive controllers that share their information to coordinate their control sequences. In this way, in addition to avoiding the need to have a controller for each objective, the overall performance of the microgrid is enhanced in terms of robustness and reliability.

(iii) It is possible to achieve economic dispatch in hybrid *ac/dc* MGs, along with the main objectives of the secondary control, which are frequency and *ac* voltage restoration on the *ac* sub-MG and *dc* voltage restoration on the *dc* sub-MG. Additionally, is it possible to restore these variables within secure bands that comply with the IEEE standard 1547-2018 [40], instead of restoring them to nominal values. In this way, more flexibility is given to the the hybrid *ac/dc* MG.

(iv) The interlinking converters in a hybrid *ac/dc* MG can communicate with *ac* DGs and *dc* DGs to transfer power from the *ac* sub-MG to the *dc* sub-

MG and vice-versa based on the economic dispatch criterion. Moreover, the predictive controller can include power rating limits in DGs and ILCs to avoid overloads.

(v) The inclusion of the dynamics of droop controllers, active power and reactive power transfer models in a predictive controller will allow the optimisation of the power contribution of each DG to the microgrid. Furthermore, a distributed control structure based on measurements and information sharing can avoid the complete modelling of a microgrid and face any load variations within a microgrid's physical capacity limits.

(vi) It is possible to share imbalances among DGs' phases in unbalanced *ac* MGs, avoiding the use of virtual impedance loops and without the need for adding extra power converters to the MG through a distributed predictive control scheme that also restores the frequency and voltage. Moreover, it is possible to limit the voltage unbalance at the output of each DG unit to comply with the IEEE standard 1547-2018 [40] within the same controller.

(vii) A set of distributed controllers can reduce the computational burden and provide a response of equal quality to a centralised controller, and are robust in the presence of changes in microgrid structure (i.e. disconnect and reconnect generation units without the need for external intervention in the controllers). They can also provide good performance when communication delays are present in the system.

1.4 Objectives

1.4.1 General objective

This PhD research thesis aims to study the design, modelling, implementation and validation of novel distributed predictive strategies for the secondary

control level of MGs, which adds to the frequency and voltage restoration, economic dispatch and imbalance sharing objectives. Within the framework of this work, the following specific objectives are pursued.

1.4.2 Specific objectives

(i) To design, implement and validate experimentally a distributed predictive control strategy for *ac* MGs to achieve economic dispatch of DGs and frequency restoration to nominal values.

(ii) To design, implement, and validate a distributed predictive control strategy for hybrid *ac/dc* MGs to achieve economic dispatch of DGs and restore within bands the frequency and *ac* voltage on the *ac* sub-MG and the *dc* voltage on the *dc* sub-MG.

(iii) To design, implement, and validate a distributed predictive control strategy for unbalanced *ac* MGs to achieve imbalance sharing among DGs and restore within bands the frequency and voltage while the unbalance at the DGs' output is kept within the recommendation of the IEEE standard 1547-2018 [40].

(iv) To validate the proposed DMPC strategies against the most demanding scenarios, which are communication delays, communication failures and disconnection/reconnection of DGs. The validation is carried out via simulation, real-time simulation and experimentally.

(v) To compare the performance of the proposed control strategies with the latest distributed strategies reported in the literature.

1.5 Contributions

The work developed during this project has resulted in the publication of three journal papers submitted to top-tier indexed journals and two international

conference papers. In addition, twelve manuscripts have been published, with the candidate as a co-author. The details of these publications related to microgrids are listed in Chapter 6. The contributions of this thesis can be summarised as follows:

For balanced *ac* MGs

(i) A novel DMPC scheme is proposed for active power economic dispatch and frequency restoration where both objectives are achieved simultaneously.

(ii) The proposed controller neither requires the modelling of the entire MG nor the modelling of the connected loads. Furthermore, this controller operates with the same usual measurements used at the primary control level; thus, the number of physical measurements is reduced when compared with previous predictive approaches [49].

(iii) The proposed DMPC scheme with the economic dispatch of DGs addresses communication delays, loss of communications and robustness in the presence of changes in microgrid structure without requiring changes in the control structure, unlike centralised MPC schemes. This validation was carried out with the experimental setup of the MGs laboratory at The University of Chile.

(iv) The DMPC includes as equality constraints the droop, the active power transfer, and the phase angle models to predict the behaviour of each DG. Additionally, terminal values and inequality constraints contribute to bound the feasible solution space. This reduces the optimisation time and enables the control strategy to be implemented in real-time controllers.

For hybrid *ac/dc* MGs

(i) A cooperative DMPC scheme that considers the interaction among ILCs, *ac* DGs and *dc* DGs in isolated H-MGs is proposed. This DMPC scheme

controls the H-MG as a single entity instead of three separated systems, giving redundancy to communications and improving the controller's dynamic response.

(ii) This work considers a DMPC strategy to control variables to specific values and within operation bands for H-MGs. For this purpose, novel cost functions are proposed to control ILCs, *ac* DGs and *dc* DGs. The proposed DMPC for secondary control can achieve accurate consensus objectives, i.e., economic dispatch of active power and reactive power. While through the use of soft constraints, the following variables are considered flexible: the frequency and average voltage of the *ac* sub-MG and the average voltage of the *dc* sub-MG. They are regulated within predefined bands that comply with the IEEE standard 1547-2018 [40]. Furthermore, by including maximum power rating constraints in the DMPC formulations, physical saturation (overloading) of *ac* DGs, *dc* DGs, and ILCs is prevented.

(iii) The proposed DMPC considers the existence of multiple ILCs. Where the cost function of the ILCs achieves simultaneously the cost-effective operation of the H-MG, averts overloading ILCs and avoids circulating currents. Moreover, to predict the behaviour of ILCs and DGs, the dynamic models that rule each of them are included as equality constraints in their respective optimisation problems.

(iv) Extensive simulation studies validate that the proposed DMPC performs well under load change, robustness in the presence of changes in microgrid structure, and communication delays scenarios. Also, this work shows that implementing the economic dispatch at the secondary level reduces the operation costs of an H-MG considerably.

For unbalanced *ac* MGs

(i) This work proposes a DMPC scheme for unbalanced MGs. The pro-

posal improves the sharing of imbalances among DG phases in *ac* MGs, avoiding the use of virtual impedance loops (as this methodology has many drawbacks [23]) and without the need for adding additional power converters to the MG.

(ii) With the DMPC mathematical model, which includes soft constraints, the proposed imbalance sharing control scheme can achieve accurate control of some variables in the MG, whereas other variables are controlled within more relaxed predefined bands. Specifically, the frequency and average voltage are regulated within predefined bands. This produces a more flexible control system than those reported in [30, 33–39, 50–53], which looks for an accurate sharing of all the variables of the MG.

(iii) The proposed DMPC approach can improve the sharing of both three-phase active and reactive power, and single-phase reactive power between the DG units. This can not be included in methods based on virtual impedance loops, as will be shown in Section 5.7.2.

(iv) The proposed control scheme achieves the sharing of imbalance, reducing the single-phase voltage deviations at the output of each DG unit, when compared with methods based on the virtual impedance loop. The proposed approach has better performance in the presence of time delays in the communication network and are robust in the presence of changes in microgrid structure. The good performance of the proposed controller was validated via real-time simulation and simulation tests.

1.6   Thesis structure

The remainder of this thesis is divided in the following chapters:

Chapter 2 presents a background of MGs' control and an extensive review of secondary control techniques for MGs and H-MGs reported in the literature. Particular attention is given to consensus-based distributed schemes and

distributed predictive schemes for economic dispatch of DGs and imbalance sharing.

Chapter 3 proposes a predictive secondary control strategy for *ac* MGs that simultaneously achieves economic dispatch and restores the MG frequency to its nominal value. The mathematical formulation of this proposal is detailed. Furthermore, the experimental validation of this technique is addressed.

Chapter 4 proposes a predictive secondary control strategy for hybrid *ac/dc* MGs that simultaneously achieves economic dispatch of active and reactive power and restores frequency and *ac* voltage on the *ac* sub-MG and *dc* voltage on the *dc* sub-MG within secure bands. The mathematical formulations for *ac* DGs, *dc* DGs and ILCs of this proposal are detailed. Furthermore, simulation validation of this technique is addressed as well as a performance comparison against other reported technique in the literature.

Chapter 5 proposes a predictive secondary control strategy for unbalanced *ac* MGs that simultaneously achieves single-phase imbalance sharing and restores frequency and voltage within secure bands. The mathematical formulation of this proposal is detailed. Furthermore, simulation and real-time simulation validation of this technique are addressed as well as a performance comparison against other reported techniques in the literature.

Chapter 6 presents the conclusions, suggests possible future research lines on the topics addressed in this work, and presents a summary of the works published during the PhD studies. Specifically, the manuscripts derived from the work presented in this thesis and MG-related papers where the candidate has contributed are presented.

Chapter 2

Literature review

2.1 Introduction

This chapter presents the state-of-the-art related to control strategies proposed for microgrids (MGs). Particular attention is given to consensus-based distributed strategies and distributed model predictive (DMPC) schemes. Also, proposals for economic dispatch and imbalance sharing are discussed extensively.

This chapter is organised as follows: Section 2.2 provides the background of the hierarchical control structure used in MGs. Section 2.3 provides a detailed explanation of the controllers involved in the hierarchical control structure for ac MGs. Similarly, Section 2.4 presents the controllers for the hierarchical control structure for dc MGs. The control of hybrid ac/dc MGs is presented in Section 2.5.

Then the latest reported schemes at the secondary control level for the aforementioned types of MG are discussed in Section 2.8. Special emphasis is given in this section to approaches that solve economic dispatch. Section 2.9 presents the main approaches to solve imbalance sharing in MGs. Then, the related solutions based on DMPC for the secondary level are discussed in Section 2.7. Finally, Section 2.10 summarises the state of the art and main benefits of the proposed strategy.

2.2   Microgrids framework

Microgrids (MGs) are an essential feature of future power systems, as they enable the full integration of distributed energy resources (DERs). These DERs are mostly based on renewable-based generation sources and aim to gradually leave behind the generation based on fossil fuels and decarbonise the planet. Harvesting electricity from renewables is now a viable option as their generation prices decrease day by day. Moreover, MGs can become the key enablers to achieve goal number 7 of the United Nations, which states: ensure access to affordable, reliable, sustainable and modern energy for all. As mentioned before, an MG acts as a single controllable entity from the grid point of view and has its own generation and storage resources with clearly defined electrical boundaries [5]. MGs aim to achieve adequate active and reactive power sharing among distributed generation (DG) units, while frequency and voltage levels must be kept within safe levels [54]. Therefore, MGs represent an attractive solution in many applications, such as terrestrial, naval or aerospace electrical grids, due to their controllability, capability to include DGs and flexibility [55]. MGs can operate in both grid-connected or island modes. In the grid-connected mode, the MG can trade energy with the main grid based on the existing power deficit or surplus. Islanded MGs can operate independently, but they can reconnect to the main grid when necessary. On the other hand, MGs that do not have a connection with the grid because of technical, geographical or economic constraints are usually called isolated MGs [6]. Isolated MGs must be controlled with extreme care because the number of DGs available to tackle voltage and overloading problems is limited [6]. Isolated MGs must autonomously regulate voltage amplitude and frequency through the MG's control system. For most DERs, power electronics (PE) interfaces are needed to connect the DERs to an MG. The sinusoidal rectifier is the most common configuration used [15]. These DERs must be controlled in a coordinated manner with care, as they do not have inertia, which can influence the stability of

an MG.
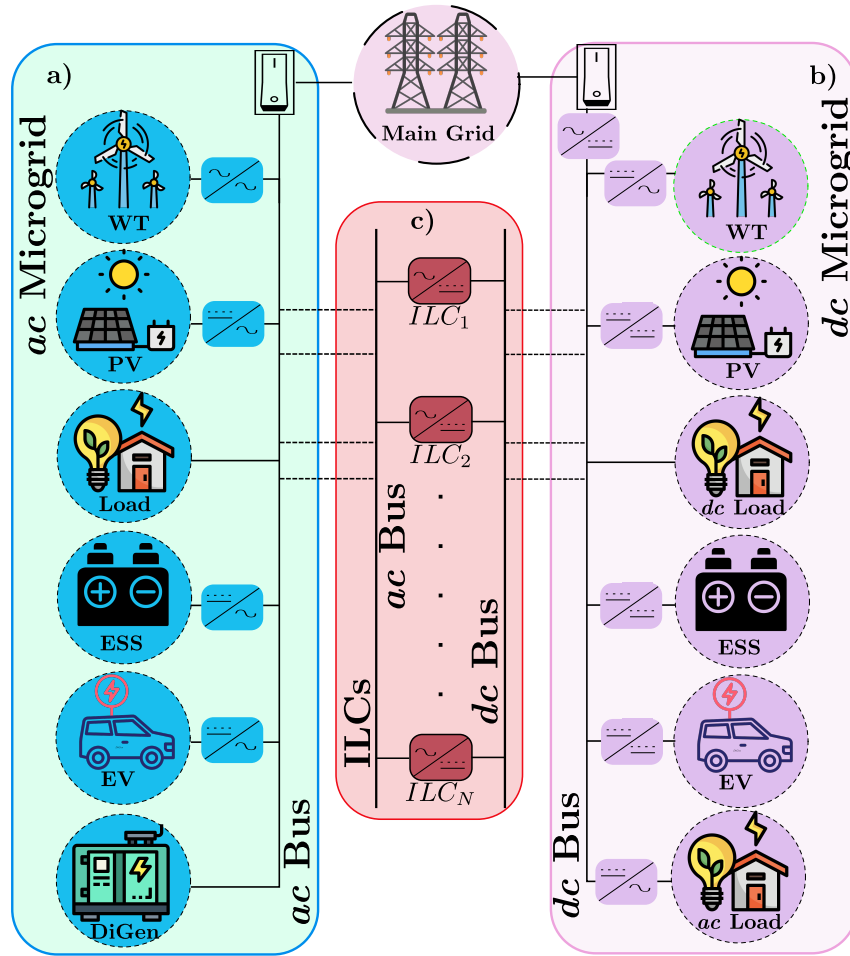
Figure 2.1: *General topology for a hybrid ac/dc microgrid. a) ac microgrid. b) dc microgrid. c) Interlinking converters.*

According to their specific electrical distribution structure, MGs can be classified as *ac* MGs [10], *dc* MGs [11] and Hybrid *ac/dc* MGs (H-MGs) [10]. Isolated *ac* MGs operate on a grid forming/supporting scheme where at least one DG works as a voltage source converter (VSC), regulating the MG voltage magnitude and frequency [56]. A general topology of an *ac* MG is presented in Fig. 2.1a. On the other hand, *dc* MGs neither require frequency regulation nor reactive power control, thus reducing the system's operational complexity. Additionally, *dc* DGs do not need to be synchronised to the utility grid [10]. A general topology of a *dc* MG is presented in Fig. 2.1b. Both *ac* and *dc* MGs can comprise renewable-based generators, such as wind turbines (WT) and photovoltaic panels (PV), as well as nonrenewable-based generators, such as diesel

generators. These generators can be connected directly to the distribution network (depending on their nature) or through PE interfaces.

Conversely, H-MGs merge the benefits of both kinds of MGs, reducing unnecessary conversion stages and increasing the power capacity and the reliability of the entire H-MG [12]. An H-MG comprises an *ac* sub-MG (Fig. 2.1a) and a *dc* sub-MG (Fig. 2.1b) connected through interlinking converters (Fig. 2.1c). The ILCs need to be controlled adequately to guarantee power flow between sub-MGs. Moreover, the infrastructure of existing *ac* MGs can be re-utilised for the deployment of H-MGs.

Typically, the control tasks of an isolated MG are split into three control levels, where each control level operates at a different time-scale [15]. The first level, which is the fastest of all (milliseconds), maintains the stability of the MG and ensures correct power sharing [54]. This control level is comprised of inner current controllers, outer voltage controllers, and droop control loops; the latter allows variations of active/reactive power to be reflected as variations of frequency/voltage, as in large power systems [15]. Droop control produces deviations in frequency and voltage amplitude. At a slower time scale (seconds), the setpoint values of frequency and voltage can be restored; the controllers used to manage this are known as the secondary control level [10]. The long-term tasks of an MG (seconds to minutes), such as economic dispatch of DGs and coordination of MGs with the main grid, are performed by the tertiary control [57].

It is worth noting that most of the control solutions proposed in MGs have been derived from large-scale electric power systems. However, latest research for *dc* MGs [18, 19], *ac* MGs [16, 17, 20] and H-MGs [21, 22] has shown that the economic dispatch should be performed in a time-scale consistent with that of the secondary control level due to the susceptibility of isolated MGs to fast changes in generation and demand. This is because MGs possess low inertia due to the use of renewables and power electronics interfaces [58, 59]. For these reasons, the secondary control level will be studied in this thesis.

There are typically three types of control architecture proposed for secondary control; these are centralised, decentralised and distributed [10], as shown in Fig. 2.2. Centralised control (see Fig. 2.2a) can give a global solution; however, it has a common point of failure in the communication network and presents a high computational burden. Decentralised controllers do not need a communication channel because each local controller takes actions based on their measurements (see Fig. 2.2b), but an optimal solution is difficult to achieve [10]. Finally, distributed controllers can achieve global objectives through information sharing (see Fig. 2.2c). They are robust against communication failures and allow connection and disconnection for the various distributed resources [60]. A detailed comparison between centralised and distributed control is presented in Table 2.1.
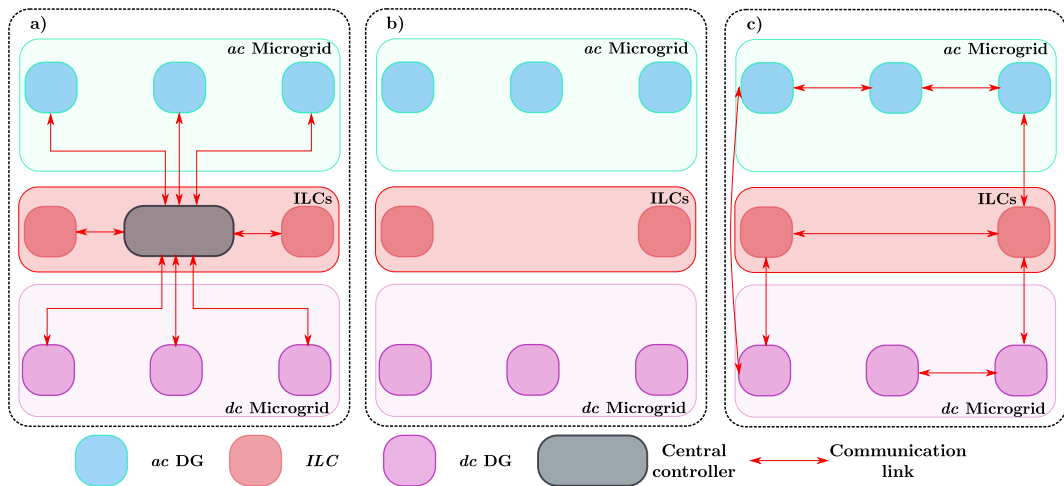
Figure 2.2: *Control structures at the secondary control level. a) Centralised. b) Decentralised. c) Distributed.*

Table 2.1: Comparison between Centralised and Distributed Control

Features	Centralised control	Distributed control
Application	Small microgrids.	Large microgrids.
Operation [60, 61]	Microgrid topology is required.	Microgrid topology is not required.
	High computational cost.	Low computational cost.
	Scalability requires changes in control.	Easy to scale.
	Decisions based on communications with all DGs.	Decisions based on local measurements and the communication with neighbours.
	Single point of failure.	Robustness in the presence of changes in microgrid structure.
	Reliability is degraded.	Reliability is maintained.
Design and implementation [10]	Powerful hardware	Embedded controllers.
	Complex algorithms.	Easier algorithms.
	Information from all units is required.	Handle local and shared information.
	Low-bandwidth communication and low communication complexity.	High-bandwidth communication and high communication complexity.

2.3 Control of *ac* MGs

2.3.1 Primary control level in *ac* MGs

The primary control level is in charge of voltage stabilisation and power sharing by fixing the current and voltage at the DGs' output. Usually, it comprises an inner current loop (faster), a voltage outer loop (slower) and droop controllers. A bandwidth separation of at least ten times is needed between these controllers for their operation [62]. The current and voltage control loops can be proportional integral (PI) controllers or proportional resonant (PR) controllers. When using PI controllers, the variables are converted into the *dq* synchronous reference frame [57]. PR controllers can be implemented directly in the *abc* natural reference frame or the $\alpha\beta$ stationary reference frame. Among the advantages of PR controllers over PI controllers, these controllers allow the implementation of positive and negative sequence loops at the same time as well as the independent control of phases [26].

The droop controllers dictate the main dynamic of this control level. The droop controllers emulate the behaviour of classical synchronous machines (mechanical/electrical). An LCL filter can be placed at the DGs' output, where the second coupling inductance can be set to ensure a predominantly inductive impedance [63, 64], as will be shown later in Section 3.3, and classical droop controllers can be used at the primary control level. To achieve active

power sharing, DG units modify the frequency of the microgrid (see Fig. 2.3a), whereas to reach proper reactive power sharing, DG units modify their voltage amplitudes (see Fig. 2.3b). As ESS are out of the scope of this work, Fig. 2.3a considers unidirectional power. Although communication-based controllers are proposed for this control level, these are not widely used because they present higher implementation costs and complexity [15, 65]. Moreover, they may not be robust in the presence of changes in microgrid structure [15, 65].
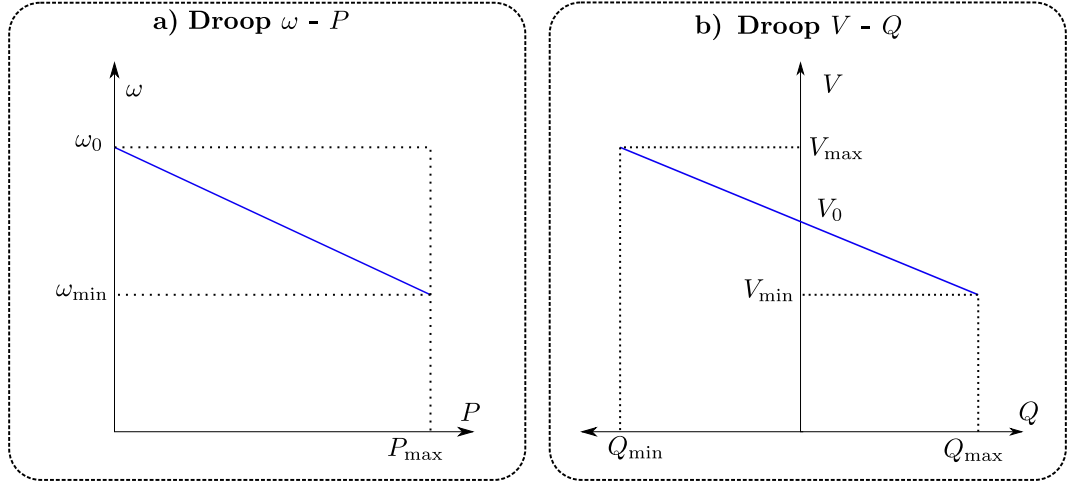
Figure 2.3: *Droop control for ac DGs*

The equations that represent the droop controllers for frequency (ω_i) - active power (P_i) and voltage (V_i) - reactive power (Q_i) of DG_i are given in (2.1).

$$\omega_i(t) = \omega_0 + M_{p\omega,i}P_i(t)$$
$$V_i(t) = V_0 + M_{qv,i}Q_i(t)$$
$$(2.1)$$

where ω_0 and V_0 are the setpoint frequency and voltage, respectively. $M_{p\omega,i}$ and $M_{qv,i}$ are the droop slopes of DG_i. These parameters can be designed as shown in (2.2).

$$M_{p\omega,i} = -\frac{\omega_0 - \omega_{\min}}{P_{\max}} \quad , \quad M_{qv,i} = -\frac{V_{\max} - V_{\min}}{Q_{\max} - Q_{\min}} \qquad (2.2)$$

where $\omega_{\min}$, $V_{\min}$ and $V_{\max}$ are the frequency and voltage amplitude limits, and $P_{\max}$, $Q_{\min}$ and $Q_{\max}$ are the active and reactive power limits of DG_i.

The main advantage of the droop control method is that communication is not required; instead, the frequency and the voltage magnitude measurement

indicates the overall deficit of active and reactive power in the MG, respectively [66]. Distributed resources are automatically connected; thus, no coordination is necessary, and the units can automatically adjust their set points to meet the overall needs of the MG. Conversely, the main disadvantage of the droop method is that, due to its operating principle, deviations in frequency and voltage are created; thus, additional controllers with a time-scale separation are needed so that they do not compromise the droop behaviour.

Note that if frequency and voltage are not restored, the variability of loads and generation based on renewable resources may cause considerable frequency excursions and, in the worst case, may lead a microgrid to instability. This is why great emphasis is given to studying techniques that guarantee voltage and frequency restoration in a microgrid, as described in the following section.

2.3.2 Secondary control level in *ac* MGs

The secondary control level has a lower bandwidth than the droop controller. Therefore, the communication network bandwidth is lower. The main tasks of the secondary control level are to restore the frequency and the voltage amplitude. The secondary controller shifts vertically the droop curves, as shown in Fig. 2.4. As explained before, there are three possible control structures at this level which are centralised, decentralised and distributed controllers. Since the MG frequency is a global variable, the frequency controller can measure the frequency at any node. However, since the voltage is not a global variable, it is necessary to define the voltage used to implement the secondary controller. Furthermore, in an MG, the existence of line impedance creates voltage drops. Hence, regulating all nodal voltages at the nominal value V_0 does not allow appropriate power-sharing among DGs [67]. For this reason, we aim for an average bus voltage regulation across the MG. In this sense, the proposed control scheme achieves the control of reactive power while regulating the average bus voltage across the MG [8, 49].
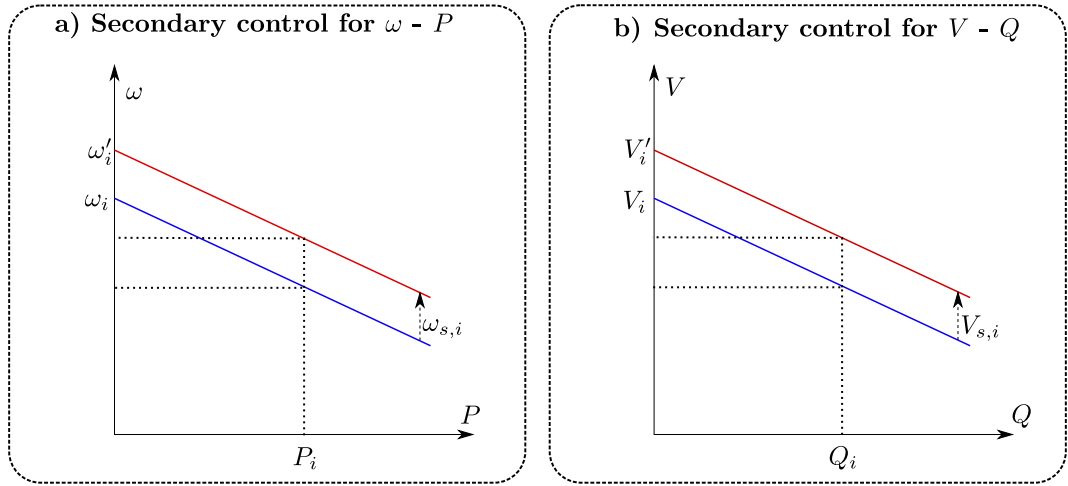
Figure 2.4: *Secondary control for ac DGs*

2.3.3 Tertiary control level in *ac* MGs

This control level is called Energy Management System (EMS) and operates on a large time scale. It usually achieves the economic dispatch of the MG and its coordination with the main grid when the MG is operating in grid-connected mode. Centralised and distributed controllers are mainly used at this control level [65, 68]. They typically require the solving an offline optimisation problem, although recently, MPC methods have been proposed at this level [69, 70]. Nevertheless, these optimisation problems use external prediction models, which are subject to uncertainty in both the power load and the generated power. Prediction models based on neural networks and fuzzy systems are the most common models used [71].

In an effort to achieve real-time operation of the EMS, [69, 70] propose a variable resolution (sample time) EMS, where the first prediction minutes are predicted with high accuracy (5 min), and the resolution decreases as the forecasted horizon is extended (60 min) to include an entire day of operation in the optimisation. These formulations consider optimal power flow and unit commitment separately, and for proper operation, these EMS need the mathematical formulation of the whole microgrid. Using the same approach described previously, [72] includes demand side management (DSM), reduces CO_2 emissions [73] and controls phase imbalance in an isolated microgrid [74].

The three previously mentioned works reported better performance in terms of an improved solution, less energy curtailed, reduced peak demand and improved load factor, but at the cost of higher computational time.

The performance of control strategies based on MPC at the tertiary level strongly depends on the accuracy of the prediction models, which in turn depends on the sampling time and aggregation level [75]. Contrary to bulk power systems, MGs can present generation fluctuations and rapid load changes. This could cause the predictions at this control level to deviate from the MG's real operating condition. For this reason latest research for *dc* MGs [18, 19], *ac* MGs [16, 17, 20] and H-MGs [21, 22] has demonstrated that the economic dispatch should be performed in a time-scale consistent with that of the secondary control level. A review of the state-of-the-art for the control of MGs is presented in Section 2.8.

2.4 Control of *dc* MGs

The control structure of *dc* MGs is similar to that described for *ac* MGs previously. The primary control level is based on a decentralised droop control, while the secondary control level restores the voltage deviation caused by the primary control. The tertiary control level exchanges energy with the main grid when a connection is possible. In the next section, only the primary and secondary control are discussed, as the tertiary control is similar to the one described for *ac* MGs.

2.4.1 Primary control level in *dc* MGs

The primary control level sets the current and voltage at the *dc* DGs' output and shares power among the *dc* DGs. These DGs are usually interfaced through *dc*-to-*dc* converters [76]. It is composed of an inner current loop (faster), voltage outer loop (slower) and droop controllers; the current and voltage control loops are usually proportional integral (PI) controllers. A bandwidth

separation of at least ten times is needed between these controllers for their operation [62].

As mentioned before, the main dynamic of this control level is dictated by the droop control. For *dc* DGs, current-voltage and power-voltage droop curves have been proposed [10]. The power *P*-voltage (*V*) droop allows the direct control of the power supplied by DGs and eases the management of *dc* DGs in hybrid *ac/dc* MGs.

In this case, to achieve active power sharing, DG units modify the output voltage (see Fig. 2.5). As ESS are out of the scope of this work, Fig. 2.5 considers unidirectional power.
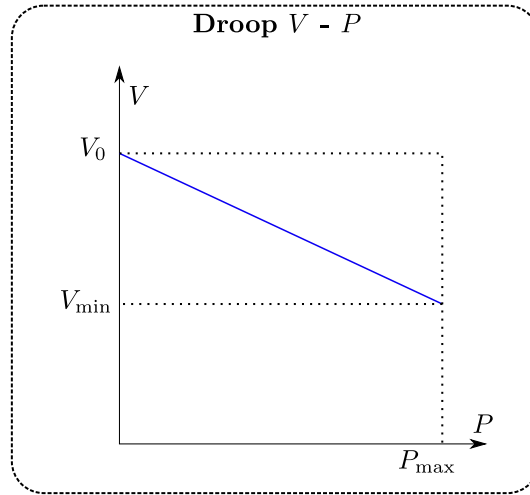
Figure 2.5: *Droop control for dc DGs*

The equation that represents the droop controller $V_i - P_i$ of DG_i is given in (2.3).

$$V_i(t) = V_0 + M_{pv,i}P_i(t) \tag{2.3}$$

where V_0 is the setpoint voltage, and $M_{pv,i}$ is the droop slope of DG_i. The slope can be designed as shown in (2.4).

$$M_{pv,i} = -\frac{V_0 - V_{\min}}{P_{\max}} \tag{2.4}$$

where $V_{\min}$ is the minimum voltage limit, and $P_{\max}$ is the active power limit of DG_i.

2.4.2   Secondary control level in *dc* MGs

The secondary control has a lower bandwidth than the droop controller. The main task of the secondary control level is to restore voltage magnitude [10]. The secondary controller shifts the droop curves vertically, as shown in Fig. 2.6. As explained before, there are three possible control structures at this level: centralised, decentralised and distributed controllers (see Fig. 2.2) [8, 10].

Since the voltage is not a global variable, it is necessary to define the voltage used to implement the secondary control. In an MG, the existence of line resistance creates voltage drops. Hence, regulating all nodal voltages at the nominal value V_0 does not enable appropriate power-sharing among the *dc* DGs. For this reason, we aim at an average bus voltage regulation across the *dc* MG. In this sense, the proposed control scheme achieves the sharing of active power while regulating the average bus voltage across the MG [8, 49]. A review of the state-of-the-art of MG's control is presented in Section 2.8.
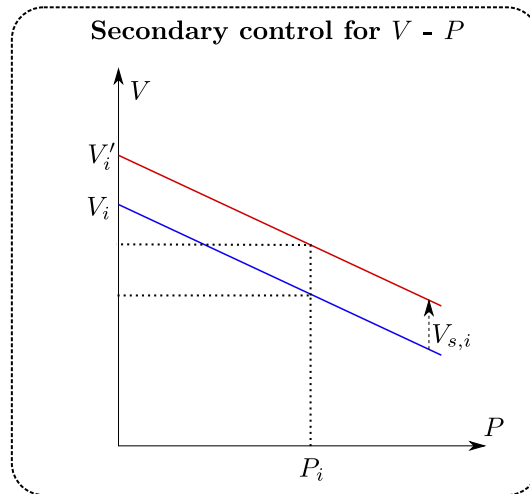
Figure 2.6: *Secondary control for dc DGs*

2.5   Control of hybrid *ac/dc* microgrids

As described in Section 2.2, a hybrid *ac/dc* microgrid (H-MG) is composed of an *ac* sub-MG and a *dc* sub-MG connected through bidirectional interlinking converters (ILCs), as shown in Fig. 2.1. The controllers of the sub-MGs were explained in Section 2.3 and Section 2.4. Therefore, only the control of the ILC is explained in the following.

ILCs control the power transference in an H-MG. There are two main approaches for controlling the power transferred through an ILC. The first one is based on the difference of the normalised deviations of the primary variables with respect to minimum and maximum allowed values, i.e., frequency of the *ac* sub-MG and voltage of the *dc* sub-MG [77, 78], which is fed to a PI controller. However, this approach losses accuracy when a secondary control regulates these variables.

The second approach includes the power management task at the secondary control level [21, 22, 38, 43, 79], where diverse objectives can be defined, such as power sharing [38, 43] and economic dispatch [21, 22]. Most of the existing approaches consider that the H-MG is composed of three independent systems [21, 22, 38, 77–79] (*ac* sub-MG, *dc* sub-MG, and ILCs) and neglect the dynamic interactions between them, which can degrade the dynamic response of the controllers. Furthermore, these formulations do not consider limits for the operation of the DGs and the ILCs. It is worth noting that no distributed model predictive control approaches for economic dispatch of H-MGs have yet been reported in the literature. A review of the state-of-the-art of MG's control is presented in Section 2.8.

2.6   Centralised and distributed model predictive control

MPC is becoming one of the most successful advanced control techniques implemented in industry [80, 81] due to its ability to handle complex systems with input and state constraints. MPC is emerging as a useful control strategy in the microgrids community [49, 68, 82] because it is a multi-variable constrained control scheme which obtains a real-time solution at each sample instant (rolling horizon). MPC consists of an objective function and a model of the process being controlled. The control includes physical and dynamic constraints [83] which, together with the objective function, are used to perform an online optimisation of the overall system. Among the advantages of MPC, the following are highlighted: modelling of complex systems, optimal solution, handling of communication delays, and better control of transients [49, 82, 84]. It is worth noting that MPC needs a good model of the system for the controller to work properly.

Centralised and distributed MPC algorithms are of interest because they can achieve global objectives. Centralised MPC schemes consider the system as a whole and perform an online optimisation [68, 83]. However, as they are complex and their computational burden increases exponentially with the number of optimisation variables [47], their application is limited to small systems. On the other hand, Distributed MPC (DMPC) solves local optimisation problems with information shared through a communication network. This structure reduces the traffic over the communication network and the computational burden. Indeed, this structure provides a fixed computational burden, as the number of optimisation variables does not increase when the system escalates [46, 47, 85]. A key aspect of DMPC is that computations for each subsystem are made in parallel.

For the implementation of MPC and DMPC, a discretisation of the system's model is used to formulate the control problem. While the discretisation of the

models does make them less exact than the original continuous-time models, it is widely accepted that a sampling time of roughly $1/15 - 1/10$ of the time constant of the main dynamic features is good in the sense that the derived model will be a good representation for its use in control [86]. In this sense, the control vector found with this model is expected to be good.

In DMPC, each local controller depends on local parameters that, in normal operation, should not change and are known. The parameters that could vary are the communication network and communication delays, affecting the predictive control modelling. However, if the DMPC includes within its formulation a model of the communication network (usually using an adjacency matrix), the controller should provide robustness when such changes occur. Moreover, MPC can provide robustness for communication delays and uncertainties due to its principle of operation, i.e., the rolling horizon mechanism [46, 85]. The controller receives new measurements and information from neighbouring subsystems at each sample time. Then, new control action sequences are computed, but only the first control actions are applied to the subsystem. After that, the whole procedure is repeated, which means a feedback mechanism is incorporated by using new measurements and neighbouring information to update the optimisation problem for the next sample time.

When considering multi-objective MPC or DMPC, weighting parameters are assigned to the objectives. These parameters will determine the relative importance of the objectives. It has been reported that if the cost function and the system's model are stated correctly, the tuning parameters will only be associated with a desired performance and will not affect the stability of the system [85]. It is recommended to normalise the objectives to ease the tuning procedure to give a sensible initial value for the weights so that the range 0 to 1 is equally important for each objective. Furthermore, it is recommended to start the tuning procedure by assigning the weight related to the control action to avoid abrupt changes in the system and later assign the weights of the remaining objectives [85].

As predictive control has a finite prediction horizon and constraints in its variables can be included, its theoretical stability analysis is not straightforward. Nevertheless, it is possible to define feasible optimisation problems with cost functions that decrease monotonically [47, 85]. There are two possible characteristics that an optimisation problem can include to guarantee feasibility and convergence. The first one is to include terminal constraints in the states to force the predicted output to exactly follow the reference during a sufficiently large horizon N_y. The second approach is to change the hard constraints for soft constraints by employing slack variables. These variables are strongly penalised in the cost function to obtain better performance [47, 85].

The main notion of including any of these characteristics is that if a feasible solution can be established and the prediction horizon (Ny) is large enough to cover the transient of the output variables, the cost function is monotonically decreasing and can be understood as a Lyapunov function, which would provide stability. Moreover, it can also be shown that the problem will be feasible in the next iteration [47, 85].

2.7   Distributed model predictive control for microgrids

Proportional integral (PI) controllers tend to be used at the secondary level [67]. However, thanks to advances in communication speeds and improved hardware capabilities of controllers, MPC and DMPC schemes are being incorporated at the secondary control level, improving the overall performance of microgrids as these controllers are multi-objective and robust against communication delays [49, 87].

Reported applications of MPC to the MG's secondary control can be divided into centralised and distributed MPC algorithms. Centralised secondary MPC controllers consider the MG as a single system and perform an online opti-

misation in order to guarantee a good performance, together with voltage, frequency and power regulation [68, 83]. However, a large communication network and high computational capability are necessary to compute the control actions. On the other hand, Distributed MPC (DMPC) solves local optimisation problems with information shared through a communication network, reducing the computational burden and traffic over the communication network. DMPC directly controls individual loads or DGs connected to the MG, requiring only partial information of the overall MG status. In this way, the computational burden is distributed across the MG, and large communication networks are avoided [49, 82, 84]. As DMPC is a distributed strategy, only the complexity of the communication network is increased.

It has been reported in [48, 49, 85, 88], that conventional controllers at the secondary level, such as proportional-integral-based (PI-based) ones, may not be robust enough to guarantee good and stable operation in the presence of uncertain and relatively large communication delays. Indeed, traditional PI-based techniques are more sensitive to delays. In such controllers, the closed-loop performance is sacrificed to endure the effects of delays [89].

The larger the delay, the more the performance is sacrificed, giving a slow dynamic response. In these controllers, if the bandwidth is not reduced, a poorer behaviour will result, i.e., significant overshoot and oscillations. Therefore, classical PI-based techniques which rely on simple gain changes are often not appropriate for systems with uncertain and potentially large delays. This phenomenon will be corroborated in this thesis through comparison tests.

Previous studies have demonstrated via small-signal modelling [88], simulation work [90] and experimentally [20, 49] that MPC and DMPC can handle a wider range of delays. MPC reduces the oscillations in the system, while other control strategies can have a predominant oscillating behaviour. These studies concluded that MPC is more robust in terms of the maximum unknown delay allowed. Therefore, in the presence of communication delays, MPC is able to compute an optimal control sequence that minimises the cost function to

obtain a smooth dynamic response in the MG.

Recently, distributed control schemes at the secondary control level based on DMPC have been reported for MGs [49, 87, 91, 92]. The authors of [87] present a feedback linearization DMPC for frequency and voltage restoration, considering the voltage and current at the LC filter output as state variables. The authors of [91] present a DMPC controller for voltage restoration, while frequency is restored using a variation of the distributed averaging proportional-integral (DAPI) controller with a finite-time observer. The authors of [92] present a DMPC controller based on a consensus version of the alternating direction method of the multipliers algorithm to regulate frequency in a networked MG system by manipulating the voltages of voltage-sensitive loads. The authors of [49] propose and validate experimentally a DMPC for frequency and voltage restoration using droop models and power transfer models; also active and reactive proportional power sharing is considered based on the concepts of [67]. The power sharing is based on consensus over the active and reactive power contributions from each generation unit in the MG using an adjacency matrix. Using external measures this controller avoids the necessity to model the MG topology. Only [93] proposes a DMPC for economic dispatch and frequency restoration via simulation at the secondary level. The work of [93] includes both operation and maintenance costs within its formulation. However, it does not use consensus for the economic dispatch, and it assumes an ideal communication network. Nevertheless, none of the DMPC methods proposed for the secondary level take into account the overall economic performance of the MG via a consensus strategy.

All of the previously reported works proposing secondary MPC or DMPC controllers for MGs have been developed considering balanced MGs [49, 68, 82–84]. However, when looking at the secondary control level, the low voltage *ac* MGs used for the distribution of electrical energy are inherently (phase) unbalanced systems since they usually have to feed unbalanced loads, leading to significant challenges for the secure and reliable operation of the MG. Adding

this to the usual aims of voltage and frequency regulation and the improvement in the sharing of both active and reactive power introduces additional control challenges to the MG secondary control [33, 94].

2.8   Distributed secondary control for microgrids in the literature

In distributed control, the consensus and cooperative control algorithms have attracted the attention of the MG community [60]. The multi-agent system (MAS) cooperative control method, in particular, aims to achieve system objectives cooperatively by mimicking the behaviour of biological phenomena [95]. Controllers based on MAS at the secondary level have been reported. For example, the authors of [67] proposed the distributed averaging proportional integral (DAPI) controller, which uses PI controllers for frequency and voltage restoration with an adjacency matrix representing the communication network of the MG. The advantage of this controller is its distributed structure; however, active power is shared proportionally among DG units.

The authors of [96] present a finite-time control approach to restore voltage and a DAPI controller to restore frequency; the former controller guarantees a fixed time convergence for voltage restoration and decouples the secondary controllers. A variation of the DAPI controller is presented in [97] where the integrative part of the control actions are shared among the DGs. This controller improves the transient of the proportional active power sharing among the DG units. However, as these controllers are based on PI controllers, they neither include dynamic models of the DGs nor include their physical power limits.

2.8.1 Distributed economic dispatch for *ac* microgrids

There is a clear tendency to integrate the economic dispatch of DGs at the secondary level and to implement distributed controllers in isolated MGs [58, 67, 98]. In a distributed fashion [16, 58, 99] demonstrated that the economic dispatch can be integrated into the same time-scale of frequency and voltage restoration. The literature distinguishes between two main approaches to achieve the distributed economic dispatch in MGs. The first one employs the distributed gradient method [100], which directly calculates a global incremental cost through a consensus algorithm, whereas the second one uses the incremental cost consensus (ICC) concept in which the incremental cost is estimated [99, 101]. The first option requires several communication iterations per sample time to find a solution which is hard to achieve in experimental microgrids. On the other hand, the ICC presents a better approach because communication among DGs is required once per sample time. In the following the related approaches based on the ICC are discussed.

The authors of [16] reformulate the optimisation problem to achieve the Karush-Kuhn-Tucker (KKT) conditions of linear optimal power flow. Then, a control action from a PI controller is added to a droop controller to achieve the economic dispatch of DGs. The authors of [99] achieved active power and reactive power dispatch, including voltage and frequency regulation in a decomposition of the optimisation problem. Nevertheless, these publications only provide simulation results. The authors of [102] proposed a MAS economic resource management in an isolated microgrid. The control strategy is tested under time-varying load conditions. Conversely, in [103] a two-stage control strategy is proposed to achieve an economical operation and restore frequency. In contrast, in [104], a grid-connected distributed resource management is presented. Two control levels are needed to achieve adequate economic dispatch. As the microgrid is connected to the distribution network, the regulation of frequency and voltage is not considered in the formulation. Nevertheless, these strategies

do not solve an actual optimisation problem and most of them do not consider operating limits in their formulation.

The authors of [105, 106] propose a distributed economic dispatch that includes power balance and ramp constraint restrictions using a distributed primal-dual consensus algorithm; the advantage of the previous technique is its speed of convergence. Time-varying communication delays are considered in the distributed optimisation through the decomposition of [107], but in this work, renewable resources are considered as constants. In [101], a distributed finite-time economic dispatch is proposed; this technique guarantees a fixed convergence time, but its formulation does not consider the regulation of voltage and frequency. Finally, [108] depicts a multi-agent system (MAS) frequency regulation at a minimum cost controller and a threshold-based demand response controller; this technique disconnects electrical load in emergency cases.

By contrast, [109] includes the minimisation of environmental objectives within its formulation, and it is tested in the presence of communication delays and noisy communication channels. In [110], BESS modelling is included in the formulation of distributed economic dispatch to provide the service of arbitrage and spinning reserve. Although the controllers proposed present different benefits, none of them is tested experimentally. As the previously described distributed controllers only use various single-input single-output (SISO) PI controllers and rely on a fixed control law, they do not guarantee an optimal solution. Moreover, they do not consider real-time changes in the operation of the MG [45]. Furthermore, most studies do not solve an optimisation problem and do no not consider physical constraints in their formulation. In addition, they perform poorly when communication delays are present in the communication network.

Economic dispatch of reactive power

Usually, only the economic dispatch of active power is considered. However, neglecting the related reactive power costs might result in increased operat-

ing costs and deviations from the optimal solutions for dispatch. For instance, [111] co-optimised the dispatch of active and reactive power in distribution networks. The results show that more than 12 % of energy losses could be reduced if reactive power is appropriately managed. The reactive power cost function, in a deregulated electricity market, can be represented by the weighted coefficients of the cost function of active power [112]. The weights are obtained through the power factor from the relation of the triangle of powers.

Recent works [112–115] have included the dispatch of reactive power along with active power in their formulation. The works of [112, 113] consider a centralised controller at the tertiary control level to address both active and reactive economic dispatch. The results show that considering the costs associated with reactive power reduces the total operation cost. The work of [115] presents a distributed approach at the tertiary level; the controller only requires local measurements and information exchange with its neighbouring buses. This paper verifies that a distributed approach can reduce the computational burden and avoid communication losses while the solution's quality is preserved compared to a centralised technique. A distributed PI approach based on the same concept of the previous methods was proposed in [114] for isolated *ac* MGs. However, none of these controllers considers equipment power limits, and only results for load changes are provided. Moreover, these controllers do not consider the existence of hybrid *ac/dc* MGs.

2.8.2   Distributed economic dispatch for *dc* microgrids

The concept of incremental cost consensus (ICC) discussed for *ac* MGs has been extended for *dc* MGs [18, 19, 100, 116, 117]. In this type of MG, the secondary controller restores the (average) voltage while ensuring economic dispatch of DGs by modifying the droop voltage control. In [100] economic dispatch of generation and local voltage regulation is achieved. The authors of [18] achieve economic dispatch of generation and average voltage regulation; however, separate communication networks are used to communicate the power

and voltage references. Similarly, [19] extends the ICC concept to multiple *dc* MGs. In [116] economic dispatch is performed without considering voltage restoration. Nevertheless, none of these controllers considers equipment power rating limits in their formulations. Only [117] considers power limits by using saturators.

The authors of [118] use droop control to estimate the MG load and generation from uncontrollable DGs. However, several parameters need to be adequately adjusted for this strategy to work. The effects of constant communication delays in distributed schemes have also been analysed using simulation work in [119]. Next, the works reported for H-MGs are presented.

2.8.3   Distributed economic dispatch for hybrid *ac/dc* microgrids

The economic dispatch of H-MGs has been usually solved through a centralised optimisation problem. These strategies can incorporate uncertainties in market prices [120] or uncertainties in generation and consumption [121]. The authors in [122, 123] include the power limits of the units in the centralised optimisation problem. Nevertheless, these approaches are subject to a single point of failure and do not provide reliability under communication failures.

Conversely, the authors of [124] proposed a two-level distributed controller for the economic dispatch of H-MGs that depends on the estimation of the MG's load. The incremental cost is included in the droop controllers of the primary level while the secondary level restores the deviations caused by the droop controllers. However, when these variables are restored the loading conditions of *ac* and *dc* sub-MGs are hard to estimate. A relative loading index (RLI) is used to extract the hidden loading status of each sub-MG and generate the power reference for the ILC. Nevertheless, this method is highly dependent on the quality of the estimation of the RLI. The works of [118, 125] also include the economic dispatch within the droop controllers design but also present

erroneous behaviour when a secondary controller is included.

Better performance can be achieved by integrating the economic dispatch in distributed approaches at the secondary level [21, 22]. For instance, [21] proposes a unified controller for economic dispatch and frequency and voltage restoration. First, ICC within sub-MGs is achieved through information sharing between the DGs; the ILC then equalises the incremental costs of the sub-MGs. However, the ILC's communication scheme, stability, and parameter design are not provided. In [22], a similar approach is presented, where an event-based control scheme is utilised to design the consensus protocol. This protocol reduces the communication burden of the MG. However, these approaches consider that the H-MG is composed of three independent systems(*ac* sub-MG, *dc* sub-MG, and ILCs) and neglect the dynamic interactions between them, which can degrade the controllers' dynamic response.

Most approaches in the literature assume fixed operational set-points for voltage and frequency [16–19, 43], and do not take advantage of the flexibility associated with the secure operational bands defined in the IEEE standard 1547-2018 [40], which suggests that DGs can operate normally as long as the frequency and the voltage are within 1% and 5% of their nominal values, respectively. It is worth noting that all the works mentioned above assume that frequency and voltages must be set to fixed setpoint values, giving up flexibility in the microgrid control system. Additionally, existing approaches are designed independently for either *ac* sub-MGs [16, 17, 44] or *dc* sub-MGs [18, 19], without accounting for the particular features of H-MGs. Also, as they are strategies based on PI controllers, it is difficult to achieve multiple parallel objectives and cope with operational constraints [45, 46].

To the best of the authors' knowledge, the problem of combined economic dispatch of active and reactive power as well as frequency and voltage restoration within secure bands in isolated H-MGs using DMPC has not been thoroughly studied in the existing literature. Furthermore, in most studies, equipment power constraints are not considered: these constraints can prevent equipment

damage. For these reasons, this thesis adopts a distributed cooperative scheme for controllers based on MPC. Each controller seeks to dispatch its controllable unit based on its generation cost and to restore the frequency and voltage amplitude deviations on the *ac* sub-MG and the voltage magnitude on the *dc* sub-MG. Furthermore, as the proposed controller includes a detailed model of the dynamics of the primary control level (controlled system), it is able to deal with variable and uncertain delays [48, 85]. Another characteristic of the proposed DMPC is that the variation of the control actions is penalised in the cost function. This penalisation prevents abrupt changes in the MG operating point, and a smooth dynamic response is obtained.

2.9   Imbalance sharing in *ac* microgrids

As MGs operate at the distribution level, their power quality is affected by the presence of unbalance between the phases [23, 24]. Unbalances directly affect the MGs' operation if they are not dealt with properly, as they can lead to inefficient operation and trigger protection systems. Unbalances are mainly caused by the presence of single-phase loads. Moreover, the integration of renewable energy resources is putting more stress on MGs, as these can be connected across all three phases or only on one single phase [24].

The secondary control schemes reported in the literature for unbalanced MG operation usually include three features (according to their control objectives): (i) Compensation of imbalance at particular points of the MG, (ii) Improving the sharing of unbalanced powers between the DG units of the MG, and (iii) Simultaneous compensation of imbalance and improvement of unbalanced power-sharing. These aims can be addressed using decentralised, centralised and distributed approaches.

The compensation of imbalance can be achieved using active power filters (APFs) to compensate unbalanced currents or unbalanced voltages at specific points of the MG [25, 26]. However, APFs are not attractive in MGs since

they constitute additional hardware and higher costs. Another more cost-effective solution is to embed imbalance compensation capabilities into the control schemes of DG units that are already available in the MG [27–29]. For instance, in [27] a master/slave based approach is proposed. A supervisory controller calculates the compensation effort (in terms of current) for each slave converter to compensate for imbalances at sensitive load buses.

Control schemes to improve the sharing of unbalanced powers between the DGs of MGs are mainly based on droop control and use virtual impedance loops. This means that negative sequence impedances are implemented to control the sharing of imbalance between the DGs. The magnitude of these virtual impedances is controlled via decentralised control schemes in [30–32], meaning that there is no coordination between the DG units (each DG works autonomously based on variables measured locally). However, better performance could be achieved via coordination between DG units (centralised and distributed approaches). In this sense, the magnitude of the negative sequence impedances are calculated in a coordinated way by a secondary centralised controller in [33–36], while in [37–39] secondary distributed controllers, based on consensus algorithms, are implemented.

It is worth noting that these papers (describing centralised and distributed systems) quantify the DGs' imbalance by defining three-phase unbalanced powers (calculated based on three-phase power theories [38, 39]), aiming to improve the sharing of these powers. However, as shown in [53] and [23], when unbalanced *ac* MGs are considered, the improvement in three-phase power sharing does not ensure that the single-phase powers are appropriately shared. In this scenario, overloading may occur in some of the DG phases, causing inappropriate behaviour in the DG and load shedding, which could affect the overall security and reliability of the MG.

Another approach to improve the sharing of imbalance is the addition of power converters to the three-phase MG to directly manage the DG phase power balance and prevent overloading of single phases [50–52]. For instance, in

[52], a multi-objective formulation is proposed to achieve per-phase imbalance sharing in a three-phase MG. An additional power converter is placed at the point of common coupling for managing single-phase power. However, adding extra power converters into the MG increases the cost of this approach making the proposals reported in [50–52] not cost-effective.

When looking for MPC-based methods to manage imbalance, only decentralised finite control set model predictive control (FCS-MPC) has been reported at the MG's primary control level [126–128]. The authors of [126] propose a decentralised FCS-MPC, where the imbalance is managed by an external loop that shares the negative sequence reactive power. The works of [127, 128] present FCS-MPC methods to improve imbalance sharing. FCS-MPC methods may produce a variable switching frequency because FCS-MPC does not use a modulator. They demand a high computational burden, as they operate at the primary control level; this is because the evaluation of the cost function is usually realised for all the switching states of the power converter. Furthermore, these are usually decentralised methods that compute local solutions; thus, an optimal solution is hard to obtain. To the authors' best knowledge, no DMPC strategy for imbalance sharing at the secondary control level has been proposed.

To summarise, imbalance sharing methods based on virtual impedance loops [30, 33–39] do not ensure a proper sharing of single-phase powers. This issue is discussed in more depth in Section 5.7.2. The solution proposed in [50–52] of adding power converters to the MG to achieve single-phase power management is not cost-effective. Finally, FCS-MPC-based methods used for the primary level for imbalance sharing require extensive processing capabilities, and since they are based on a decentralised approach, do not provide a cooperative solution.

To avoid the drawbacks of these approaches, we propose a novel secondary DMPC control scheme for improving the sharing of imbalances. This proposal avoids the use of virtual impedance loops; moreover, it does not require

additional converters in the MG. In this case, contrary to the reported MPC-based methods for imbalance sharing, the proposed control algorithm achieves a global solution via consensus objectives which do not require an extensive computational burden (thanks to the distributed approach). The imbalance sharing is achieved by controlling the single-phase reactive powers of the DGs. In particular, the proposed strategy uses a modified single-phase $Q - V$ droop scheme, where one additional secondary control action is introduced per phase. With the multi objective DMPC, it is possible to formulate a predictive controller that considers the dynamic behaviour of the MG main variables. This technique uses a reduced number of control actions to achieve all the control objectives (see Section 5.2). Furthermore, the proposed secondary control scheme can regulate simultaneously the imbalance sharing and power quality of each DG. This has not previously been explored extensively: the works published in [33, 39] are the only ones reported so far.

These simultaneous objectives are of paramount importance since, as discussed in [33, 34], imbalance sharing methods increase the voltage imbalance at the output of the DGs. Therefore, these imbalances should be regulated to avoid power quality issues as defined by IEEE standard 1547-2018 [40]. A well-used index to determine the power quality of an MG is the phase voltage unbalance rate index (PVUR), which is defined Section 5.3.4. Thus, a control technique must improve imbalance sharing without exceeding the maximum PVUR value recommended in the IEEE standard 1547-2018 for PVUR [40].

2.10 Discussion

This section presented the hierarchical control structures of *ac* MGs, *dc* and H-MGs. The corresponding controllers at each control level and their functionalities were explained. The main advantages of distributed control against centralised and decentralised control were also discussed. A review of the current state-of-the-art in distributed control approaches applied to isolated

ac, *dc* and hybrid *ac/dc* MGs was presented. Special emphasis was given to consensus-based approaches and distributed model predictive control approaches.

The latest consensus-based strategies for economic dispatch were presented. Their operation principles, main characteristics and limitations were detailed. Moreover, imbalance sharing methods reported so far were also discussed and analysed in detail.

The review shows that despite the advances in control strategies, the economic dispatch of H-MGs and the sharing of imbalances have not been studied thoroughly. Moreover, there are still research gaps that DMPC-based strategies can solve to improve the entire system's reliability and operation. On the other hand, DMPC presents several advantages against classical PI-based approaches. This is because DMPC models the main dynamics of the controlled system and allows the inclusion of hard and soft constraints, allowing to represent physical limitations and achieve a more flexible regulation of certain variables.

The distributed structure of the predictive controllers provides robustness in the presence of changes in microgrid structure while better performance against communication delays and communication failures is secured. Another advantage of the distributed structure of the proposed strategies is their easy scalability. In addition, the proposed strategies are easy to deploy in current operating systems as they use the usual measurements of the primary control level and do not need the addition of extra power converters. Instead, all the desired functionalities are incorporated directly into the formulations of the predictive controllers.

The following sections present the proposed controllers. The first proposal for *ac* MGs is presented in Chapter 3. This controller considers the restoration of frequency to its nominal value and economic dispatch of DGs in balanced *ac* MGs. The second proposal, described in Chapter 4, achieves economic dispatch of *ac* DGs, *dc* DGs and manages the power transference of ILCs

based on an economic criterion in H-MGs. Frequency and *ac* voltage on the *ac* sub-MG and *dc* voltage on the *dc* sub-MG are also regulated within secure bands based on the IEEE standard 1547-2018 [40] to provide flexibility to the H-MG operation.

The last proposed strategy, described in Chapter 5, is able to manage imbalance sharing in unbalanced *ac* MGs while the maximum unbalanced voltage at the DGs output is regulated to fulfil the maximum values stated in the IEEE standard 1547-2018 [40]. This strategy also considers the regulation of frequency and voltage within secure bands based on the IEEE standard 1547-2018 [40].

Finally, Chapter 6 presents the conclusions, possible future research paths and the publications realised during the PhD studies.

Chapter 3

DMPC scheme for frequency regulation and active power dispatch in *ac* microgrids

3.1   Introduction

In this Chapter, the proposed distributed model predictive control (DMPC) strategy for economic dispatch and frequency restoration for isolated *ac* microgrids (MGs) is detailed. In the DMPC scheme of this chapter, each DG can economically dispatch active power by employing an incremental cost consensus (ICC) approach and can also restore the MG's frequency to its nominal value whilst satisfying physical constraints.

The main challenge for this Chapter is to develop the local models and cost function required to tackle simultaneously the aforementioned objectives. A local prediction model of the DGs primary control level is included in each DMPC to predict its future behaviour. These are in the form of droop control and active power transfer models. In addition, the DMPC strategy has to be able to recognise and update its calculations when the MG is subject to external phenomena including, communication delays, communication failures and the disconnection/reconnection of DGs.

This chapter is organised as follows: Section 3.2 presents the derivation of the incremental cost from the usual centralised economic dispatch. Then, its extension for the distributed scheme is designed. Section 3.3 introduces the proposed strategy. The dynamic prediction models are presented in Section 3.4. The DMPC formulation is then described in Section 3.5. The experimental setup and validation tests are explained in detail in Section 3.6. Finally, Section 3.7 summarises the main benefits of the proposed strategy.

3.2   Centralised economic dispatch

Consider a three-phase balanced *ac* MG with a set of $\mathbb{N}$ DGs, where $\mathbb{N} = \{1, ..., N\}$. The traditional centralised approach to economically dispatching active power in an MG can be expressed as the optimisation problem in (3.1).

$$\underset{\mathbf{P}}{\text{minimise}} \quad \sum_{i=1}^{N} \mathbb{C}_i(P_i) \tag{3.1a}$$

$$\text{subject to} \quad \sum_{i=1}^{N} P_i = P_D \tag{3.1b}$$

Economic dispatch establishes the lowest cost dispatch of controllable DG units, whilst ensuring that the total load is met. It is composed of a cost function that minimises a quadratic cost (3.1a) subject to the power balance constraint (3.1b). $\mathbb{N}$ is the set of DGs in the MG, $\mathbf{P} = \{P_i : i \in \mathbb{N}\}$, P_i is the active power contribution of DG i, P_D is the total MG load, and $\mathbb{C}_i(P_i)$ is a convex cost function described in (3.4a). The traditional centralised approach to economic dispatch (3.1) requires a unique central controller, and its failure could compromise the economic dispatch of the entire MG . It presents a high computational burden [8, 10]. Therefore, a distributed control is a better alternative for higher reliability and security for the operation of the MG [129]. Assuming strong duality holds e.g. Slater's constraint qualification condition holds, the problem may be expressed through its Lagrange dual [130]. The

Lagrangian function of the economic dispatch problem is:

$$\mathbb{L}\left(P_i, \eta\right) = \sum_{i=1}^{N} \mathbb{C}_i\left(P_i\right) + \eta\left(P_D - \sum_{i=1}^{N} P_i\right) \tag{3.2}$$

where the Lagrange multiplier η is associated with the power balance constraint. The Karush–Kuhn–Tucker (KKT) stationary condition for the problem is defined in (3.3a) [16]. From (3.3a) it is possible to establish that at the optimal point, the incremental cost (IC) function is defined by (3.3b).

$$\frac{\partial \mathbb{L}}{\partial P_i} = \nabla \mathbb{C}_i(P_i) - \eta = 0 \quad i \in \mathbb{N} \tag{3.3a}$$

$$\eta = \nabla \mathbb{C}_i(P_i) \quad i \in \mathbb{N} \tag{3.3b}$$

The generation cost function for the $i - th$ DG is stated in (3.4a) [59], where a_i, b_i and c_i are constant cost parameters defined in Section 3.6.2, and P_i is its active power contribution. Therefore, by using (3.4a) in (3.3b), the IC for the $i - th$ DG is given by (3.4b).

$$\mathbb{C}_i(P_i) = a_i P_i^2 + b_i P_i + c_i \tag{3.4a}$$

$$\eta_i(P_i) = 2a_i P_i + b_i \tag{3.4b}$$

The economic dispatch problem redistributes the power contribution of all DGs to reach the same optimal dispatch point η (3.3b) (KKT stationary condition), where η corresponds to the (unique) dual variable associated with the demand-supply balance equation of the MG's economic dispatch problem (3.1b). Therefore, a distributed cooperative predictive scheme can be designed that ensures the condition of $\eta_i = \eta_j = \eta$ in steady state, where η_j is the IC of neighbouring DGs. Note that this distributed scheme intrinsically meets the demand-supply balance.

Based on the IC, a new distributed predictive cooperative control strategy is

designed, aiming to provide an economic dispatch of active power and at the same time regulating the frequency. This DMPC control strategy is based on the work presented in [49]. It is worth noting that in [49] economic dispatch is not considered. Also, in this first proposal the DMPC formulation for the coupling between voltage regulation and reactive power sharing is not considered. However, the DAPI controller reported in [67] is used to solve for voltage restoration and reactive power sharing.

3.3 Proposed DMPC scheme

The following explanations and mathematical analysis are made for the $i-th$ DG, as the analysis is analogous for the rest of the DGs. The proposed controller neither depends on the MG's electrical topology nor on adjacent physical measurements i.e. only the typical measurements at the output filter and voltage observers are required. Therefore, the number of buses and distribution lines are irrelevant. At the DG's output, an LCL filter is used, where the second inductance (L_i) is designed to ensure a predominantly inductive impedance [63, 64], as shown in the electrical configuration of Fig. 3.1. This allows the decoupling of active and reactive power and the implementation of the classic droop controllers in the power converters [8].

To predict the power contribution of the $i-th$ DG, the phase angle deviation $(\delta\theta_i)$ between the local unit and the MG is determined [131]. For this, the voltage measurement (V_i) at the output of the LC filter is used. Then using a phase locked loop (PLL), its frequency (ω_i) and phase angle (θ_i) are estimated. In addition, the voltage $(\hat{V}_i^B)$ at the connection bar node (after the coupling inductances L_i) is estimated by virtual meters based on non-linear reduced-order observers to reduce the hardware, while the performance of the controller is maintained. Then, the MG's frequency $(\hat{\omega}_i^B)$ and phase angle $(\hat{\theta}_i^B)$ are estimated using a PLL, as shown at the bottom of Fig. 3.1.

The voltage observer is based on [132], and its main advantage is its linear
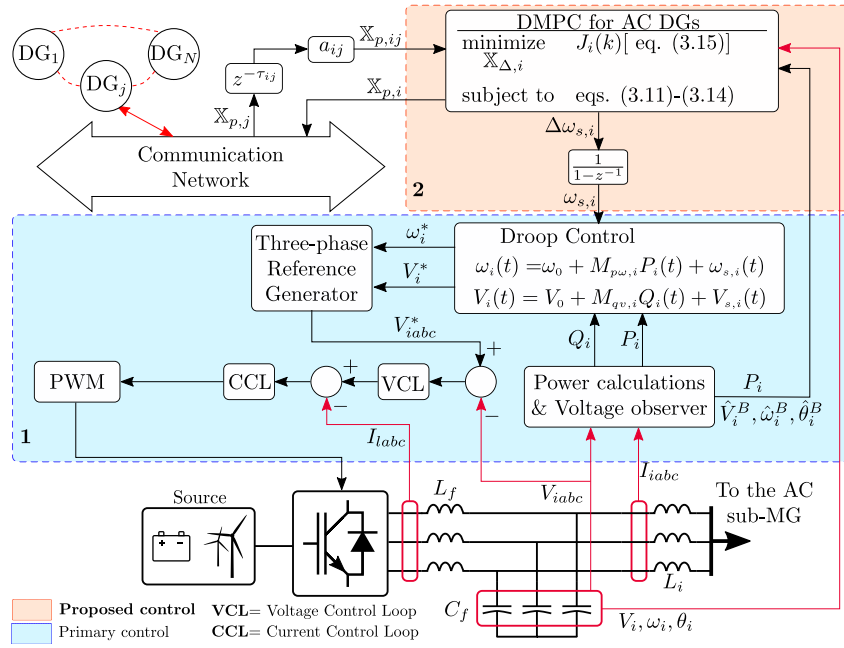
Figure 3.1: *Distributed economic dispatch with frequency restoration for the $i-th$ DG*

dynamic for the estimation error. Therefore, the observer gains can be tuned via pole placement, improving the transient performance of the observer and the convergence rate of the estimation error. It also has a low computational burden. The basis of the observer is detailed as follows. The observer works in the $\alpha-\beta$ framework. The estimated states are defined by $\hat{V}_{\alpha,i}^B = V_m sin(\theta_i)$ and $\hat{V}_{\beta,i}^B = V_m cos(\theta_i)$, where V_m depends on the $abc-\alpha\beta$ transformation used. The observer's state space formulation is obtained from Kirchhoff's voltage law, whereas its inputs are the measured values of V_i and i_i (at the LCL filter), both in the $\alpha - \beta$ framework. A detailed explanation of the development of the voltage observer is presented in the Appendix A.

The controller scheme for the $i-th$ DG is depicted in Fig. 3.1. It is configured as a voltage source converter (VSC) with its respective LCL output-filter. Two control layers are highlighted. The primary control level (cyan box in Fig. 3.1) is made up of $\omega - P$ and $V - Q$ droop controllers, outer voltage (slower) and inner current (faster) cascaded Proportional-Resonant (PR) controllers. The voltage observer also operates at this control level.

At the secondary level (orange box in Fig. 3.1), the predictive controller for

economic dispatch and frequency restoration is presented. This controller receives as inputs the local measurements/estimates ($P_i(k)$, $V_i(k)$, $\omega_i(k)$, $\theta_i(k)$, $\hat{V}_i^B(k)$, $\hat{\omega}_i^B(k)$, $\hat{\theta}_i^B(k)$) of the $i-th$ DG unit and the results of the optimisation problems of communicated neighbouring units $\mathbb{X}_{p,ij}$. The controller has two outputs, which are the frequency control action (vector $_\Delta\omega_{s,i}$) and the results of the local optimisation problem $\mathbb{X}_{p,i}$ (vector of predicted values), both defined in Section 3.5.3. Whereas the former passes through a discrete integrator to ensure zero error in steady-state, the latter is sent via the communication network. Note that both objectives of this proposal (frequency restoration and economic dispatch) are achieved with the same control action $_\Delta\omega_{s,i}$. Next, the dynamic models that rule the behaviour of the DMPC scheme are presented.

3.4 Dynamic models used for the design of the DMPC strategy

3.4.1 Communication network model

As distributed control schemes require information exchange, a full-duplex communication network is considered. This network allows the consensus objectives to be achieved through cooperation between the MG DGs [133]. To accomplish a consensus objective, all distributed controllers must converge to the same steady-state value, also known as a consensus value. This communication structure considers both latency and connectivity phenomena. Latency represents the time interval (τ_{ij}) for a data packet to be transmitted from source to destination, whereas the connectivity is represented by the $N \times N$ adjacency matrix A. The terms a_{ij} (3.5) of a non-negative A represent information flow among DGs at time instant k.

$$a_{ij}(k) = \begin{cases} 1 & \text{Data from DG}_j \text{ arrives at DG}_i \text{ at } k \\\\ 0 & \text{Data from DG}_j \text{ does not arrive at DG}_i \text{ at } k \\\\ 0 & j = i \end{cases} \tag{3.5}$$

where $k = nT_{sec}, n \in \mathbb{Z}^+$, and T_{sec} is the sample time of the controller.

As the communication is bidirectional, the associated graph is undirected. Thus, $\tau_{ij} = \tau_{ji}$ and $a_{ij}=a_{ji}$ [42, 133, 134]. A fully meshed communication network can be used as primary setup; however, this topology can change as long as at least one communication path exists between all DGs in the MG (i.e., there is a spanning tree) [42, 133, 134]. An example of the adjacency matrix of an MG with four DGs is depicted in Fig. 3.2. This matrix encodes the communication topology of the MG.
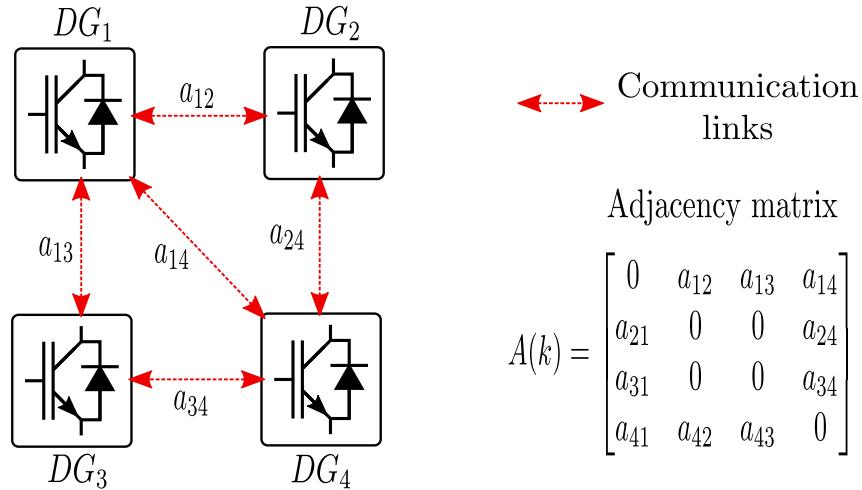
Figure 3.2: *Example of an MG with four DGs and its adjacency matrix*

The adjacency matrix A is initialised at the beginning of the simulation based on communication topology at that sample time. Then, this matrix is updated (by verifying the communication links) at each sample time based on the information received on each DG from its directly communicating neighbouring DG units. Note that each DG only knows (interacts with) its direct communication links and not the entire network. Furthermore, an asynchronous communication protocol is used; thus, no global clock is necessary to ensure that the sharing of information is globally synchronised [135, 136].

3.4.2   Dynamic models

To model the dynamics of the MG, the frequency at each node, along with the active power flow, are considered. Since these variables are coupled, in this work they are modelled using the droop (3.6), phase angle difference (3.7) and power transfer (3.8) equations . In particular, the $i - th$ DG unit is modelled as the node at the output of its LCL filter, as shown at the bottom of Fig. 3.1. The $i - th$ DG is connected to the MG through the second inductance (L_i) of the LCL filter.

The droop model for frequency $\omega_i(t)$ - active power $P_i(t)$ for the local $i - th$ DG is presented in (3.6).

$$\omega_i(t) \;=\; \omega_0 + M_{p\omega,i}P_i(t) + \omega_{s,i}(t) \tag{3.6}$$

where ω_0 is the nominal frequency, $M_{p\omega,i}$ is the droop slope that defines the linear relation between the frequency and the active power $P_i(t)$, and $\omega_{s,i}(t)$ is the secondary control action (after the discrete-time integrator, see Fig. 3.1) for the i-th unit. This relationship allows the DGs to interpret active power changes in the MG by producing a frequency deviation; furthermore, through this model, the primary and secondary control levels interact.

To determine the power contribution from the $i - th$ DG to the MG, the phase angle difference is determined. The phase angle difference $(\delta\theta_i)$ between the local DG unit and the MG through a coupling inductance (L_i) of the LCL output filter is defined in (3.7) [131].

$$\delta\theta_i(t) \;=\; \theta_i(t) - \hat{\theta}_i^B(t) \;=\; \int_0^t \left[\omega_i(\tau) - \hat{\omega}_i^B(\tau)\right] \, d\tau \tag{3.7}$$

where θ_i, ω_i are the phase angle and frequency before the coupling inductance (L_i), and $\hat{\theta}_i^B$ and $\hat{\omega}_i^B$ are the phase angle and frequency after the coupling inductance (L_i), respectively.

The power transfer equation (3.8) is included to govern the active power contribution from each DG unit to the MG.

$$P_i(t) \;=\; B_i V_i(t) \hat{V}_i^B(t) \sin\left(\delta\theta_i(t)\right) \tag{3.8}$$

where $V_i(t)$ and $\hat{V}_i^B(t)$ are the voltages before and after the coupling inductance L_i, and $B_i = 1/(L_i \cdot \omega_0)$ [131]. Note that this model only requires local measurements and the estimation of the voltage $(\hat{V}_i^B)$ after the coupling inductance to predict the active power contribution. Therefore, the use of an admittance matrix is avoided with this formulation, ensuring robustness in the presence of changes in microgrid structure.

3.4.3   Discrete time models

Prior to defining the prediction models, a discretisation of the models in (3.6), (3.7) and (3.8) is needed. These models are discretised using the forward Euler method, where $k = nT_{sec}, n \in \mathbb{Z}^+$, and T_{sec} is the sample time of the controller. As integrators are placed at the output of the predictive controllers to ensure zero error in steady-state (See Fig. 3.1) [45], the incremental operator (3.9) is applied to (3.6); thus, the optimisation problem is expressed as a function of the control action variation $(\vartriangle\omega_{s,i})$.

$$\vartriangle f(k) = [f(k) - f(k-1)] \tag{3.9}$$

Additionally, a Taylor expansion is applied around the measured/estimated point $\{\omega_i(k), \hat{\omega}_i^B(k), V_i(k), \hat{V}_i^B(k), \delta\theta_i(k), P_i(k)\}$ to linearise the power transfer model (3.8). The resulting linear discrete models are shown in (3.10). A detailed explanation of the discretisation and linearisation processes is given in Appendix B. Note that having linear models ensures that the computational burden will remain within the recommendations for the secondary control level.

$$\omega_i(k{+}1) = \omega_i(k){+}M_{p\omega,i}[P_i(k{+}1){-}P_i(k)]{+}\vartriangle\omega_{s,i}(k) \tag{3.10a}$$

$$\delta\theta_i(k{+}1) = \delta\theta_i(k){+}T_{sec}\left[\omega_i(k{+}1){-}\hat{\omega}_i^B(k)\right] \tag{3.10b}$$

$$P_i(k{+}1) = P_i(k){+}[\delta\theta_i(k{+}1){-}\delta\theta_i(k)]B_i V_i(k)\hat{V}_i^B(k)\cos(\delta\theta_i(k)) \tag{3.10c}$$

The models described in this section are included in the in DMPC strategy in the following section.

3.5   Formulation of the distributed model predictive control

Unlike [43, 49, 67], where the aim was that all generation units contribute to the power-sharing of active power proportionally to their maximum power rating, in this work, a more cost-effective formulation is proposed that meets the economic dispatch, where the most economical generation units are the ones that contribute most to the power-sharing as long as power limits are not exceeded. Additionally, this proposed controller restores the MG frequency to its nominal value.

DMPC uses the discrete-time model of the system, presented in (3.10), to predict the behaviour of the DGs over a prediction horizon (N_y), and a sequence of control actions (N_u) is calculated through a numerical optimisation problem that minimises a cost function (see (3.11) in Section 3.5.1). The predicted sequences for the variables and control actions are contained in the vector $\mathbb{X}_i$ (defined in Section 3.5.3), which is the solution to the optimisation problem. Only the first control action is applied to the system, and the optimal control problem is repeated at each sample time with updated measures[45]. A challenge in the implementation of MPC strategies at the secondary control level is the definition of an optimisation problem with a low computational burden which can be solved in a short sample period [46, 49]. The optimisation problem and how it is solved are detailed in the next section.

3.5.1   Cost function

The multiobjective cost function is stated in (3.11) and is composed of three weighted terms, where each term seeks a specific objective.

$$J_i(k)=\sum_{m=1}^{N_y}\lambda_{1i}(\overline{\omega}_i(k+m)-\omega_0)^2+\sum_{m=1}^{N_u}\lambda_{2i}(\triangle\omega_{s,i}(k+m-1))^2$$

$$+\sum_{j=1,j\neq i}^{N}\sum_{m=1}^{N_y}\lambda_{3i}a_{ij}(k)(\eta_i(k+m)-\eta_j(k+m-\hat{\tau}_{ij}))^2 \tag{3.11}$$

The first term represents the restoration of the average frequency $(\overline{\omega}_i)$ to its nominal value, which is calculated only with the information communicated from other DGs. The second term penalises the control action sequence required to carry out (at the same) time both the regulation and consensus objectives; note also, the overshoot and settling time are adjusted with this term. The third term achieves the economic dispatch through a cooperative consensus over the predicted ICs between the local DG and the neighbouring (communicating) DGs. Therefore, the condition $\eta_i = \eta_j = \eta$ in steady state is enforced within the cost function. The terms $\lambda_{1i}, \lambda_{2i}$ and λ_{3i} are the tuning parameters explained in Section 3.6, and $\hat{\tau}_{ij}$ is the estimation of the communication delay, which is assumed to be one sample period at the secondary level.

3.5.2 Predictive models and constraints

The set of equations of (3.10) is generalised in (3.12) to predict the response of the $i-th$ DG at $k+m$ steps ahead, where $m \in \mathbb{Z}^+$. Note that although the coefficients produced in the linearisation are updated each sample time, they are constant during the optimisation.

$$\omega_i(k+m)=\omega_i(k+m-1)+M_{p\omega,i}[P_i(k+m)-P_i(k+m-1)]+\triangle\omega_{s,i}(k+m-1) \tag{3.12a}$$

$$\delta\theta_i(k+m)=\delta\theta_i(k+m-1)+T_{sec}\big[\omega_i(k+m)-\hat{\omega}_i^B(k)\big] \tag{3.12b}$$

$$P_i(k+m)=P_i(k)+[\delta\theta_i(k+m)-\delta\theta_i(k)]B_iV_i(k)\hat{V}_i^B(k)\cos(\delta\theta_i(k)) \tag{3.12c}$$

In addition to the previous models, a set of operational constraints are included in the DMPC formulation. These are equality constraints to ensure appropri-

ate performance of the controller and inequality constraints to guarantee the solution is within the equipment power ratings of each DG.

Equation (3.13a) represents a local average frequency approximation ($\overline{\omega}_i$). This average is calculated with only the information communicated from the other DGs (ω_j), which is determined by the adjacency term a_{ij}. Also, the term $\hat{\tau}_{ij}$ is the estimate of the time-delay. These two terms provide robustness against communication failures and latency effects, respectively. The terminal constraint (3.13b) is included to guarantee convergence of the distributed predictive scheme to the tracked value (nominal frequency) at the end of the prediction horizon N_y [47].

$$\overline{\omega}_i(k+m) = \frac{\omega_i(k+m) + \sum_{j=1}^{N} a_{ij}(k)\omega_j(k+m-\hat{\tau}_{ij})}{1 + \sum_{j=1}^{N} a_{ij}(k)} \tag{3.13a}$$

$$\overline{\omega}_i(k+N_y) = \omega_0 \tag{3.13b}$$

The generalisation of the incremental cost (IC) model for the prediction horizon is expressed in (3.14). This term is used in the cost function to achieve the economic dispatch of DGs, as will be shown in (3.11).

$$\eta_i(k+m) = 2a_i P_i(k+m) + b_i \tag{3.14}$$

Finally, the active power contribution of the $i-th$ DG is limited to its physical maximum power rating through the inequality constraint (3.15); hence, the space solution is bound.

$$P_{i,\min}(k) \leq P_i(k+m) \leq P_{i,\max}(k) \tag{3.15}$$

Note that the control action variation ($\delta\omega_{s,i}$) will be zero after the frequency regulation and incremental cost consensus objectives have been met when the DG is in steady-state. At this point, the cost function will take the value of zero. Moreover, as no constraints are associated with the control action, the desired objectives will always be achieved. Additionally, because a terminal

restriction for frequency regulation is incorporated (3.13b), the controller's convergence is ensured. By imposing this terminal constraint, the controller is forced to follow the reference during a sufficiently large horizon (N_y). The main notion is that if a feasible solution can be established and the prediction horizon (Ny) is large enough to cover the transient of the output variables, the cost function is monotonically decreasing and can be understood as a Lyapunov function, which would provide stability [47, 85]. Moreover, it can also be shown that the problem will be feasible in the next iteration. Therefore, considering that the optimisation problem is always feasible and its convergence is guaranteed, it is possible to state that the controller will remain stable.

3.5.3 Formulation of the quadratic programming

The proposed DMPC comprises a quadratic cost function, linear equality constraints and linear inequality constraints; thus, it is convex and can be synthesised in a canonical quadratic programming (QP) formulation. Due to the convexity of the proposed controller, the global minimum can be achieved. The cost function (3.11) with its respective equality and inequality constraints (3.12)-(3.15) are included in a QP formulation (3.16) via the matrices/vectors $H_i, A_i, B_i, A_{eq,i}, B_{eq,i}, F_i$.

$$
\begin{aligned}
&\underset{\mathbb{X}_i}{\text{minimise}} && J_i(k) := \tfrac{1}{2}\mathbb{X}_i^T H_i \mathbb{X}_i + F_i^T \mathbb{X}_i \\
&\text{subject to} && A_i \mathbb{X}_i \leq B_i \\
& && A_{eq,i}\mathbb{X}_i = B_{eq,i}
\end{aligned}
\tag{3.16}
$$

The output of the QP problem is (3.17), where the set of predicted variables is contained in $\mathbb{X}_{p,i}$ (3.18) and the optimal control sequence is given by $\mathbb{X}_{\Delta,i}$ (3.19). Note that thanks to the distributed structure of the controller, the number of predicted variables is fixed. Therefore, the computational burden does not increase when new DGs are introduced into the MG. This is of high importance for the scalability of control techniques at the secondary control

level.

$$\mathbb{X}_i = \{\mathbb{X}_{p,i}, \mathbb{X}_{\Delta,i}\} \tag{3.17}$$

$$\mathbb{X}_{p,i} = \{\overline{\omega}_i(k+m), \omega_i(k+m), \delta\theta_i(k+m),$$
$$P_i(k+m), \eta_i(k+m)\}_{m=1}^{N_y} \tag{3.18}$$

$$\mathbb{X}_{\Delta,i} = \left\{\Delta\omega_{s,i}(k+m-1)\right\}_{m=1}^{N_u} \tag{3.19}$$

Following the principle of MPC, only the first predicted control action of $\mathbb{X}_{\Delta,i}$ is applied in the frequency-active power droop controller, i.e. $\Delta\omega_{s,i}(k)$. The optimisation is then repeated each sample time with updated measurements/estimations. Moreover, the predictions $(\mathbb{X}_{p,i})$ are shared to achieve the cooperative objectives.

To compute the QP problem (3.16), the QPKWIK algorithm is used, which is a stable variation of the classic active-set method [137]. This solver is able to generate C_{++} code to run on the experimental setup. The methodology to solve the DMPC scheme is described in Algorithm 1, which details all the necessary steps to achieve the cooperative objectives.

Algorithm 1 DMPC solution for DG_i

Inputs: Measurements and estimations:$\{\omega_i(k), \hat{\omega}_i^B(k), V_i(k), \hat{V}_i^B(k),$
   $\delta\theta_i(k), P_i(k)\}$
   Received information:$\mathbb{X}_{ij}, \forall j = \{1, ..., p\}$
Outputs: $\mathbb{X}_i, \Delta\omega_{s,i}(k)$
   Initialisation :
 1: Compute matrix/vector coefficients of $H_i, A_i, B_i, A_{eq,i}, B_{eq,i}, F_i$
 2: **for** every k **do**
 3:    Compute adjacency terms a_{ij} according to the received information.
 4:    According to the received information, compute the sum of frequency and incremental cost from
       (3.13a) and (3.11).
 5:    Update matrices/vector $H_i, A_i, B_i, A_{eq,i}, B_{eq,i}, F_i$ from (3.16) according to the results of step 4 and
       the measurements/estimations $\{\omega_i(k), \hat{\omega}_i^B(k), V_i(k), \hat{V}_i^B(k), \delta\theta_i(k), P_i(k)\}$.
 6:    Solve QP problem using QPKWIK algorithm.
 7:    **if** $\mathbb{X}_i$ is feasible and $t < k + T_{sec}$ **then**
 8:       Extract $\Delta\omega_{s,i}(k)$ from $\mathbb{X}_i$.
 9:    **else**
10:       $\Delta\omega_{s,i}(k) = 0$.
11:    **end if**
12:    Update controller outputs and send $\mathbb{X}_i$ to neighbour DGs if it is feasible
13: **end for**

3.6   Experimental results

3.6.1   Experimental MG configuration

The performance of the proposed DMPC control strategy was assessed in a case study using the experimental MG configuration illustrated in Fig. 3.3a. This experimental MG was built in the MGs Control Lab at the University of Chile[1]. The DGs are emulated by real-time controlled power units from the *Triphase*® company, part of National Instruments. The MG comprises three *ac* DG units, which are emulated by the PM15F120 (DG_1 and DG_2) and PM5F60 (DG_3) *Triphase*®, as shown in Fig. 3.3b. Each DG unit is controlled by a real-time target (RTT) computer, in which the DMPC control algorithm is uploaded. Table 3.1 presents the MG electrical parameters. Furthermore, Table 3.2 and Table 3.3 present the DG parameters, including their operating costs which were obtained from [16]. In Table 3.3, a_i, b_i and c_i are the constant generating cost parameters used in the quadratic cost function (3.4b). These parameters represent the generating cost of the DGs and their operating point efficiency.

---

[1]https://www.die.cl/sitio/home/investigacion/laboratorios/laboratorio-de-control-de-micro-redes/

a)

b)
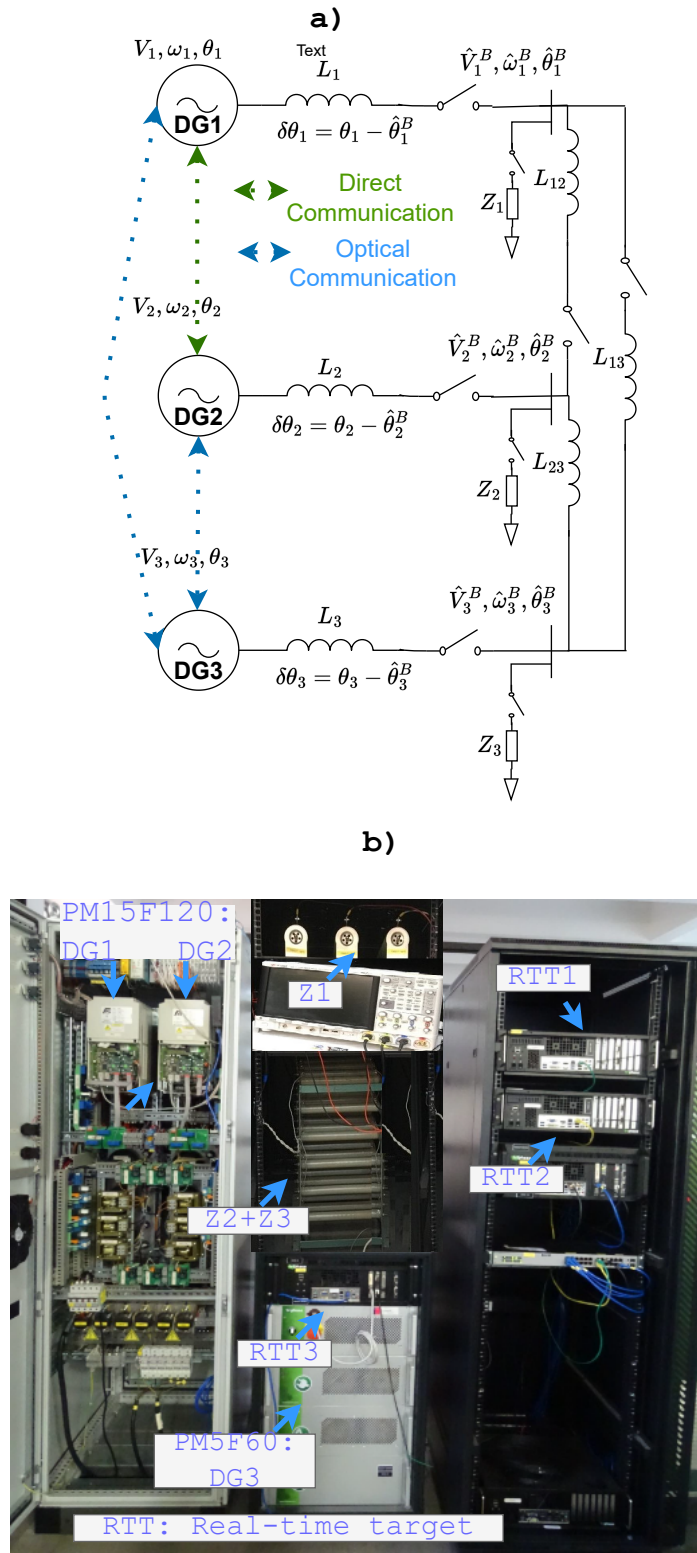
Figure 3.3: *a) MG Diagram, b) Experimental MG setup*

Table 3.1: MG electrical parameters

Parameter	Description	Value
T_{prim}[s]	Primary level sample period	1/16E3
Z_1 [Ω]	Load 1	35 (0.64 KW)
Z_2 [Ω]	Load 2	15 (1.5 KW)
Z_3 [Ω]	Load 3	22 (1.02 KW)
L_i [mH]	Coupling inductance	2.5
L_{ij} [mH]	Distribution line inductance	2.5
ω_0 [rad/s]	Nominal frequency	100π
V_0 [V]	Nominal voltage (peak)	150
ω_c [rad/s]	Droop controller cutoff frequency	2π

Table 3.2: Power ratings and droop slopes

Parameter	**Description**	DG_1-DG_3
P^{max} [Kw]	Maximum power rating	2.1
$M_{p\omega}$ $\frac{rad}{sW}$	$P - \omega$ droop coefficients	-2.38E-4
M_{qv} $\frac{V}{VAR}$	$Q - V$ droop coefficients	-4.8E-3

Table 3.3: DG operating costs

Parameter	DG_1	DG_2	DG_3
a[$/kW^2$]	0.264	0.4	0.5
b[$/kW$]	0.067	0.1	0.125
c[$]	0	0	0

3.6.2 Design parameters and test scenarios used to evaluate the DMPC

Table 3.4 presents the DMPC design parameters and weighting factors. All the design parameters were selected aiming to reduce the overall computational burden. This is because the computational burden increases significatively with the sample time, and the prediction and control horizons [47]. While the sample time was selected considering the open loop rise time ($T_r = 0.7s$) of the MG's frequency (operating with only the primary control enabled) as $T_{sec} = 0.7/14 = 0.05s$ [86], the prediction and control horizons were selected

as 5 samples because with these values, the traffic over the communication network is reduced. The minimum estimated delay corresponds to one sample period at the secondary level sample time.

The weighting factors were tuned following the guidelines in [89], i.e., looking for a trade-off between the control objectives and, if needed giving more importance to one objective compared to the rest of the objectives. The load changes scenario was used to tune the controller. Note that this scenario does not consider failures such as communication delays/failures and topology changes. However, the results show that the proposed controller achieves good performance even when these issues occur in the MG. First, the weight related to the control action variation (λ_{2i}) was highly penalised for avoiding undesired behaviours in the DGs. Then, as frequency regulation is the main task of the secondary control level, the weight associated with this objective (λ_{1i}) was fixed. Finally, the weight associated with the incremental cost consensus (λ_{3i}) was established.

Note that the latter weight is smaller than the other weights. This is because the incremental cost consensus depends on the active power, which is larger than the frequency. Therefore, a smaller weighting factor is needed to make this objective comparable to the other objectives. It is worth highlighting that these weighting factors will not affect the steady-state solution of the controller. Indeed they are only related to the convergence speed of the objectives.

Table 3.4: Controller parameters and weights

Parameter	Description	Value
T_{sec} [s]	Controller sample time	0.05
$\hat{\tau}_{ij}$ [s]	Estimated communication delay	0.05
Ny	Prediction horizon	5
Nu	Control horizon	5
λ_{1i} [$(\frac{s}{rad})^2$]	Average frequency error	18.5E2
λ_{2i} [$(\frac{s}{rad})^2$]	Frequency control action	4.7E4
λ_{3i} [$(\frac{1}{W})^2$]	Active power dispatch	1.01E-4

The controller was tested under four scenarios using the experimental MG, shown in Fig. 3.3. The first scenario presents the DMPC's performance when the MG experiences load changes. The second scenario shows the behaviour of the MG when there are latency effects over the communication network. The third scenario shows the effects of a failure in the communication network. Finally, the last scenario validates the robustness in the presence of changes in microgrid structure, where DG_2 is disconnected and reconnected from/to the MG. These four test scenarios were selected because these are the most common phenomena that a controller at the secondary level confronts [49, 135]. A distributed controller has to perform well against communication issues, such as communication delays and failures. In addition, the possibility of disconnecting and reconnecting DGs to the MG without changes in the programming of the controllers is essential. Moreover, as voltage restoration and reactive power sharing are not the focus of this first proposal, their results are presented just for the base case.

3.6.3   *Scenario I* (base case) - Load changes

This scenario presents the performance of the proposed controller in the MG when there are several load impacts. During the whole test, the adjacency matrix is not changed and is represented by (3.20).

$$A(k) = \begin{bmatrix} a_{11} & a_{12} & a_{13} \\ a_{21} & a_{22} & a_{23} \\ a_{31} & a_{32} & a_{33} \end{bmatrix} = \begin{bmatrix} 0 & 1 & 1 \\ 1 & 0 & 1 \\ 1 & 1 & 0 \end{bmatrix} \tag{3.20}$$

The test starts with the primary control enabled (internal loops and droop control) and two loads connected (Z_1 and Z_2) at different nodes to observe that without the DMPC controller, the DG units share active power equally (see Fig. 3.4a before 10s) and the frequency deviates from its nominal value (see Fig. 3.4c before 10s) with an operating cost of 0.8293 $\$/h$ (American dollars/hour), shown in Fig. 3.4d (before 10 s).
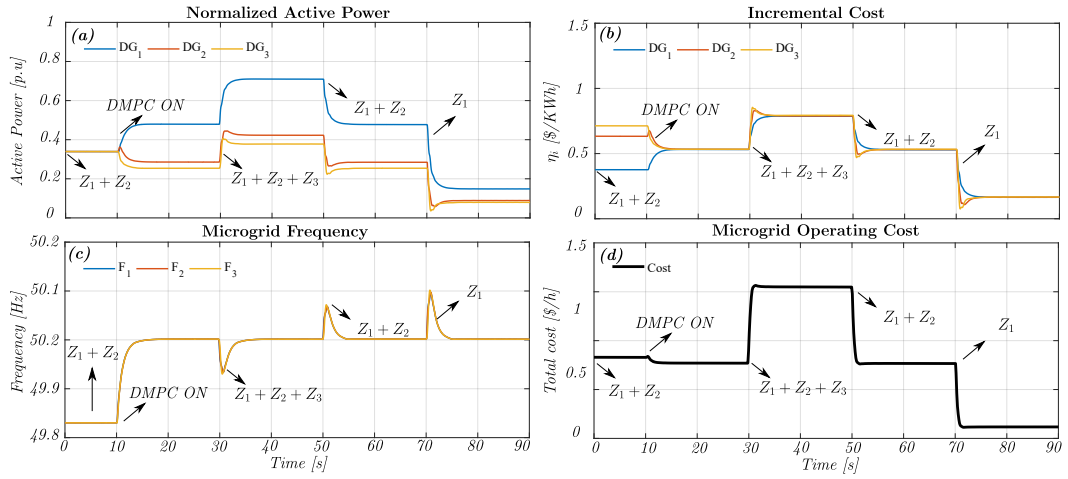
Figure 3.4: *Load changes - base case: a) Active power contribution, b) Incremental cost consensus, c) Frequency regulation, d) Total operation cost*

At $t = 10s$, the secondary controller is enabled, so the active power is redistributed, as observed in Fig. 3.4a, and the frequency is restored to its nominal value, as observed in Fig. 3.4c. Once the controller is enabled the active power is redispatched according to the DG's operating costs in Table 3.3 via the consensus over the incremental cost (η), as shown in Fig. 3.4b. The operating cost is reduced from $0.8293 \$/h$ to $0.7696 \$/h$. This cost reduction may seem small in monetary terms due to the small size of the MG; however, it could be significant in percentage terms in a larger MG. Indeed the reduction cost is 7.2%. As DG_1 is the least expensive unit, it takes the majority of the load followed by DG_2, which has an intermediate cost. Furthermore, DG_3 takes the lowest load as it is the most expensive unit to operate. At 30 seconds, the MG is subjected to its total load (i.e. Z_3 is connected). Finally, the loads Z_3 and Z_2 are disconnected at $t = 50$ and $t = 70$, respectively. Fig. 3.4a, Fig. 3.4b and Fig. 3.4c show that during all the load perturbations the controller provides a smooth response without large overshoots and with a settling time below 3 seconds for both objectives. Moreover, the proposed DMPC reduces the operating cost (as shown in Fig. 3.4d) during the entire test.

In addition, it is shown that the proposed DMPC controller does not affect the performance of the DAPI controller for normalised reactive power sharing and voltage restoration, as shown in Fig. 3.5a and Fig. 3.5b, respectively. It is worth

noting that there is better regulation of voltage than reactive power sharing. This is because these two objectives are opposed in the DAPI controller [67], and more weight was given to regulation of voltage.
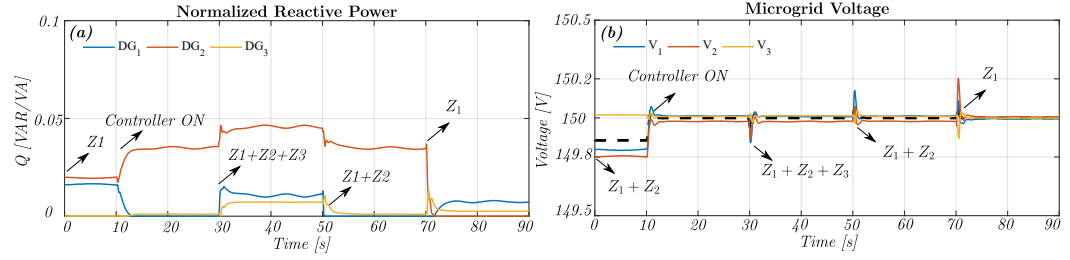
Figure 3.5: *Load changes - base case: a) Reactive power contribution, b) Voltage regulation*

3.6.4   *Scenario II* - Communication delay

This test presents the performance of the proposed controller when there is a constant delay (τ_{ij}) in all links of the communication network, whilst the estimated delay $(\hat{\tau}_{ij})$ is kept constant at one sample, as shown in (3.13a) and (3.11). For each test, the same load perturbations of *scenario I* are applied. Two cases were considered: a) small time-delay $(\tau_{ij}=0.25s)$ and b) large time-delay $(\tau_{ij} = 1s)$. Note that the worst-case scenario represents a delay of 20 samples, which is four times the prediction horizon N_y. These values for the delays were obtained from related works published in the literature [16, 17]. These works establish that for the operating time of the secondary control level a time delay of 1 second is considered as a large delay. Moreover as this delay is in the whole communication network, this is the worst possible scenario. This is because the dynamic response of the controller will depend on the largest delay.

The results of the controller performance are presented in Fig. 3.6. The frequency restoration is the most affected variable when communication delays are present. Fig. 3.6a and Fig. 3.6b show the frequency of each DG for the cases of small time-delay $(\tau_{ij}=0.25s)$, and large time-delay $(\tau_{ij}=1s)$, respectively. It is observed that the larger the time-delay the larger the overshoot

and settling time. However, these two parameters are still small, even for the worse case-scenario, i.e. for (τ_{ij}=1s) the overshoot is negligible (less than 0.3%) and the settling time is below ten seconds.
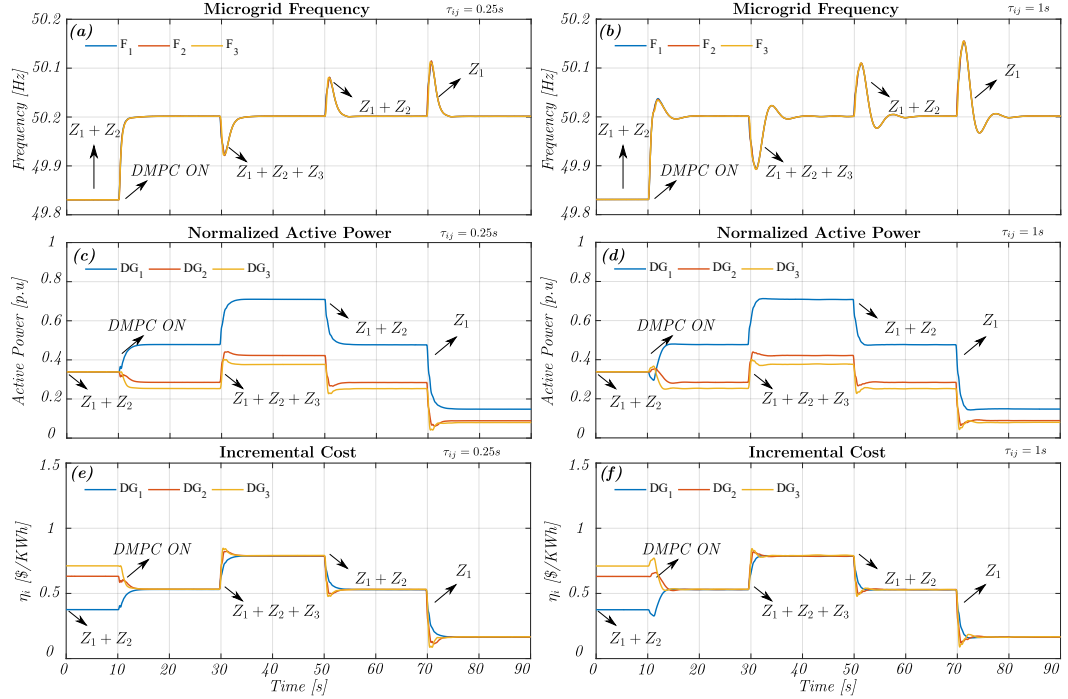
Figure 3.6: *Communication delays: a) Frequency regulation for $\tau_{ij} = 0.25s$, b) Frequency regulation for $\tau_{ij} = 1s$, c) Active power contribution for $\tau_{ij} = 0.25s$, d) Active power contribution for $\tau_{ij} = 1s$, e) Incremental cost consensus for $\tau_{ij} = 0.25s$, f) Incremental cost consensus for $\tau_{ij} = 1s$*

The active power dispatch for the same two time-delays is presented in Fig. 3.6c Fig. 3.6d, while the IC consensus for both time-delays is shown Fig. 3.6e Fig. 3.6f. For both variables, it is observed that the settling time is practically unaffected; even in the worst case (τ_{ij}=1s), the settling time is lower than five seconds. The overshoot slightly increases, as the time-delay increases. This is seen most when the controller is activated; nevertheless, it is still negligible. From these results, it is possible to establish that the DMPC is robust against communication delays over and above the prediction horizon. This is because the DMPC uses the rolling horizon property, which determines the appropriate control sequence even with past information from neighbouring DGs [46].

3.6.5   *Scenario III* - Communication link failure

To analyse the performance of the controller against communication link failures, the following test was carried out. The test begins with two loads connected at different nodes (Z_1 and Z_2). At $t = 10s$, the controller is enabled. A communication failure is forced at $t = 30s$ between DG_1 and DG_2, so the adjacency matrix is modified as shown in (3.21), and the control algorithm identifies automatically the failure by calculating (3.13a) and (3.11) only with the information received. Z_3 is connected at $t = 50s$ and disconnected at $t = 70s$. Finally, the communication link is restored at $t = 90s$.

$$A(k) = \begin{bmatrix} a_{11} & a_{12} & a_{13} \\ a_{21} & a_{22} & a_{23} \\ a_{31} & a_{32} & a_{33} \end{bmatrix} = \begin{bmatrix} 0 & 0 & 1 \\ 0 & 0 & 1 \\ 1 & 1 & 0 \end{bmatrix} \tag{3.21}$$

The results are shown in Fig. 3.7. It is observed that the controller performance is not impaired, and the control objectives are achieved. Therefore, the DMPC strategy is robust against communication failures. Nevertheless, the transient response is different, specifically, the settling time is increased to nearly ten seconds. This is because the communication matrix (A) is not complete (3.21), and the control objectives are directly related to known information from the neighbouring DGs. A detailed explanation of the effects of the communication network on the controller performance is presented in Section 5.5.3 and Section 5.7.1.
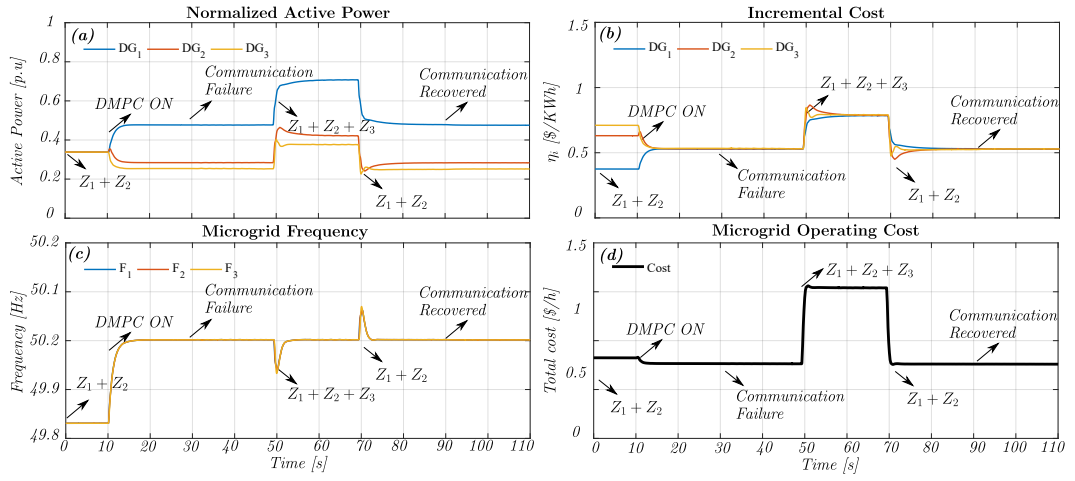
Figure 3.7: *Communication failure: a) Active power contribution, b) Incremental cost consensus, c) Frequency regulation, d) Total operation cost*

3.6.6 *Scenario IV* - Robustness in the presence of changes in microgrid structure

This test presents the controller's response when an unscheduled failure occurs in a specific DG. The test starts with two loads connected at $t = 0s$ (Z_1 and Z_2) and the controller is enabled and at $t = 10s$, where the adjacency matrix is represented by (3.20). At $t = 30s$ DG_2 is taken out of service, i.e. DG_2 is disconnected from both the electrical system and the communication network. Thus, the adjacency matrix is modified as shown in Fig. 3.8c at $t = 30s$. The MG continues operating with DG_1 and DG_3 connected. Next at $t = 50s$, the total load is connected. At $t = 70s$, after a synchronisation routine, DG_2 is reconnected to the MG. Finally, Z_3 is disconnected at $t = 90s$.

Note that although DG_2 is disconnected from the MG, it is not turned off. Only its secondary control is disabled, but its primary control continues operating. When DG_2 is disconnected or reconnected the adjacency matrix is updated, and the remaining controllers identify this failure by calculating (3.13a) and (3.11) only with the information received. Therefore, the remaining DG units optimise the consensus terms with only the operating units.

Fig. 3.8a presents the active power contribution. It is observed that when DG_2 is disconnected although both DG units increase their contributions,
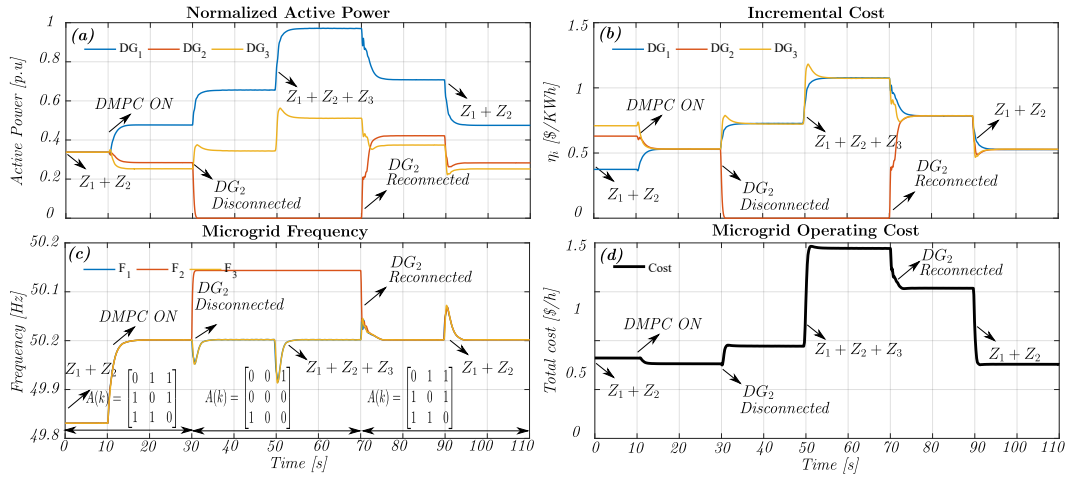
Figure 3.8: *Robustness in the presence of changes in microgrid structure: a) Active power contribution, b) Incremental cost consensus, c) Frequency regulation, d) Total Operation cost*

DG_1 takes the majority of the load; however, its maximum power rating is not exceeded. Fig. 3.8b shows that the IC consensus is achieved during all the disturbances. However, when DG_2 is disconnected the MG operating cost increases (see Fig. 3.8b at $t = 30s$). This is because DG_3, which is the most expensive, increases it power contribution. Similarly, Fig. 3.8b presents the frequency restoration. It is observed that the operating DGs restore the frequency adequately during the whole test without overshoots or long settling times. Therefore, the proposed DMPC scheme is robust in the presence of changes in microgrid structure and always respects the physical power rating of the DGs.

3.7   Discussion

This Chapter presented a novel distributed predictive control strategy to cope with economic dispatch and frequency regulation for isolated *ac* microgrids. The proposed controller is able to maintain frequency regulation and economic dispatch simultaneously, respecting the maximum power limits of each DG unit. The proposed strategy achieves the economic dispatch of DGs in a distributed fashion through the incremental cost consensus concept. Moreover,

the proposed strategy considers only the communication links between neighbouring communicated DGs.

The dynamic performance of the controller is evaluated experimentally and discussed under four test scenarios. The controller effectively tackles the disconnection and reconnection of DGs and communication link issues, i.e., communication delays and communication failures. It is verified that the rolling horizon property of the DMPC scheme provides robustness against large communication delays. Moreover, the distributed structure of the controller provides robustness against communication link failures.

This proposed strategy and its experimental validation were presented in the journal paper:

A. Navas-Fonseca, J. S. Gomez, J. Llanos, E. Rute, D. Saez, and M. Sumner, "Distributed Predictive Control Strategy for Frequency Restoration of Microgrids Considering Optimal Dispatch," in IEEE Transactions on Smart Grid, vol. 12, no. 4, pp. 2748-2759, July 2021, doi: 10.1109/TSG.2021.3053092, [**Q1-IF 8.960 - published**].

The following chapter formulates the application of the DMPC strategy for the operation of hybrid *ac/dc* microgrids and the inclusion of voltage and reactive power control in the proposed predictive control strategy for *ac* DGs. For the operation of hybrid *ac/dc* MGs (H-MGs), predictive models and cost functions for the control of *dc* DGs and interlinking converters (ILCs) need to be developed. Additionally, new models and additional objectives are included in the formulation for *ac* DGs to control reactive power and voltage restoration. A detailed explanation of the DMPC scheme for the operation of H-MGs is provided in the following chapter.

Chapter 4

DMPC scheme for frequency and voltage regulation within bands and the economic dispatch of active and reactive power for hybrid *ac/dc* microgrids

4.1 Introduction

In this Chapter, the distributed model predictive control (DMPC) strategy is proposed for the economic dispatch of active and reactive power and frequency and voltage regulation within bands for isolated hybrid *ac/dc* microgrids (H-MGs). In this DMPC scheme, all the DGs of the H-MG can achieve active power economic dispatch while the DGs of the *ac* sub-MG can also provide reactive power economic dispatch. In contrast to the previous approach, the frequency and *ac* voltage on the *ac* sub-MG and the *dc* voltage on the *dc* sub-MG are regulated within secure bands through the use of soft constraints.

Additionally, equipment operating constraints are not exceeded.

The main challenge for this chapter is to design the local dynamic models and cost functions of *ac* generators, *dc* generators and interlinking converters (ILCs) to tackle these objectives simultaneously. A local prediction model is included in each DMPC to predict its future behaviour, i.e., droop control, and active and reactive power transfer models. Moreover, the DMPC strategy has to be able to recognise and update its calculations when the MG is subject to external phenomena such as, communication delays, communication failures and the disconnection/reconnection of DGs and ILCs.

This chapter is organised as follows: Section 4.2 presents the derivation of the incremental cost from the usual centralised economic dispatch for H-MGs. In a similar fashion, Section 4.3 shows the derivation of the reactive marginal cost (RMC). Section 4.4 describes the communication structure of the H-MG. Section 4.5 introduces the proposed strategy for ILCs. Then, the DMPC formulation for ILCs is described in Section 4.6. The proposed strategy for *dc* DGs is presented in Section 4.7, and its DMPC formulation is detailed in Section 4.8. The proposed strategy for *ac* DGs is presented in Section 4.9, and its DMPC formulation is described in Section 4.10. The simulation setup and validation tests are explained in detail in Section 4.11. Finally, Section 4.12 summarises the main benefits of the proposed strategy.

4.2   The active power economic dispatch problem

The usual centralised approach to economically dispatching active power in an H-MG can be expressed as the optimisation problem in (4.1) [21]. The objective function minimises a quadratic cost function subject to the power balance constraint with $\mathbf{P} = \{P_i : i \in \mathbb{N}_{ac} \cup \mathbb{N}_{dc}\}$, where $\mathbb{N}_{ac}$ and $\mathbb{N}_{dc}$ are the sets of *ac* and *dc* DGs, respectively. P_i is the active power contribution of DG

i. The aggregated active power load on the *ac* and *dc* sub-MGs are P_D^{ac} and P_D^{dc}, respectively. The quadratic cost function for DG_i is expressed in (4.2), where a_i, b_i and c_i are the cost coefficients of DG_i, defined in Section 4.11.

$$\underset{\mathbf{P}}{\text{minimise}} \quad \sum_{i \in \mathbb{N}_{ac} \cup \mathbb{N}_{dc}} \mathbb{C}_i(P_i) \tag{4.1a}$$

$$\text{subject to} \quad \sum_{i \in \mathbb{N}_{ac} \cup \mathbb{N}_{dc}} P_i = P_D^{ac} + P_D^{dc} \tag{4.1b}$$

$$\mathbb{C}_i(P_i) = a_i P_i^2 + b_i P_i + c_i \tag{4.2}$$

However, as demonstrated in [17–19, 44], this optimisation problem when operated in a centralised framework is susceptible to a single-point-of-failure and has a high computational burden if it is solved using a centralised approach. For these reasons, a distributed controller is a more reliable and secure solution. The optimisation problem of (4.1) can be expressed in a distributed way through the incremental cost criterion [16, 17, 20]. Following the same procedure explained previously for *ac* MGs in Section 3.2, the Lagrangian function of (4.1) can be expressed as follows.

$$\mathbb{L}(P_i, \eta) = \sum_{i \in N_{ac} \cup N_{dc}} \mathbb{C}_i(P_i) \\ + \eta \left(P_D^{ac} + P_D^{dc} - \sum_{i \in N_{ac} \cup N_{dc}} P_i \right) \tag{4.3}$$

$$\frac{\partial \mathbb{L}(P_i, \eta)}{\partial P_i} = 0 \quad \Longleftrightarrow \quad \eta = \frac{\partial \mathbb{C}_i(P_i)}{\partial P_i}, \quad i \in \mathbb{N}_{ac} \cup \mathbb{N}_{dc} \tag{4.4}$$

From the stationary condition (4.4), the incremental cost (IC) or Lagrange operator η can be obtained. To accomplish the economic dispatch of active power in the H-MG, all DGs must achieve the same IC, i.e., $\eta = \eta_i = \eta_j$ where $i, j \in \mathbb{N}_{ac} \cup \mathbb{N}_{dc}$.

4.3 The reactive power economic dispatch problem

As the total generation costs of *ac* DGs are associated with both the active and reactive power supplied, it is necessary to co-optimise the production of reactive power in the *ac* sub-MG [138]. For this purpose, similar to the IC principle described in Section 4.2, the reactive marginal cost (Ψ_i) in (4.5) is proposed to minimise the production of reactive power in a distributed fashion [112, 113].

$$\Psi_i = 2a_i' \, S_{i,res} \, Q_i + b_i' \quad i \in \mathbb{N}_{ac} \tag{4.5}$$

where Q_i is the reactive power of *ac* DG i and $S_{i,res}$ is the residual apparent power capacity of the $i - th$ *ac* DG as a function of its rated capacity, i.e., $S_{i,res} = (S_{i,max} - S_i)/S_{i,max}$. The cost coefficients $a_i' = a_i \, sin^2(\phi)$ and $b_i' = b_i \, sin(\phi)$ depend on the active power cost parameters (defined in Section 4.11) and the power factor angle ϕ. To accomplish the economic dispatch of reactive power in the *ac* sub-MG, all *ac* DGs must achieve the same reactive marginal cost (RMC), i.e., $\Psi = \Psi_i = \Psi_j$ where $i, j \in \mathbb{N}_{ac}$. Based on the principles of incremental cost (IC) and reactive marginal cost (RMC), a novel cooperative DMPC strategy is proposed. This strategy minimises the operational costs of both active and reactive power while the frequency and voltage variables on the H-MG are regulated within predefined bands. The development of the distributed predictive strategies for ILCs, *dc* DGs and *ac* DGs is explained in detail in the following sections.

4.4 Communication structure

Although *ac* DGs, *dc* DGs and ILCs have different operating principles, they can interact with each other [43]. In this way, information can be shared globally to achieve cooperative control objectives via a fully-meshed communication

network. Consider an H-MG composed of a set of $\mathbb{N}$ nodes (DGs or ILCs), where $\mathbb{N} = \mathbb{N}_{ac} \cup \mathbb{N}_{dc} \cup \mathbb{N}_{ILC}$. The subsets of *ac* DGs, *dc* DGs, and ILCs are represented for $\mathbb{N}_{ac} = \{1, ..., N_{ac}\}$, $\mathbb{N}_{dc} = \{1, ..., N_{dc}\}$, and $\mathbb{N}_{ILC} = \{1, ..., N_{ILC}\}$, respectively. Each node (DG or ILC) includes a model of the full-duplex communication network. This model considers both latency and connectivity issues. Latency (represented in sampling periods) is characterised as the end to end communication delay (τ_{ij}), i.e., total time for a data packet to be transmitted from source to destination. Connectivity represents the information flow among nodes at time instant k and is stated by the $\mathbb{N} \times \mathbb{N}$ non-negative adjacency matrix $\boldsymbol{A}$ (defined in Section 4.11). The entries a_{ij} of the adjacency matrix $\boldsymbol{A}$ are 1 if there is communication between node j and node i at time instant k or 0 otherwise, where $k = nT_{sec}, n \in \mathbb{Z}^+$, and T_{sec} is the DMPC sample time.

As a full-duplex communication network is used, the associated communication graph is *undirected*. Thus, $\tau_{ij} = \tau_{ji}$ and $a_{ij}=a_{ji}$ [42]. We consider that the *undirected* graph in this work is *connected*, which implies that there must be at least one communication path between any two nodes (i.e., there is a spanning tree). Therefore, the H-MG's topology can vary as long as there is at least one communication path between all its nodes.

4.5 Proposed DMPC scheme for interlinking converters (ILCs)

As stated in the introduction section, ILCs transfer active power bidirectionally between the *ac* and *dc* sub-MGs. In this way, to achieve the economic dispatch of active power in an H-MG, the ILC should equalise the incremental costs (ICs) of both sub-MGs, i.e., the condition $\eta_i^{ac} = \eta_j^{dc} = \eta$ must hold, where $i \in \mathbb{N}_{ac} \land j \in \mathbb{N}_{dc}$ and η is the optimal IC value. The control diagram of the ILC_h with $h \in \mathbb{N}_{ILC}$ is shown in Fig. 4.1.
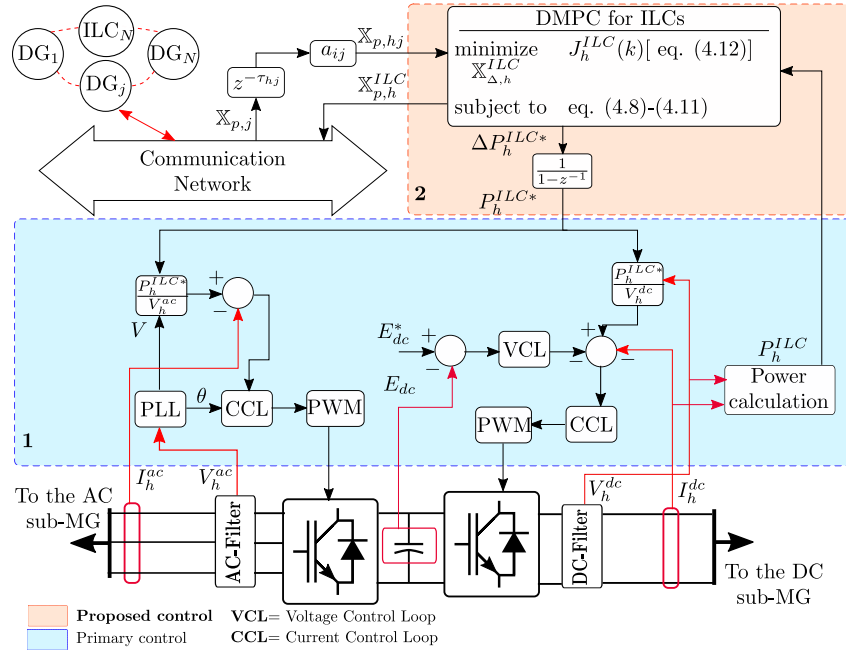
Figure 4.1: *Control diagram of $DMPC_i$ for ILCs.*

Two control levels are distinguished. As a back-to-back configuration is used for each ILC, the primary level comprises a current controller on both *ac* and *dc* sides. The proposed DMPC is presented at the secondary level (orange box in Fig. 4.1). The DMPC receives as inputs the local active power measurement (P_h^{ILC}) and the active power predictions of communicated *ac* DGs, *dc* DGs, and ILCs. The controller has two outputs, which are the active power variation (vector $_\Delta P_h^{ILC}$) and the results of the local optimisation problem $\mathbb{X}_{p,h}^{ILC}$ (vector of predicted values), both defined in Section 4.6.1. The former passes through a discrete integrator to ensure zero error in steady-state, Whereas the latter is sent via the communication network. Furthermore, the ILCs can be connected to any electrical node in the H-MG as they share information with the DGs of both sub-MGs.

4.5.1   Dynamic models used for the design of the controller for interlinking converters

Considering that the losses in ILC_h are negligible, the power contribution ($P_{h,i}^{ILC}$) to ILC_h from the $i-th$ *ac* DG (P_i^{ac}) can be computed as (4.6a).

Similarly, the power contribution $(P_{h,j}^{ILC})$ to ILC_h from the $j-th$ dc DG (P_j^{dc}) can be calculated as (4.6b).

$$P_i^{ac}(k) = P_i^{ac}(k-1) + P_{h,i}^{ILC}(k-1) \quad \forall\ i \in \mathbb{N}_{ac} \qquad (4.6a)$$

$$P_j^{dc}(k) = P_j^{dc}(k-1) - P_{h,j}^{ILC}(k-1) \quad \forall\ j \in \mathbb{N}_{dc} \qquad (4.6b)$$

These models are the basis for determining the power transference for each ILC that comprises the H-MG. Note that (4.6a) considers that the *ac* sub-MG is receiving active power form the *dc* sub-MG through the ILC, whilst (4.6b) considers that the *dc* sub-MG is providing power to the *ac* sub-MG through the ILC.

4.6 Formulation of the DMPC for ILCs

The following explanations and mathematical analysis is performed for the $h-th$ ILC, as the analysis is analogous for the rest of the ILCs. The optimisation problem with its cost function and constraints are described in Section 4.6.1 and Section 4.6.2, respectively. The predicted variables and control actions sequence of this optimisation problem are contained in the vector $\mathbb{X}_h^{ILC}$ (defined in Section 4.6.2), which is the solution to the optimisation problem (4.7). Only the first control action is applied to the system, and the optimal control problem is repeated at each sample time with updated measures[45]. The optimisation problem and how it is solved is detailed in the next section.

4.6.1 Cost function

The cost function of the DMPC scheme for ILC_h is composed of three terms and is described in (4.7) where N_y and N_u are the prediction and the control horizons, respectively.

$$J_h^{ILC}(k) = \sum_{k=1}^{N_u} \lambda_{1h}(\triangle P_h^{ILC}(k+m-1))^2$$

$$+ \sum_{i \in \mathbb{N}_{ac}} \sum_{j \in \mathbb{N}_{dc}} \sum_{k=1}^{N_y} \lambda_{2h} a_{hi}(k) a_{hj}(k) \left(\eta_i^{ac}(k+m-\hat{\tau}_{hi}) - \eta_j^{dc}(k+m-\hat{\tau}_{hj}) \right)^2 \quad (4.7)$$

$$+ \sum_{l \in \mathbb{N}_{ILC}} \sum_{k=1}^{N_y} \lambda_{3h} a_{hl}(k) \left(\frac{P_h^{ILC}(k+m)}{P_{h\,\max}^{ILC}} - \frac{P_l^{ILC}(k+m-\hat{\tau}_{hl})}{P_{l\,\max}^{ILC}} \right)^2$$

The first term penalises the variation of the control action sequence to minimise the control effort and improve the controller's transient behaviour. The second term equalises the ICs of the sub-MGs by transferring power from the the most economical side to the most expensive side. When all DGs achieve a consensus on the IC, the economic dispatch equilibrium is reached. This objective is strengthened in each DG controller, as will be explained in Section 4.7 and Section 4.9. The third term ensures that when there are multiple ILCs, the power transferred per ILC is proportional to its maximum power rating with $l \in \mathbb{N}_{ILC}$, thus, avoiding overloading the ILCs. The terms λ_{1h} to λ_{3h} are positive tuning parameters explained in Section 4.11. Note that the consensus objectives (economic dispatch of DGs and power sharing of ILCs) are updated only with the predicted information from neighbouring *agents* (connected), represented by the terms $a_{hi}(k)$, $a_{hj}(k)$ and $a_{hl}(k)$, and the estimated delays $\hat{\tau}_{hi}$, $\hat{\tau}_{hj}$ and $\hat{\tau}_{hl}$.

4.6.2   Prediction models and constraints

The set of prediction models included in the DMPC scheme of ILC_h are described as follows. The previous discrete time models of (4.6) are generalised for $k + m$ steps ahead in (4.8a) and (4.8b), where $m \in \mathbb{Z}^+$. Additionally, the incremental operator (3.9) is applied to derive the power contributions as a function of their variation $(\triangle P_{h,i}^{ILC})$.

$$P_i^{ac}(k+m) = 2P_i^{ac}(k+m-1) - P_i^{ac}(k+m-2)$$
$$+ \triangle P_{h,i}^{ILC}(k+m-1) \quad \forall\, i \in \mathbb{N}_{ac} \tag{4.8a}$$

$$P_j^{dc}(k+m) = 2P_j^{dc}(k+m-1) - P_j^{dc}(k+m-2)$$
$$- {}_\Delta P_{h,j}^{ILC}(k+m-1) \quad \forall \, j \in \mathbb{N}_{dc} \tag{4.8b}$$

To obtain the active power reference variation ($_\Delta P_h^{ILC}$) for ILC_h, the power contributions from each communicated DG are added in (4.9a). Where the terms $a_{ih}(k)$ and $a_{jh}(k)$ represent the communication from the ac DG_i and from the dc DG_j to ILC_h, respectively. A discrete time integrator is used to obtain the power reference for ILC_h, ensuring zero error in steady-state, as shown in Fig. 4.1. Note that $P_h^{ILC} > 0$ indicates that power is flowing from the dc sub-MG to the ac sub-MG. Conversely, $P_h^{ILC} < 0$ indicates that power is flowing from the ac sub-MG to the dc sub-MG.

$$_\Delta P_h^{ILC}(k+m-1) = \sum_{i \in \mathbb{N}_{ac}} a_{ih}(k) {}_\Delta P_{h,i}^{ILC}(k+m-1) =$$
$$\sum_{j \in \mathbb{N}_{dc}} a_{jh}(k) {}_\Delta P_{h,j}^{ILC}(k+m-1) \tag{4.9a}$$

The incremental cost (IC) models for ac DGs and dc DGs are presented in (4.10a) and (4.10b), respectively.

$$\eta_i^{ac}(k+m) = 2a_i P_i^{ac}(k+m) + b_i \quad \forall \, i \in \mathbb{N}_{ac} \tag{4.10a}$$

$$\eta_j^{dc}(k+m) = 2a_j P_j^{dc}(k+m) + b_j \quad \forall \, j \in \mathbb{N}_{dc} \tag{4.10b}$$

Finally, the ILC's maximum active power rating model is included in (4.11) to guarantee that the power reference required is within the equipment limits of ILC_h.

$$P_{h,min}^{ILC} \le P_h^{ILC}(k+m-1) \le P_{h,max}^{ILC} \tag{4.11}$$

The proposed DMPC comprises a quadratic cost function (4.7), linear equality constraints and linear inequality constraints (4.8)-(4.11); thus, it is convex and can be synthesised in a canonical quadratic programming (QP) formulation. Moreover, the methodology to solve the DMPC scheme is similar to the one

described in Algorithm 1. The optimisation vector of the QP problem, $\mathbb{X}_h^{ILC}$ in (4.12), comprises the predicted variables $\mathbb{X}_{p,h}^{ILC}$ and the control decisions $\mathbb{X}_{\Delta,h}^{ILC}$ presented in (4.13) and (4.14), respectively.

$$\mathbb{X}_h^{ILC} = \{\mathbb{X}_{p,h}^{ILC}, \mathbb{X}_{\Delta,h}^{ILC}\} \tag{4.12}$$

$$\mathbb{X}_{p,h}^{ILC} = \{P_i^{ac}(k+m), P_j^{dc}(k+m), P_h^{ILC}(k+m), \eta_i^{ac}(k+m), \eta_j^{dc}(k+m)\}_{k=1}^{N_y} \tag{4.13}$$

$$\mathbb{X}_{\Delta,h}^{ILC} = \{\Delta P_h^{ILC}(k+m-1)\}_{k=1}^{N_u} \tag{4.14}$$

The predicted variables are sent to the communication network to achieve the consensus objectives and the first control decision, $\Delta P_h^{ILC}(k)$, is applied to ILC_h, after passing through an integrator (see Fig. 4.1). At each sample time the optimisation problem is computed with updated measures (forming a rolling horizon) [47]. The following section explains the development and formulation of the DMPC strategy for dc DGs, which interacts with the DMPCs of the ILCs described in this section and the DMPCs of the ac DGs described in Section 4.9.

4.7 Proposed DMPC scheme for *dc* Generators

The control scheme for the dc DG_i is depicted in Fig. 4.2, where the primary control (lower half) is based on $P - V$ droop control [18, 43] and the proposed DMPC scheme for secondary level is presented in the orange box. The local measurements/estimates ($P_i^{dc}(k)$, $V_i^{dc}(k)$, $\hat{V}_i^{dc,B}(k)$) and the results of the optimisation problems from connected neighbouring units are the inputs of the DMPC. The controller has two outputs, which are the voltage control action (vector $\Delta V_{s,i}^{dc}$) and the results of the local optimisation problem $\mathbb{X}_{p,i}^{dc}$ (vector of predicted values), both defined in Section 4.8.1. The former passes through a

discrete integrator to ensure zero error in steady-state, Whereas the latter is sent via the communication network.
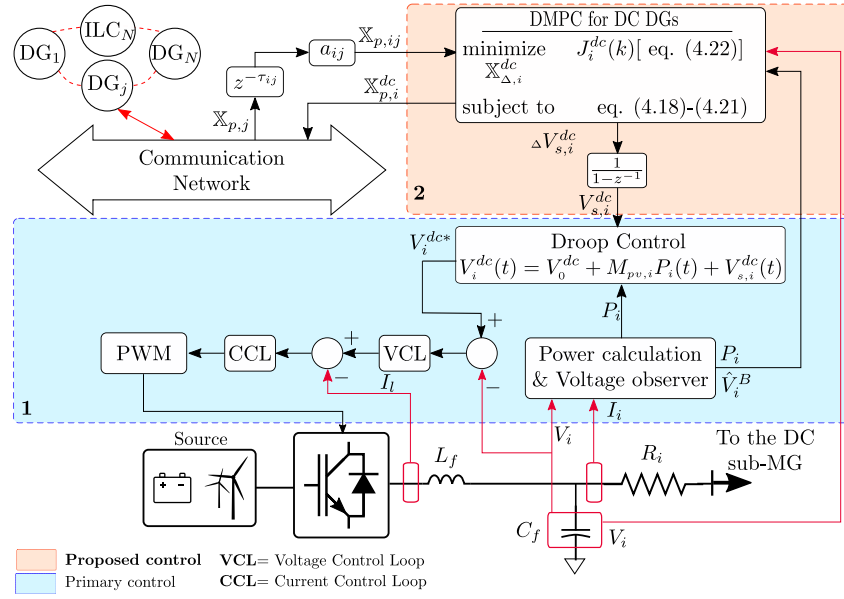
Figure 4.2: *Control diagram of DMPC$_i$ for dc DGs.*

4.7.1 Dynamic models used for the design of the controller for *dc* generators

To model the dynamics of the *dc* DGs, the voltage at each node, along with the active power flow, are considered. Since these variables are coupled, in this work, they are modelled using the droop (4.15) and active power transfer (4.16) equations.

The droop model for $P - V$ for the local $i - th$ *dc* DG is given in (4.15).

$$V_i^{dc}(t) = V_0^{dc} + M_{pv,i}P_i^{dc}(t) + V_{s,i}^{dc}(t) \tag{4.15}$$

where V_i^{dc} is the output voltage of *dc* DG_i, P_i^{dc} is the active power transferred to the MG, computed by (4.16), V_0^{dc} is the nominal voltage of the *dc* sub-MG, $M_{pv,i}$ is the droop slope, and $V_{s,i}^{dc}$ is the secondary control action.

Equation (4.16) determines the power contribution of DG_i to the MG. This equation is reformulated to avoid dependence on the output current (I_i^{dc}) of DG_i.

$$P_i^{dc}(t) = V_i^{dc}(t)I_i^{dc}(t) = G_i V_i^{dc}(t)(V_i^{dc}(t) - \hat{V}_i^{dc,B}(t)) \qquad (4.16)$$

Note that by using (4.16) a complete electrical model of the MG is not needed. Moreover, (4.16) only uses local measurements and the voltage estimation $\hat{V}_i^{dc,B}$ after the coupling resistor R_i (with $G_i = 1/R_i$).

4.8 Formulation of the DMPC for *dc* generators

The following explanations and mathematical analysis are performed for the $i-$th dc DG, as the analysis is analogous for the rest of dc DGs. The optimisation problem with its cost function and constraints are described in Section 4.8.1 and Section 4.8.2, respectively. The predicted variables and control actions sequence are contained in the vector $\mathbb{X}_i^{dc}$ (defined in Section 4.8.2), which is the solution to the optimisation problem (4.17). Only the first control action is applied to the system $(\Delta V_{s,i}^{dc}(k))$, and the optimal control problem is repeated at each sample time with updated measures [45]. The optimisation problem and how it is solved is detailed in the next section.

4.8.1 Cost function

The multiobjective cost function is stated in (4.17) and is composed of four quadratic weighted terms, where each term seeks a specific objective.

$$
\begin{aligned}
J_i^{dc}(k) = & \sum_{j \in \mathbb{N}_{dc}} \sum_{m=1}^{N_y} \lambda_{1i} a_{ij}(k) \left(\eta_i^{dc}(k+m) - \eta_j^{dc}(k+m-\hat{\tau}_{ij}) \right)^2 \\
& + \sum_{j \in \mathbb{N}_{ac}} \sum_{m=1}^{N_y} \lambda_{2i} a_{ij}(k) \left(\eta_i^{dc}(k+m) - \eta_j^{ac}(k+m-\hat{\tau}_{ij}) \right)^2 \qquad (4.17) \\
& + \sum_{m=1}^{N_y} \left[\lambda_{3i}(V_{aux,i}^{dc}(k+m))^2 \right] + \sum_{k=1}^{N_u} \lambda_{4i}(\Delta V_{s,i}^{dc}(k+m-1))^2
\end{aligned}
$$

The first term achieves the consensus over the ICs within the dc DGs, while the second term performs the consensus for the ICs of the ac DGs. The latter

objective only works when the ILCs are enabled; the controller verifies the ILCs status (1:ON, 0:OFF) at each sample time. The third term achieves the regulation of the average *dc* voltage within a band by penalising the auxiliary variable $V_{aux,i}^{dc}$. This term temporally relaxes the average *dc* voltage regulation constraint (4.21b), allowing the average *dc* voltage to take transient values outside its predefined band when the MG is disturbed. The last term penalises the control effort to achieve all the previous objectives with good transient behaviour. The terms λ_{1i} to λ_{4i} are positive tuning parameters explained in Section 4.11. Note that the cooperative objectives (IC consensus with *dc* DGs and with *ac* DGs) are updated only with the predicted information of connected neighbouring DGs, represented by the terms $a_{ij}(k)$, and the estimated delays $\hat{\tau}_{ij}$.

4.8.2   Predictive models and constraints

The following equations present the prediction models included as equality and inequality constraints in the DMPC formulation for *dc* DGs. Models (4.18) and (4.19) are the discretised versions of (4.15) and (4.16) via the forward Euler method, where in the former, the incremental operator (3.9) was applied and in the latter a Taylor expansion around the measured/estimated point $\{V_i^{dc}(k),\ \hat{V}_i^{dc,B}(k), P_i^{dc}(k)\}$ is used. The derivation of this predictive model is detailed in Appendix D.

$$
\begin{aligned}
V_i^{dc}(k+m) =& M_{pv,i}[P_i^{dc}(k+m) - P_i^{dc}(k+m-1)] \\
& + V_i^{dc}(k+m-1) + {}_{\Delta}V_{s,i}^{dc}(k+m-1)
\end{aligned}
\tag{4.18}
$$

$$
\begin{aligned}
P_i^{dc}(k+m) =& [V_i^{dc}(k+m) - V_i^{dc}(k)]G_i[2V_i^{dc}(k) - \hat{V}_i^{dc,B}(k)] \\
& + P_i^{dc}(k)
\end{aligned}
\tag{4.19}
$$

Model (4.20a) represents the IC of the $i-th$ *dc DG*, while a local average *dc* voltage approximation $(\overline{V}_i^{dc})$ is computed in (4.20b). Note that $\overline{V}_i^{dc}$ also depends on the communication terms $a_{ij}(k)$ and the estimated delay $(\hat{\tau}_{ij})$.

$$\eta_i^{dc}(k+m)=2a_i P_i^{dc}(k+m)+b_i \tag{4.20a}$$

$$\overline{V}_i^{dc}(k+m)=\frac{V_i^{dc}(k+m)+\sum\limits_{j\in\mathbb{N}_{dc}}a_{ij}(k)V_j^{dc}(k+m-\hat{\tau}_{ij})}{1+\sum\limits_{j\in\mathbb{N}_{dc}}a_{ij}(k)} \tag{4.20b}$$

The active power contribution is limited within the DG's power rating in (4.21a). Finally, the soft constraint (4.21b) works in conjunction with the cost function (see third term of (4.17)) to regulate the average *dc* voltage in a predefined band within the recommendation of IEEE standard 1547-2018 [40] and avoid unfeasible solutions [47].

$$P_{i,\min}^{dc}\leq P_i^{dc}(k+m)\leq P_{i,\max}^{dc} \tag{4.21a}$$

$$\overline{V}_{min}^{dc}\leq\overline{V}_i^{dc}(k+m)+V_{aux,i}^{dc}(k+m)\leq\overline{V}_{max}^{dc} \tag{4.21b}$$

$V_{aux,i}^{dc}$ is an auxiliary variable that acts as a slack variable.

The proposed DMPC is synthesised in a QP formulation. The methodology to solve the DMPC scheme is similar to the one described in Algorithm 1. The optimisation vector of the QP problem, $\mathbb{X}_i^{dc}$ in (4.22), comprises the predicted variables $\mathbb{X}_{p,i}^{dc}$ and the control decisions $\mathbb{X}_{\Delta,i}^{dc}$ presented in (4.23) and (4.24), respectively.

$$\mathbb{X}_i^{dc}=\{\mathbb{X}_{p,i}^{dc},\mathbb{X}_{\Delta,i}^{dc}\} \tag{4.22}$$

$$\mathbb{X}_{p,i}^{dc}=\{\overline{V}_i^{dc}(k+m),V_i^{dc}(k+m),P_i^{dc}(k+m),\eta_i^{dc}(k+m)\}_{k=1}^{N_y} \tag{4.23}$$

$$\mathbb{X}_{\Delta,i}^{dc}=\{{}_\Delta V_{s,i}^{dc}(k+m-1)\}_{k=1}^{N_u} \tag{4.24}$$

The predicted variables are sent to the communication network and the first control decision, ${}_\Delta V_{s,i}^{dc}(k)$, is applied to the $i-th$ *dc* DG, after passing through an integrator (see Fig. 4.2). At each sample time the optimisation problem is

computed with updated measures (forming a rolling horizon) [47]. The following section explains the development and formulation of the DMPC strategy for ac DGs, which interacts with the DMPCs for dc DGs described in this section and the DMPCs of ILCs described Section 4.5.

4.9 Proposed DMPC scheme for ac Generators

Unlike the DMPC strategy presented in Chapter 3, which considers active power economic dispatch and frequency regulation, the following DMPC scheme for ac DGs also considers the economic dispatch of reactive power and the regulation of ac voltage. Moreover, this strategy regulates both frequency and voltage within secure bands following the recommendations of the IEEE standard 1547-2018 [40], instead of restoring these variables to nominal values. The following explanations and mathematical analysis are performed for the $i - th$ ac DG, as the analysis is analogous for the rest of ac DGs.

The control scheme for the ac DG_i is depicted in Fig. 4.3, where the primary controller is based on frequency-active power $(\omega - P)$ and voltage-reactive power $(V - Q)$ droop controllers, as well as outer voltage (slower) and inner current (faster) cascaded Proportional-Resonant (PR) controllers. In the MG context, a common assumption is that the impedances are predominantly inductive. By doing that, it is possible to decouple both active and reactive powers and thus, the droop controllers $P - \omega$ and $Q - V$ are decoupled [15], i.e., active and reactive powers can be controlled by the frequency and the amplitude of the DG unit output voltage, respectively. In order to fulfil the assumption of an inductive line, an LCL output filter is used: In this method, the second inductance of the LCL filter (L_i) is directly connected to the line impedance. Thus, the line impedance can be set to be predominantly inductive by choosing the proper parameters for the LCL filter of the DG units [63, 64].

The proposed DMPC for the secondary level is presented in the orange box. Its inputs are the local measurements/estimates ($P_i(k)$, $V_i^{ac}(k)$, $\omega_i(k)$, $\theta_i(k)$, $\hat{V}_i^{ac,B}(k)$, $\hat{\omega}_i^B(k)$, $\hat{\theta}_i^B(k)$) and the results of the optimisation problems of connected neighbouring units. To model the behaviour of *ac* DGs, the voltage and frequency at each node, along with the active and reactive power flows, are considered. Since these variables are coupled, in this thesis they are modelled using the droop, power transfer and phase angle equations. In particular, the $i-th$ *ac* DG unit is modelled as the node at the output of its LCL filter, as shown at the bottom of Fig. 4.3, through its voltage V_i^{ac}, its angular speed ω_i, and its phase angle θ_i. The $i-th$ unit is connected to the rest of the MG through inductor L_i.
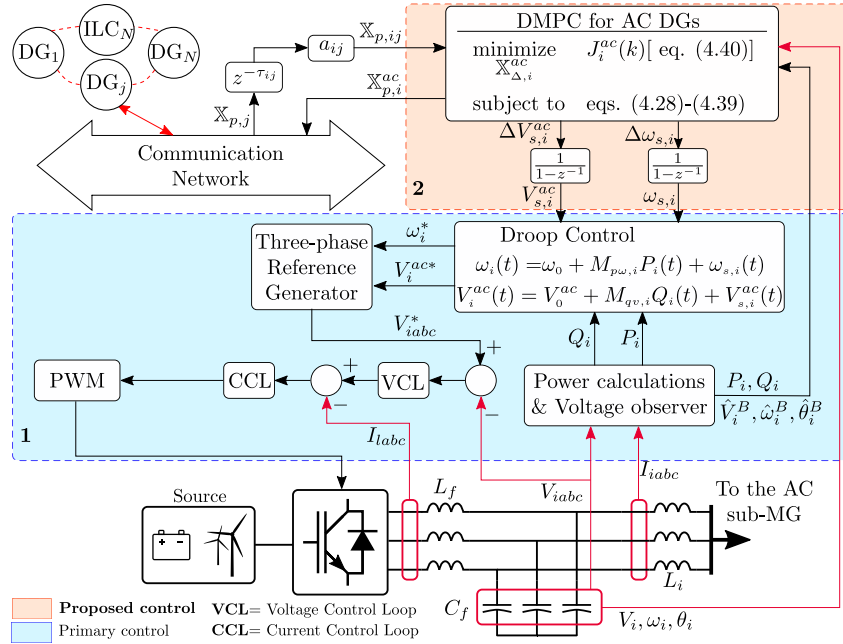
Figure 4.3: *Control diagram of DMPC$_i$ for ac DGs.*

Unlike previous approaches [49] where external sensors are used, a sensorless scheme is employed to estimate the voltage after the coupling inductor L_i (at the connection bus); thus, only the usual voltage and current measurements at the LCL filter are needed. The estimated voltages $\hat{V}_i^{ac,B}$ are computed using a reduced-order state observer based on [139] and explained in detail in Appendix A. Finally, the angular frequency and phase angle at the coupling point $\hat{\omega}_i^B$ and $\hat{\theta}_i^B$, respectively, are estimated using phase-locked loops (PLLs).

4.9.1   Dynamic models used for the design of the controller for *ac* generators

The dynamic models for the angular speed (3.6), phase angle difference (3.7) and active power transference (3.8) introduced before in Chapter 3 are also used in this controller. Thus, in this section, only the new dynamic models included in the DMPC formulation are presented.

The $V - Q$ droop model, which allows that a variation in the reactive power (Q_i) be reflected as a voltage variation (V_i) is presented in (4.25).

$$V_i^{ac}(t) = V_0^{ac} + M_{qv,i}Q_i(t) + V_{s,i}^{ac}(t) \tag{4.25}$$

where V_i^{ac} is the output voltage of *ac* DG_i, Q_i is the active power transferred to the MG, computed by (4.26), V_0^{ac} is the nominal voltage of the *ac* sub-MG, $M_{qv,i}$ is the droop slope, and $V_{s,i}^{ac}$ is the secondary control action.

The reactive power contribution of *ac* DG_i is computed in (4.26).

$$Q_i(t) = B_i \left[(V_i^{ac}(t))^2 - V_i^{ac}(t)\,\hat{V}_i^{ac,B}(t) \cos\left(\delta\theta_i(t)\right) \right] \tag{4.26}$$

where, $B_i = 1/(\omega_0 L_i)$, is the nominal admittance of the coupling inductor L_i.

4.10   Formulation of the DMPC for *ac* generators

In a similar fashion to the models presented in Section 3.4.2, the models of Section 4.9.1 are discretised using the forward Euler method. Furthermore, the incremental operator (3.9) is applied in (4.25) to express the optimisation problem as a function of the control action variation ($\Delta V_{s,i}^{ac}$) and a Taylor expansion is applied in (4.26) to linearise the reactive power transfer model. The procedure to obtain the all the prediction models is detailed in Appendix B. The optimisation problem with its cost function and constraints are described in Section 4.10.1 and Section 4.10.2, respectively. The predicted variables and

control actions sequence are contained in the vector $\mathbb{X}_i^{ac}$ (defined in Section 4.10.2), which is the solution to the optimisation problem (4.27). Only the first control action is applied to the system, and the optimal control problem is repeated at each sample time with updated measures [45]. The optimisation problem and how it is solved are detailed in the next section.

4.10.1   Cost function

The multiobjective cost function is stated in (4.27) and is composed of seven quadratic weighted terms, where each term seeks a specific objective.

$$
\begin{aligned}
J_i^{ac}(k) = & \sum_{j \in \mathbb{N}_{ac}} \sum_{m=1}^{N_y} \lambda_{1i} a_{ij}(k) \left(\eta_i^{ac}(k+m) - \eta_j^{ac}(k+m-\hat{\tau}_{ij}) \right)^2 \\
& + \sum_{j \in \mathbb{N}_{dc}} \sum_{m=1}^{N_y} \lambda_{2i} a_{ij}(k) \left(\eta_i^{ac}(k+m) - \eta_j^{dc}(k+m-\hat{\tau}_{ij}) \right)^2 \\
& + \sum_{j \in \mathbb{N}_{ac}} \sum_{m=1}^{N_y} \lambda_{3i} a_{ij}(k) \left(\Psi_i(k+m) - \Psi_j(k+m-\hat{\tau}_{ij}) \right)^2 \qquad (4.27) \\
& + \sum_{m=1}^{N_y} \left[\lambda_{4i} (\omega_{aux,i}(k+m))^2 + \lambda_{5i} (V_{aux,i}^{ac}(k+m))^2 \right] \\
& + \sum_{m=1}^{N_u} \left[\lambda_{6i} (\Delta V_{s,i}(k+m-1))^2 + \lambda_{7i} (\Delta \omega_{s,i}(k+m-1))^2 \right]
\end{aligned}
$$

The first term achieves the consensus over the ICs within the *ac* DGs, while the second term performs the consensus for the ICs of the *dc* DGs. The latter objective works only when the ILCs are enabled; the controller verifies the ILCs status (1:ON, 0:OFF) at each sample time. The third term performs the consensus over the RMC, hence guaranteeing the economic dispatch of reactive power. The fourth and fifth terms regulate the frequency and the average *ac* voltage within bands by penalising the auxiliary variables $\omega_{aux,i}$ $V_{aux,i}^{ac}$, respectively. These terms temporally relax the frequency constraint (4.38) and the average *ac* voltage constraint (4.39), allowing these variables to take values outside their predefined bands for a short period of time.

The sixth term penalises any variations of the voltage control action, and the

seventh term penalises any variation of the frequency control action. The controller achieves all the previous objectives with good transitory behaviour with only two control actions ($\Delta V_{s,i}^{ac}$ and $\Delta \omega_{s,i}$). The terms λ_{1i} to λ_{7i} are positive tuning parameters explained in Section 4.11. Note that the cooperative objectives (IC consensus with *ac* DGs and with *dc* DGs and RMC consensus) are updated only with the predicted information of connected neighbouring DGs, represented by the terms $a_{ij}(k)$, and the estimated delays $\hat{\tau}_{ij}$.

4.10.2 Predictive models and constraints

The linear discrete time prediction models included in the controller to rule its behaviour are detailed as follows. Model (4.28) represents the incremental cost (IC) prediction model for the $i-th$ ac DG while (4.29) is its reactive marginal cost (RMC) prediction model; both models were derived in Section 4.2 and Section 4.3, respectively.

$$\eta_i^{ac}(k+m) = 2a_i\ P_i^{ac}(k+m)\ +\ b_i \tag{4.28}$$

$$\Psi_i(k+m) = 2a_i'(k)\ S_{i,res}(k)\ Q_i(k+m)\ +\ b_i'(k) \tag{4.29}$$

Model (4.30) represents the $\omega - P$ droop control, and model (4.31) is the $V - Q$ droop control.

$$\begin{aligned}\omega_i(k+m) =& \omega_i(k+m-1) + M_{p\omega,i}\left[P_i^{ac}(k+m) - P_i^{ac}(k+m-1)\right] \\ &+ \Delta\omega_{s,i}(k+m-1)\end{aligned} \tag{4.30}$$

$$\begin{aligned}V_i^{ac}(k+m) =& V_i^{ac}(k+m-1) + M_{qv,i}\left[Q_i(k+m) - Q_i(k+m-1)\right] \\ &+ \Delta V_{s,i}^{ac}(k+m-1)\end{aligned} \tag{4.31}$$

Model (4.32) calculates the phase angle deviation ($\delta\theta_i$) due to the inductance L_i of the LCL output filter (see at the bottom of Fig. 4.3). This model is used to predict the active and reactive power contributions of ac DG_i to the MG, where $\hat{\omega}_i^B(k)$ is the frequency estimated after L_i.

$$\delta\theta_i\left(k+m\right)=\delta\theta_i\left(k+m-1\right)+T_{sec}\left[\omega_i\left(k+m\right)-\hat{\omega}_i^B\left(k\right)\right] \tag{4.32}$$

The active power contribution from *ac* DG_i to the MG is computed by the linearised model (4.33).

$$P_i^{ac}(k+m)=P_i^{ac}\left(k\right)+\left[V_i^{ac}\left(k+m\right)-V_i^{ac}\left(k\right)\right]B_i\hat{V}_i^{ac,B}\left(k\right)\sin\left(\delta\theta_i\left(k\right)\right)$$
$$+\left[\delta\theta_i\left(k+m\right)-\delta\theta_i\left(k\right)\right]B_iV_i^{ac}\left(k\right)\hat{V}_i^{ac,B}\left(k\right)\cos\left(\delta\theta_i\left(k\right)\right) \tag{4.33}$$

where $B_i=1/(L_i\cdot\omega_0)$, $V_i^{ac}\left(k\right)$ and $\hat{V}_i^{ac,B}\left(k\right)$ are the voltage measurements and estimations before and after the inductance L_i, $P_i^{ac}(k)$ is the active power measurement, and $\delta\theta_i\left(k\right)$ is the phase angle deviation measurement. It is worth noting that, unlike (3.12c), a linear term is added to the active power prediction model. This is because the formulation considers the DG's voltage control (see Appendix B).

Similarly, the reactive power contribution from *ac* DG_i to the MG is determined by the linearised model (4.34), where $Q_i(k)$ is the reactive power measurement.

$$Q_i\left(k+m\right)=Q_i\left(k\right)+\left[\delta\theta_i\left(k+m\right)-\delta\theta_i\left(k\right)\right]B_iV_i^{ac}\left(k\right)\hat{V}_i^{ac,B}\left(k\right)\sin\left(\delta\theta_i\left(k\right)\right)$$
$$+\left[V_i^{ac}\left(k+m\right)-V_i^{ac}\left(k\right)\right]B_i\left[2V_i^{ac}\left(k\right)-\hat{V}_i^{ac,B}\left(k\right)\cos\left(\delta\theta_i\left(k\right)\right)\right] \tag{4.34}$$

The active and reactive power contributions are bounded within the DG's power rating $(S_{i,max})$ through the linearised triangular constraint in (4.35). The procedure to obtain the power rating constraint is detailed in Appendix C.

$$\left|P_i^{ac}\left(k\right)\right|+\left|Q_i\left(k\right)\right|+\text{sign}\left(P_i^{ac}\left(k\right)\right)\left[P_i^{ac}\left(k+m\right)-P_i^{ac}\left(k\right)\right]$$
$$+\text{sign}\left(Q_i\left(k\right)\right)\left[Q_i\left(k+m\right)-Q_i\left(k\right)\right]\leq S_{i,\max} \tag{4.35}$$

Local approximations of the average frequency $(\overline{\omega}_i)$ and the average *ac* voltage $(\overline{V}_i^{ac})$ are computed by models (4.36) and (4.37), respectively. Note that both average approximations are updated only with the predicted information from connected neighbouring *ac* DGs, represented by the terms $a_{ij}(k)$, and the estimated delays $\hat{\tau}_{ij}$.

$$\overline{\omega}_i(k+m) = \frac{\omega_i(k+m) + \sum\limits_{j\in\mathbb{N}_{ac}} a_{ij}(k)\omega_j(k+m-\hat{\tau}_{ij})}{1 + \sum\limits_{j\in\mathbb{N}_{ac}} a_{ij}(k)} \tag{4.36}$$

$$\overline{V}_i^{ac}(k+m) = \frac{V_i^{ac}(k+m) + \sum\limits_{j\in\mathbb{N}_{ac}} a_{ij}(k)V_j^{ac}(k+m-\hat{\tau}_{ij})}{1 + \sum\limits_{j\in\mathbb{N}_{ac}} a_{ij}(k)} \tag{4.37}$$

Finally, soft constraints (4.38) and (4.39) work together with the cost function (see fourth and fifth terms of (4.27)) to maintain both average frequency and average *ac* voltage within predefined bands according to the recommendation of IEEE standard 1547-2018 [40] and avoid unfeasible solutions [47] by using the auxiliary variables $\omega_{aux,i}$, $V_{aux,i}^{ac}$.

$$\overline{\omega}_{min} \leq \overline{\omega}_i(k+m) + \omega_{aux,i}(k+m) \leq \overline{\omega}_{max} \tag{4.38}$$

$$\overline{V}_{min}^{ac} \leq \overline{V}_i^{ac}(k+m) + V_{aux,i}^{ac}(k+m) \leq \overline{V}_{max}^{ac} \tag{4.39}$$

The proposed DMPC is synthesised in a QP formulation, similar to (3.16). Moreover, the methodology to solve the DMPC scheme is similar to the one described in Algorithm 1. The optimisation vector of the QP problem, $\mathbb{X}_i^{ac}$ in (4.40), comprises the predicted variables $\mathbb{X}_{p,i}^{ac}$ and the control decisions $\mathbb{X}_{\Delta,i}^{ac}$ presented in (4.41) and (4.42), respectively. The former is sent to the communication network and the first control decisions of the latter, $_\Delta V_{s,i}^{ac}(k)$, and $_\Delta\omega_{s,i}(k)$, are applied to *ac* DG_i, after passing through discrete integrators (see Fig. 4.3). At each sample time the optimisation problem is computed with updated measures (rolling horizon) [47].

$$\mathbb{X}_i^{ac} = \{\mathbb{X}_{p,i}^{ac}, \mathbb{X}_{\Delta,i}^{ac}\} \tag{4.40}$$

$$\mathbb{X}_{p,i}^{ac} = [\eta_i^{ac}(k+m), \omega_i(k+m), \delta\theta_i(k+m), V_i^{ac}(k+m),$$

$$\omega_{aux,i}(k+m), V_{aux,i}^{ac}(k+m), P_i^{ac}(k+m), \Psi_i(k+m), \quad (4.41)$$

$$Q_i(k+m), \overline{\omega}_i(k+m), \overline{V}_i^{ac}(k+m)]_{m=1}^{N_y}$$

$$\mathbb{X}_{\Delta,i}^{ac} = [\Delta V_{s,i}^{ac}(k+m-1), \Delta\omega_{s,i}(k+m-1)]_{m=1}^{N_u} \quad (4.42)$$

In summary, all the proposed DMPCs in this chapter have quadratic cost functions with linear constraints; thus, their respective minimums can be reached [45, 47]. Note that in models (4.19), (4.29) and (4.32) to (4.35) all the variables at time instant k are local measurements and estimations produced in the discretisation and linearisation of the continuous time models; they are not predicted variables. Hence, all the previous models are linear. The distributed structure inherently addresses communication issues and connection and reconnection of DGs and ILCs scenarios. Moreover, each DG or ILC performs its own optimisation locally; thus, the computational burden is reduced and does not increase when more DGs or ILCs are added to the H-MG. The controllers identify when the ILCs are enabled before performing the economic dispatch in the entire H-MG. In contrast, when there are no ILCs available, the sub-MGs work independently, i.e. the economic dispatch is performed in each sub-MG, and the voltage (and frequency for the *ac* sub-MG) is regulated within appropriate bands.

4.11 Simulation results

To evaluate the performance of the proposed DMPC scheme, the H-MG in Fig. 4.4 was simulated using the electrical parameters described in Table 4.1. The PLECS blockset® was used to build the MG electrical model, and the Matlab/Simulink® environment was used to implement the controllers.

The system comprises an *ac* sub-MG with 5 *ac* DGs, a *dc* sub-MG with 5 *dc* DGs and two interlinking converters (ILCs) that connect both sub-MGs.
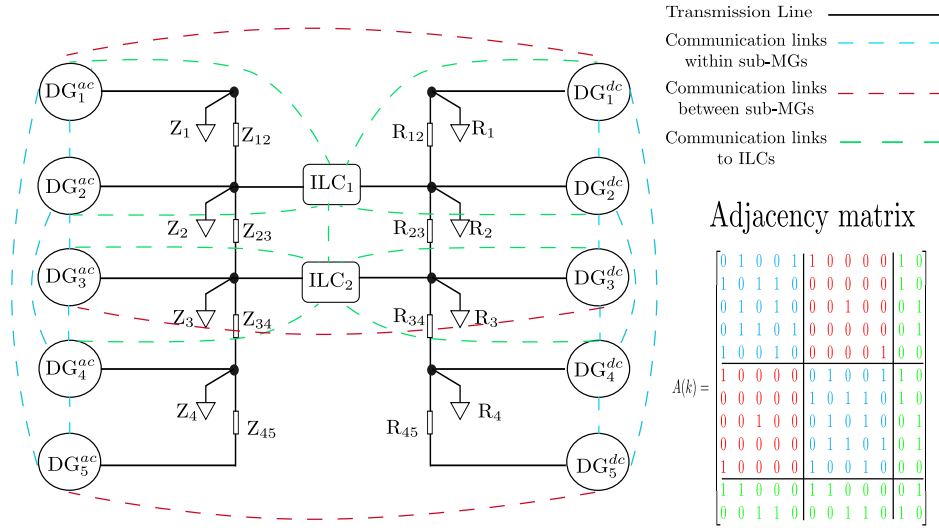
Figure 4.4: *Hybrid ac/dc MG topology for the validation of the DMPC scheme*

The *ac* distribution lines are inductive-resistive (RL), while the *dc* distribution lines are resistive (R). There are four RL loads on the *ac* sub-MG and four R loads on the *dc* sub-MG. The ILCs' maximum power ratings are given in Table 4.1 while the cost and operating parameters of the *ac* DGs and *dc* DGs are given in Table 4.2. In Table 4.2, a_i, b_i and c_i are the constant generating cost parameters used in the quadratic cost function (4.2). These parameters represent the generating cost of the DGs and their operating point efficiency. Note that in Fig. 4.4 the dashed lines represent the communication network, and its associated adjacency matrix $\boldsymbol{A}$ is also shown. The subsections of the matrix $\boldsymbol{A}$ in cyan represent the communication links within the *ac* sub-MG or within the *dc* sub-MG. In contrast, the subsections in red represent the communication links between sub-MGs, and the subsections in green are the communication links to the ILCs from both sub-MGs. From left to right (and top to bottom), the elements of A belong to *ac* DGs, *dc* DGs and ILCs, respectively.

The MG electrical model was built in PLECS blockset®, and the primary and secondary controllers were implemented in Matlab/Simulink® environment. The primary level consists of the droop, inner voltage and current controllers. The inner voltage and current controllers were implemented as

self-tuning proportional-resonant controllers for *ac* variables and proportional-integral controllers for *dc* variables. The following simplifications were considered in the simulator since their high-bandwidth dynamics are much faster than that of the studied controllers, and they are not relevant on the time-scale of the proposed controllers:

- The DGs are simulated as regulable voltage sources.

- The modulation techniques (PWM, SVM) of the converters are not considered.

- The switching of the switching devices is not considered.

Table 4.1: MG parameters and loads

Parameter	Description	Value
T_{prim}	Primary level sample time [s]	$1/(16 \cdot 10^3)$
L_i	$i-th$ *ac DG* coupling inductance $[mH]$	2.5
Z_{ij}	*ac* sub-MG distribution lines $[\Omega]$	$0.7 + j2.5 \cdot 2\pi$
R_i	$i-th$ *dc DG* coupling resistor $[\Omega]$	0.67
R_{ij}	*dc* sub-MG distribution lines $[\Omega]$	0.78
$Z_1; Z_2$	*ac* sub-MG loads $[kVA]$	5.7+j2.3; 1.5+j0.2
$Z_3; Z_4$	*ac* sub-MG loads $[kVA]$	2+j0.5; 2.3+j0.3
$R_1; R_2; R_3; R_4$	*dc* sub-MG loads $[kW]$	3.36; 1.32; 1.13; 1.11
$P_{1,max}^{ILC}; P_{2,max}^{ILC}$	ILCs power rating	5.0; 3.0
ω_0	*ac* sub-MG nominal frequency	$2\pi \cdot 50$
V_0^{ac}	*ac* sub-MG nominal voltage	220
V_0^{dc}	*dc* sub-MG nominal voltage	400

4.11.1 Design parameters and test scenarios used to evaluate the DMPC for H-MGs

The DMPC design parameters and weighting factors are presented in Table 4.3. All the design parameters were selected to reduce the computational burden. The sample time was selected considering the open loop rise time ($T_r = 0.7s$) of

Table 4.2: DGs parameters

dc DGs parameters					
Parameter	DG_1^{dc}	DG_2^{dc}	DG_3^{dc}	DG_4^{dc}	DG_5^{dc}
a [$/kWh^2$]	0.35	0.37	0.46	0.51	0.52
b [$/kWh$]	1.8	2.9	2.0	2.6	1.6
c [$]	0	0	0	0	0
Power capacity ($P_{i,max}$) [kW]	2.5				
$P-V$ droop coefficient (M_{pv}) [$\frac{V}{W}$]	$-1.2 \cdot 10^{-2}$				
ac DGs parameters					
Parameter	DG_1^{ac}	DG_2^{ac}	DG_3^{ac}	DG_4^{ac}	DG_5^{ac}
a [$/kWh^2$]	0.39	0.44	0.49	0.55	0.66
b [$/kWh$]	2.9	2.3	2.4	1.5	1.9
c [$]	0	0	0	0	0
Power capacity ($S_{i,max}$) [kVA]	3				
$P-\omega$ droop coefficient ($M_{p\omega}$) [$\frac{rad}{sW}$]	$-3.33 \cdot 10^{-4}$				
$Q-V$ droop coefficient (M_{qv}) [$\frac{V}{VAR}$]	$-1.5 \cdot 10^{-2}$				

the *ac* sub-MG's frequency (operating with only the primary control enabled) as $T_{sec} = 0.7/14 = 0.05s$ [86]. The weighting factors were tuned following the guidelines in [89], i.e., looking for a trade-off between the control objectives and, if needed giving more importance to one objective over the rest of the objectives. The average *ac* voltage and *dc* voltage are limited to a band of ± 5 [V] of their nominal values V_0^{ac} and V_0^{dc}, respectively, while the frequency is limited to a band of $\pm \pi$ [rad/s] of the nominal value ω_0. Although the limits are fixed for all the test scenarios, these can be modified as long as they comply with IEEE standard 1547-2018 [40].

The controller was tested under three scenarios using the H-MG simulator, shown in Fig. 5.3. The first scenario presents the DMPC's performance when the H-MG experiences *ac* and *dc* load changes on both sub-MGs. The second scenario shows the behaviour of the MG when two issues are present simultaneously. These issues are communication path failures and disconnection and connection of *ac* DGs, *dc* DGs and ILCs. The last scenario presents a comparison between the proposed DMPC and a reported technique based on

the distributed averaging proportional-integral (DAPI) controller. For this scenario, both controllers are tested when the entire communication network has communication delays. These three test scenarios were selected because these are the most common phenomena that a controller at the secondary level confronts [49, 135]. A distributed controller must perform well against communication issues, such as communication delays and failures. In addition, the possibility of disconnecting and reconnecting DGs and ILCs to the H-MG without changes in the programming of the controllers is essential.

Table 4.3: DMPC parameters and Weights

Parameter	Description	Value
T_{sec} [s]	Controller sample time	0.05
$\hat{\tau}_{ij}$ [s]	Estimated communication delay	0.05
Ny	Prediction horizon	10
Nu	Control horizon	10
DMPC for ILC weights		
λ_{1h} $[(kWh/\$)^2]$	Active power dispatch for DGs	$4 \cdot 10^0$
λ_{2h} [-]	Active power consensus for ILCs	$4 \cdot 10^4$
λ_{3h} $[(1/kW)^2]$	ILC control action (ΔP_h^{ILC})	$5 \cdot 10^3$
DMPC for dc DGs parameters and weights		
$[V_{max}; Vmin]$	Average voltage predefined band	[395,405]
λ_{1i} $[(kWh/\$)^2]$	Active power dispatch with dc DGs	$3.5 \cdot 10^{-4}$
λ_{2i} $[(kWh/\$)^2]$	Active power dispatch with ac DGs	$3.5 \cdot 10^{-4}$
λ_{3i} $[(1/V)^2]$	Average voltage regulation	$7 \cdot 10^3$
λ_{4i} $[(\frac{1}{V})^2]$	Voltage control action variation	$16 \cdot 10^2$
DMPC for ac DGs parameters and weights		
$[V_{max}; Vmin]$	Average voltage predefined band	[215,225]
$[\omega_{max}, \omega_{min}]$ $[rad/s]$	Frequency predefined band	$[101\pi, 99\pi]$
λ_{1i} $[(kWh/\$)^2]$	Active power dispatch with ac DGs	$2.1 \cdot 10^{-3}$
λ_{2i} $[(kWh/\$)^2]$	Active power dispatch with dc DGs	$2.1 \cdot 10^{-3}$
λ_{3i} $[(kVAR/\$)^2]$	Reactive power dispatch	$4.2 \cdot 10^1$
λ_{4i} $[(\frac{s}{rad})^2]$	Average frequency regulation	$3.8 \cdot 10^6$
λ_{5i} $[(1/V)^2]$	Average voltage regulation	$5.0 \cdot 10^5$
λ_{6i} $[(\frac{s}{rad})^2]$	Frequency control action variation	$4.5 \cdot 10^6$
λ_{7i} $[(\frac{1}{V})^2]$	Voltage control action variation	$1.9 \cdot 10^4$

4.11.2   *Scenario I* (base case) - Load changes

This test evaluates the performance of the proposed DMPC scheme when the MG is subject to *ac* and *dc* load steps. For the whole test the communication network does not vary, i.e., the adjacency matrix A is kept constant and is described in Fig. 4.4. The test starts with both *ac* DGs and *dc* DGs enabled and working only with the primary control while the ILC is disabled. Hence, the *ac* sub-MG and the *dc* sub-MG are working separately, and its dynamic is fixed by the droop controller. Additionally Z_1, Z_2, R_1, and R_2 are connected at their respective nodes (see Fig. 4.4). Note that as the DMPC controllers are disabled, there is neither consensus in the incremental cost (IC) nor consensus in the reactive marginal cost (RMC) (see Fig. 4.5.a and Fig. 4.5.b before $t = 10s$); therefore, active and reactive power are not economically dispatched (see Fig. 4.5.c and Fig. 4.5.d before $t = 10s$). Furthermore, the frequency and voltages of the H-MG are outside of the established bands (see Fig. 4.6.b, Fig. 4.6.c and Fig. 4.6.d before $t = 10s$).
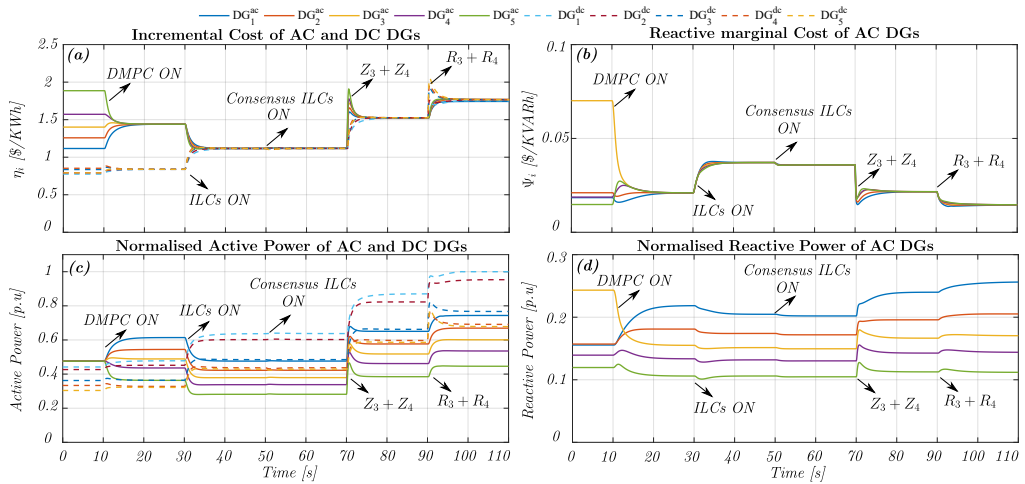
Figure 4.5: *Load changes: a) Incremental cost consensus, b) Reactive marginal cost consensus, c) Active power, d) Reactive power*

At $t = 10s$, the predictive controllers for the sub-MGs are enabled, but the ILCs are still disabled, so there is no power transference between the sub-MGs yet. Therefore, the DMPC controllers optimise the DGs' performance locally, i.e., the second terms (objectives) in the cost functions of (4.17) and (4.27) are
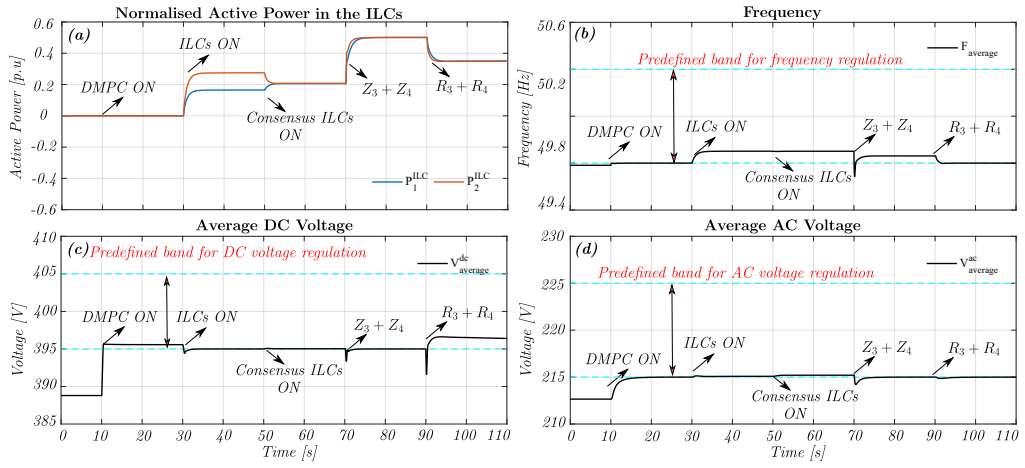
Figure 4.6: *Load changes: a) Active power through the ILCs, b) Frequency regulation, c) Average dc voltage regulation, d) Average ac voltage regulation. The dashed cyan lines represent the predefined band limits for frequency and voltages.*

disabled. It is observed that on the ac sub-MG, consensus on both the IC and RMC are achieved (see Fig. 4.5.a and Fig. 4.5.b at $t = 10s$). The consensus values for IC and RMC are achieved as all the ac DGs achieve the same value in steady-state. Thus, both active and reactive power are redispatched economically, considering generating costs (see Fig. 4.5.c and Fig. 4.5.d at $t = 10s$). Moreover, both frequency and average ac voltage are regulated within the established bands (see Fig. 4.6.b and Fig. 4.6.d at $t = 10s$). Similarly, on the dc sub-MG, the consensus on the IC is achieved, hence active power is redispatched based on the DGs' generation costs, as shown in Fig. 4.5.a and Fig. 4.5.c at $t = 10s$. Additionally, the average dc voltage is regulated within its established band (see Fig. 4.6.c at $t = 10s$).

The ILCs and their DMPC strategies are enabled at $t = 30s$, but initially only the IC consensus objective (second term) in (4.7) is enable. Thus, the ILCs equalise the ICs on both sub MGs to achieve global economic dispatch (see Fig. 4.5.a at $t = 30s$), but they do not transfer active power proportionally to their power rating (see Fig. 4.6.a at $t = 30s$), which could cause overloading in the ILCs. Fig. 4.5.c shows that the DGs on the dc sub-MG increase their power contribution to transfer power to the ac sub-MG because they have lower generation costs (see Table 4.2) while the ac DGs decrease theirs, as they are more expensive. At $t = 50s$, the power consensus on the ILCs is enabled

(third term) in (4.7). Therefore, both ILCs transfer power proportionally to their power rating, as shown in Fig. 4.6.a at $t = 50s$.

Then, at $t = 70s$ the total ac load (Z_3 and Z_4) is connected. As the dc DGs are cheaper, they increase their power contribution more than the ac DGs (see Fig. 4.5.c at $t = 70s$) to transfer more through the ILCs (see Fig. 4.6.a at $t = 70s$) and achieve the consensus value (see Fig. 4.5.a at $t = 70s$). This takes the frequency and voltages outside of their bands for a short time; however, these variables are regulated immediately by the DMPC controllers, as shown in Fig. 4.6.b, Fig. 4.6.c, and Fig. 4.6.d at $t = 70s$. Finally, at $t = 90s$, R_3 and R_4 are connected; hence, the H-MG is subject to its total load. Due to the dc sub-MG increasing their load consumption and the dc DGs being cheaper, this new load is mostly supplied by its local DGs. Moreover, as two dc DGs almost reach their power rating limit, the ac DGs also increase their power contribution to supply the remaining load. Therefore, the power transferred through the ILCs is reduced.

It is observed that the economic dispatch of active and reactive power is fulfilled under this demanding operating condition. In addition, even though the disturbances are sudden, the frequency and voltages are regulated within their bands at all times. The results show that the proposed DMPC scheme achieves all the objectives without large overshoots and with settling times below 8 seconds for all the scenarios tested, and all the equipment constraints have been respected

4.11.3   *Scenario II* - Combined communication link failures and robustness in the presence of changes in microgrid structure

This test evaluates the performance of the DMPC scheme when two of the most common failures occur, i.e., communication link failures, and disconnection and reconnection of DGs and ILCs. The test starts with the predictive

controllers of the *ac* DGs, *dc* DGs and ILCs enabled. Loads Z_1, Z_2 and R_1 to R_4 are connected at their respective nodes (see Fig. 4.4). A communication failure is forced at $t = 10s$ between the communication channels of DG_1^{ac} to DG_1^{dc}, DG_3^{ac} to DG_3^{dc} and DG_5^{ac} to DG_5^{dc} (see red dashed lines in Fig. 4.4). Note that when these communication links fail, the H-MG is coordinated through the communication links to the ILCs (see green dashed lines in Fig. 4.4), and the DGs only communicate with the neighbouring DGs within their corresponding sub-MGs. Furthermore, the adjacency matrix is modified when the communication links fail.
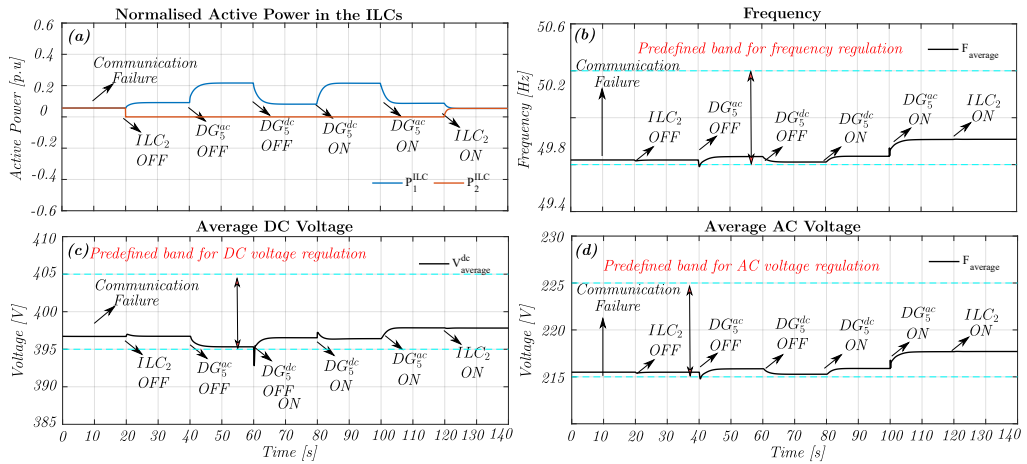
Figure 4.7: *Communication failure and robustness in the presence of changes in microgrid structure test: a) Active power through the ILCs, b) Frequency regulation, c) Average dc voltage regulation, d) Average ac voltage regulation. The dashed cyan lines represent the predefined band limits for frequency and voltages.*

The control algorithms of *dc* DGs and *ac* DGs automatically identify the failure and change the consensus calculations. Specifically, the second terms in (4.17) for *dc* DGs and (4.27) for *ac* DGs, respectively, are not considered in the controller. The predictive controllers do not suffer any noticeable deterioration in performance, as shown in Fig. 4.7 and Fig. 4.8 at $t = 10s$. Note that the communication links are not reestablished for the remain of the test. Then at $t = 20s$, $t = 40s$, and $t = 60s$ three unscheduled failures occur in the H-MG, i.e. ILC_2, DG_1^{ac}, and DG_1^{dc} are disconnected, respectively, from both the electrical system and the communication network. The MG continues operating with the remaining connected DGs and ILC until $t = 80s$, where DG_1^{dc} is reconnected
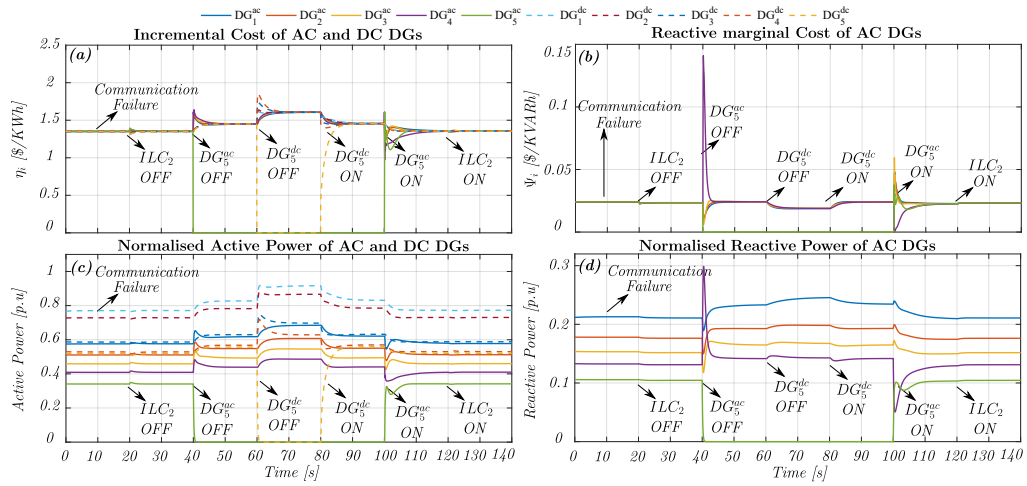
Figure 4.8: *Communication failure and robustness in the presence of changes in microgrid structure test: a) Incremental cost consensus, b) Reactive marginal cost consensus, c) Active power, d) Reactive power*

to the MG. In a similar way, DG_1^{ac}, after a synchronisation routine, and ILC_2 are reconnected at $t = 100s$ and $t = 120s$, respectively.

The results in Fig. 4.7 and Fig. 4.8 show that the controller performance is not affected by both phenomena, and the remaining operating DGs and ILCs achieve the consensus objectives, even when both failures are present at the same time. Nevertheless, the transient response is different; both overshoot and settling time increase slightly. This is because the adjacency matrix is not complete, and the consensus objectives depend on the known information of the neighbouring DGs and ILCs. Note that when DG_1^{dc} and DG_1^{ac} are reconnected (see Fig. 4.8 at $t = 80s$ and $t = 100s$), these DG units achieve the consensus objectives in a longer time. Next the performance of the proposed strategy against a DAPI-based strategy under the presence of communication delays is evaluated.

4.11.4 *Scenario III* - Comparison against a DAPI-based strategy without economic dispatch for H-MGs

This section presents a comparison study between the proposed DMPC strategy and the reported technique in [43]. The DAPI-based method in [43] shares active and reactive power proportionally to the DGs' power rating without

considering the DGs generation costs and restores frequency and voltage to nominal values. The same simulator and adjacency matrix (A) presented in Fig. 4.4 is used for this comparison study. The selected scenario is communication delays, one of the most common phenomena in distributed controllers. A communication delay of one second is applied in the entire communication network ($\tau_{ij} = 1s$) for the whole test. For this test, both the proposed DMPC strategy and the DAPI strategy [43] start with all their functionalities enabled and all the loads connected except R_3 and R_4. Fig. 4.9 presents on the left-hand side the results of active power contribution and active power transference through the ILCs for [43], while the results of these variables for the proposed DMPC are on the right-hand side. Conversely, Fig. 4.10 presents in each graph a performance comparison of both control strategies.
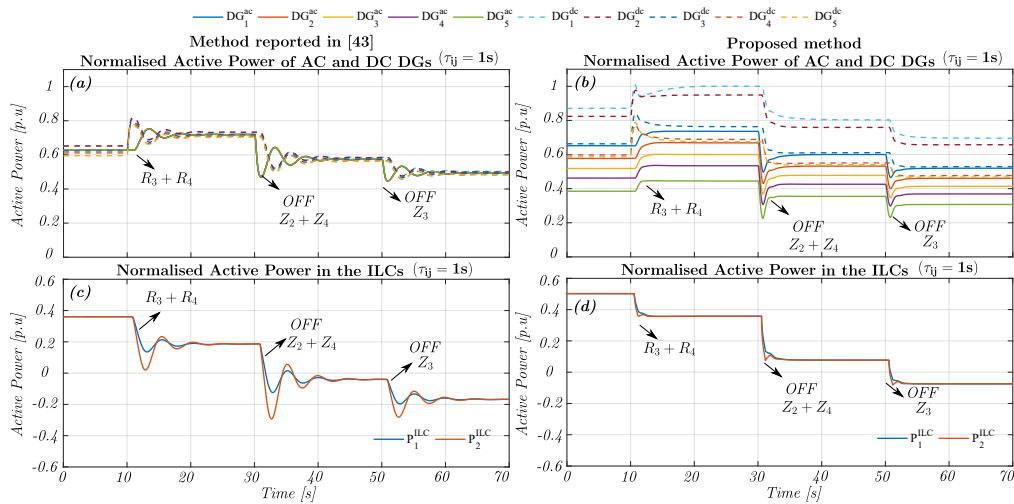
Figure 4.9: *Comparison between the proposed DMPC scheme and a DAPI-based method for ($\tau_{ij} = 1s$): a)-b) Active power for both methods, c)-d) Active power through the ILCs for both methods.*

At $t = 10s$, the H-MG is subject to its total load, i.e., R_3 and R_4 are connected. It is observed that the DAPI controller shares power proportionally while the proposed DMPC dispatches the DGs considering their operation costs (see Fig. 4.9.a and Fig. 4.9.b at $t = 10s$). The proposed DMPC transfers more active power through the ILCs than the DAPI controller (see Fig. 4.9.c and Fig. 4.9.d at $t = 10s$); this is because the DMPC achieves the economical dispatch point by dispatching more power from the dc DGs, as these are cheaper
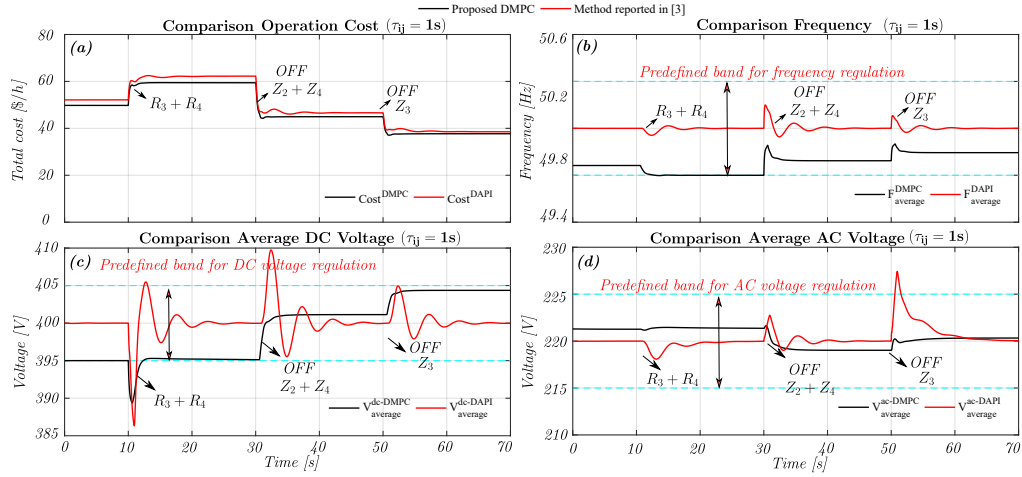
Figure 4.10: *Comparison between the proposed DMPC scheme and a DAPI-based method for $(\tau_{ij} = 1s)$: a) Total operating cost, b) Frequency regulation, c) Average dc voltage regulation, d) Average ac voltage regulation. The dashed cyan lines represent the predefined band limits for frequency and voltages.*

(see Table 4.2). Furthermore, when the H-MG has its total load connected, the operation cost is reduced by up to 4.55%, i.e., from 62.25 $/h$ to 59.42 $/h$, as shown in Fig. 4.10.a. Regarding frequency and voltage, the DAPI controller restores these variables to nominal values while the proposed DMPC provides more flexibility to the H-MG and regulates them only when they are outside their established bands, as shown in Fig. 4.10.b, Fig. 4.10.c and Fig. 4.10.d. It is crucial to note that the DAPI controller is highly affected by the large communication delay $(\tau_{ij} = 1s)$; this controller presents larger overshoots and long settling times compared to the DMPC in all their controlled variables. This poor performance is because the DAPI controller does not provide a delay compensation mechanism. On the other hand, the proposed DMPC controller has a delay estimation and uses a rolling horizon, which corrects the control action sequences and provides robustness against the effects of delays [65].

Finally, at $t = 30s$ and at $t = 50s$, Z_2 and Z_4, and Z_3 are disconnected, respectively. The results during these events are consistent with the previously described performance. In summary, the communication delay affects the behaviour of [43] significantly by increasing its overshoots and settling time, while the proposed DMPC is slightly affected with negligible overshoots. Moreover, the proposed DMPC has a lower operating cost during the entire test. This

is because the proposed DMPC uses the DGs of the H-MG cost-effectively. The cost reduction may seem small in monetary terms due to the small size of the H-MG, but it could be significant in percentage terms in a larger H-MG. Furthermore, the DMPC scheme can simultaneously regulate variables to specific values and within bands, providing more flexibility to the H-MG while equipment constraints are satisfied. Additionally, the DMPC can tackle more control objectives with fewer control actions, while in the DAPI method, a new controller needs to be designed (added) for each control objective to be addressed.

4.12 Discussion

This Chapter presented a novel DMPC strategy for isolated H-MGs to tackle simultaneously the economic dispatch of both active power and reactive power and the regulation within bands of frequency and voltage (fulfilling IEEE standard 1547-2018 [40]). Specifically, the frequency and the average *ac* voltage on the *ac* sub-MG and the average *dc* voltage on the *dc* sub-MG are regulated within bands. The DMPC scheme considers the H-MG as a single entity by modelling the behaviour and interaction of *ac* DGs, *dc* DGs and ILCs. Furthermore, the dynamic performance of the DMPC scheme is evaluated and discussed for load impacts and communication issues, such as communication delays and communication link failures. The distributed structure of the control scheme allows the disconnection and reconnection DGs and ILCs. In all the tests, the DMPC fulfils its objectives without exceeding the maximum power rating limits, preventing any overloading of DGs and ILCs. In summary, the simulation results demonstrated the main advantages of the proposed strategy, which are:

- Active and reactive economic dispatch is achieved among *ac* and *dc* DGs when a load is connected to either side of the H-MG and when a DG or ILC is disconnected and reconnected to the H-MG.

- The frequency and *ac* voltage in the *ac* sub-MG and the *dc* voltage on the *dc* sub-MG are restored within secure bands in steady-state under all the analysed cases.

- The ILCs transfer active power based on the DGs' generation costs, thus reducing the total operation cost of the H-MG.

- The DMPC scheme operates appropriately with a reduced communication network, where DGs and ILCs are communicated only with neighbouring agents. Moreover, global objectives are achieved through information sharing.

- DGs and ILCs can easily be connected to or disconnected from the H-MG, and the control structure, demonstrating the robustness in the presence of changes in microgrid structure of the proposed strategy.

- The superior behaviour of the DMPC scheme against usual DAPI-based controllers is demonstrated under communication issues.

The development of these strategies and their validation were presented in the following papers:

A. Navas-Fonseca, C. Burgos-Mellado, J. S. Gómez, E. Espina, J. Llanos, D. Sáez, M. Sumner, and D. E. Olivares, "Distributed predictive secondary control with soft constraints for optimal dispatch in hybrid AC/DC microgrids," in IEEE Transactions on Smart Grid, 2022 , [**Q1-IF 8.960 - under review**].
A. Navas-Fonseca, C. Burgos-Mellado, J. Gomez, J. Llanos, E. Espina, D Saez, M. Sumner, "Distributed Predictive Control using Frequency and Voltage Soft Constraints in AC Microgrids including Economic Dispatch of Generation" IECON 2021 – 47th Annual Conference of the IEEE Industrial Electronics Society, 2021, pp. 1-7, doi: 10.1109/IECON48115.2021.9589500.
A. Navas-Fonseca, C. Burgos, E. Espina, E. Rute, D. Saez, M. Sumner, "Distributed Predictive Secondary Control for Voltage Restoration and Economic

Dispatch of Generation for DC Microgrids," 2021 IEEE Fourth International Conference on DC Microgrids (ICDCM), 2021, pp. 1-6, doi: 10.1109/ICDCM50975.2021.9504612.

This chapter concludes the application of DMPC for the economic dispatch of DGs in H-MG. The next chapter presents the application of DMPC to solve the other pressing problem considered in this thesis: the presence of unbalance between the phases in MGs. To this end, new prediction models and a novel cost function are proposed. The following chapter provides a detailed explanation of the proposed control strategy's development and validation.

Chapter 5

DMPC scheme for phase imbalance sharing and frequency and voltage regulation within bands in *ac* microgrids

5.1   Introduction

In this Chapter, the distributed model predictive control (DMPC) strategy for imbalance sharing and the regulation of frequency and voltage within bands for isolated *ac* microgrids (MGs) is proposed. In the DMPC scheme of this chapter, each DG will achieve per-phase reactive power sharing, three-phase active power sharing and will also restore the MG's frequency and voltage within recommended operating bands that comply with IEEE standard 1547-2018 [40] while operating equipment constraints are satisfied.

The main challenge for the techniques proposed in this Chapter is to design the local models and a cost function to tackle simultaneously the control objectives proposed. A local prediction model of the DG's primary control level is included in each DMPC to predict its future behaviour, i.e., the active power - frequency droop control and the active power transfer models

as well as per-phase reactive power - voltage droop control and per-phase reactive power transfer models. Moreover, the DMPC strategy has to be able to recognise and update its calculations when the MG is subject to external phenomena such as communication delays, communication failures and disconnection/reconnection of DGs.

This chapter is organised as follows: Section 5.2 introduces the proposed strategy for imbalance sharing. The dynamic prediction models are presented in Section 5.3. Then, the DMPC formulation is described in Section 5.4. The MG simulator and validation tests are explained in detail in Section 5.5. Additionally, real-time simulation validation is presented in Section 5.6, and a comparison analysis is detailed in Section 5.7. Finally, Section 5.8 summarises the main benefits of the proposed strategy.

5.2   Proposed DMPC scheme

In this section, a three-phase unbalanced ac MG composed of $\mathbb{N}$ DGs is considered. Within the general structure of an MG, a local model for each DG is considered. Fig. 5.1 shows the control of the $i-th$ DG with $i=\{1, \cdots, N\}$. The following explanations and mathematical analysis are made for the $i-th$ DG, as the analysis is analogous for the rest of the DGs.

In this work, each DG is connected to an LCL filter, where the second inductance (L_i) is set to ensure an impedance which is predominantly inductive [63, 64], as shown in the electrical configuration of Fig. 5.1. The primary control of the $i-th$ DG is shown at the bottom of Fig. 5.1. The primary control is achieved by means of a droop equation for the active and reactive power of each unit. The $P-\omega$ droop equation takes into account the three-phase active power of each DG to calculate the angular speed ω_i. The droop equation for the reactive power is defined for each phase x with $x=\{a, b, c\}$ as shown in Fig. 5.1.

This novel approach allows the introduction of small imbalances in the output

voltage (V_x) of the DG units with $x=\{a,b,c\}$, enabling unbalanced power sharing. Indeed, as stated in the introduction section, the sharing of imbalance can only be achieved by increasing the voltage imbalance at the DG units' output. This issue is taken into account for the proposed method, which enables the sharing of unbalanced powers and at the same time regulates the maximum unbalanced voltage at the DGs to enable the maximum values stated in IEEE standard 1547-2018 [40]. In this work, the Phase Voltage Unbalance Rate index (PVUR) is used to quantify the level of imbalance in the output voltage of the DG units (see Section 5.3.4). To create the single-phase $Q-V$ droops, a Quadrature Signal Generator (QSG) is applied in the voltage and current measurements of each phase, as shown in Fig. 5.2.
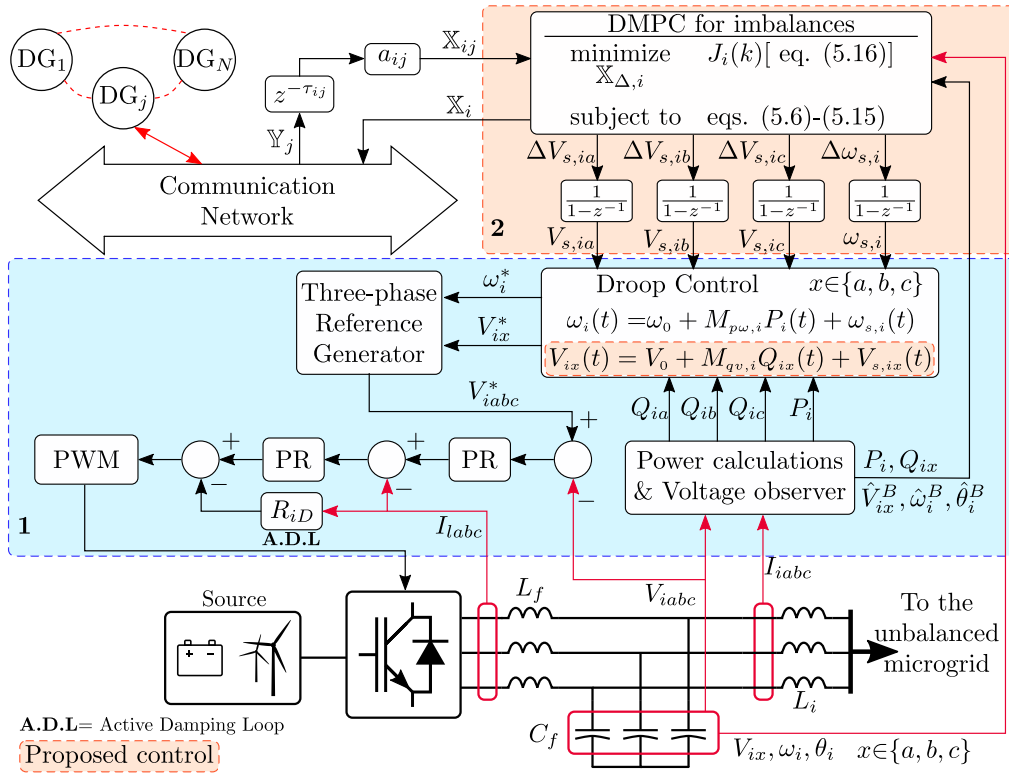
Figure 5.1: *General control diagram of DMPC$_i$ for imbalance sharing.*

The QSG creates a 90-degree shifted signal when applied to sinusoidal signals, thus, creating the virtual β components from the voltage and the current measurements, while only the α components are actually measured. These QSGs are implemented using all-pass filters, and they present good performance when operating around the MG nominal frequency [23, 53]. The output of the re-

active power droop control is the DG output voltage in the natural reference frame V_{iabc}. The DG voltage and current are then regulated through outer and inner cascaded Proportional-Resonant (PR) controllers (see Fig. 5.1).
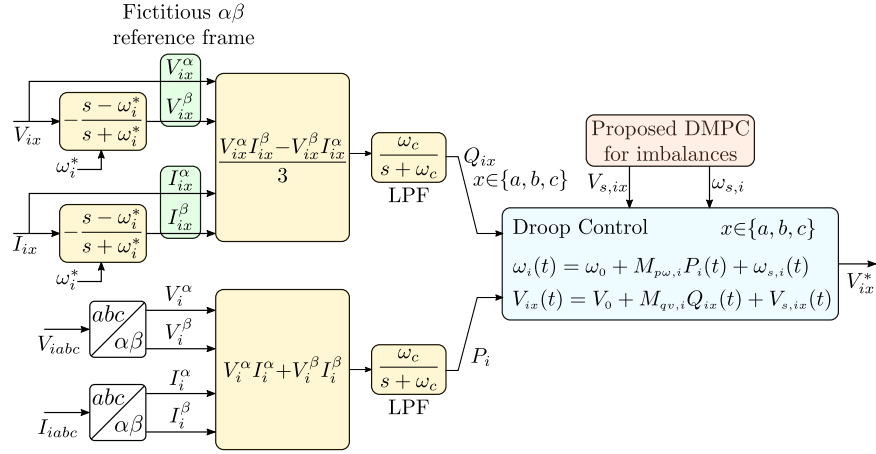
Figure 5.2: *Single-phase droop controller.*

At the top of Fig. 5.1 the DMPC controller of DG_i is presented. This controller receives as inputs the local estimates and measurements ($\{\omega_i(k), \hat{\omega}_i^B(k), V_i(k), V_{ix}(k), \hat{V}_i^B(k), \hat{V}_{ix}^B(k), \delta\theta_i(k), P_i(k), Q_{ix}(k)\}$ with $x=\{a,b,c\}$) from the primary control level and state variable predictions from neighbour units, connected via a communication network. The DMPC outputs are the frequency variation, the per-phase voltage variations (vectors $_\Delta\omega_{s,i}$ and $_\Delta V_{s,ix}$ with $x=\{a,b,c\}$), and the predictions of the local optimisation problem $\mathbb{X}_{p,i}$, defined in Section 5.4. While the control actions are processed by discrete-time integrators to ensure zero error in steady-state, the predictions are sent directly through the communication network. It is worth noting that the same communication principle described previously in Section 3.4.1 is used in this control strategy.

5.3 Dynamic models used for the design of the DMPC strategy

To model the dynamics of the MG, the voltage and frequency at each node, along with the active and reactive power flows, are considered. Since these variables are coupled, in this thesis they are modelled using the droop, power

transfer and phase angle equations. In particular, the $i-th$ DG unit is modelled as the node at the output of its LCL filter, as shown at the bottom of Fig. 5.1, through the per-phase voltages V_{ix} with $x=\{a, b, c\}$, its angular speed ω_i, and its phase angle θ_i. The $i - th$ unit is connected to the rest of the MG through inductor L_i. Unlike previous approaches [49] where external sensors are used, a sensorless scheme is employed to estimate the per-phase unbalanced voltage after the coupling inductor (at the connection bus); thus, only the usual voltage and current measurements at the LCL filter are needed. The per-phase estimated voltages $\hat{V}_{ix}^B$ with $x=\{a, b, c\}$ are computed using a reduced-order state observer based on [139] and explained detail in Appendix A. Also, the average voltage magnitude of the phases $\hat{V}_i^B$ is calculated. Finally, the angular frequency and phase angle at the coupling point $\hat{\omega}_i^B$ and $\hat{\theta}_i^B$, respectively, are estimated using PLLs.

5.3.1   Droop control

To share the active and reactive power between the units belonging to the MG, the angular speed and output voltage of each DG are computed using droop control. The droop models are included in the DMPC scheme because droop controllers rule the MG's behaviour, and through these models, the secondary control interacts with the primary control. For the $i - th$ unit, the active power is regulated through its instantaneous angular frequency $\omega_i(t)$ through the $\omega - P$ droop shown previously in (3.6).

It should be pointed out that a single-phase P-ω droop scheme is not considered in this work because this approach may produce differences in each phase frequency, especially during the transients, which could be a drawback if the MG is feeding three-phase loads, such as motors [53].

The reactive power is shared evenly per phase. Consequently, it is necessary to regulate the reactive power independently for each output phase. In this case, the droop control law for the phase $x=\{a, b, c\}$ is shown in (5.1).

$$V_{ix}(t) = V_0 + M_{qv,i}Q_{ix}(t) + V_{s,ix}(t) \tag{5.1}$$

The reactive power is regulated by controlling the magnitude of the output voltages V_{ix} with $x=\{a, b, c\}$. In addition, the nominal voltage V_0 is the same for all output phases, and the droop slope for the reactive power $Q_{ix}(t)$ is $M_{qv,i}$. Finally, the outputs of the secondary control are $V_{s,ix}(t)$ for phases $x=\{a, b, c\}$ of the $i-th$ unit (after the discrete-time integrators, see Fig. 5.1).

The average voltage magnitude of the phases $V_i(t)$ of the $i-th$ unit is also included, and is given by:

$$V_i(t) = \frac{1}{3}\sum_x V_{ix}(t) \qquad x=\{a, b, c\} \tag{5.2}$$

5.3.2   Phase angle model

To estimate the active and reactive power transferred from the $i-th$ unit to the rest of the MG, its deviation angle $\delta\theta_i(t)$ is employed. The phase angle $\delta\theta_i(t)$ is defined as the angular difference between the output of the LC filter of the $i-th$ unit and the node after the coupling inductor L_i. This model was presented in (3.7)

5.3.3   Power transfer models

To estimate the active and reactive power contribution from the $i-th$ unit to the MG, the power flow through its coupling inductor (L_i) is considered. By using this approach it is possible to avoid the use of the admittance matrix of the whole MG, reducing modelling complexity and enhancing the robustness in the presence of changes in microgrid structure. The active power from DG_i to the rest of the MG was presented in (3.8). Conversely, the reactive power needs to be calculated for each output phase $x=\{a, b, c\}$ to adequately share reactive power in each phase:

$$Q_{ix}(t) = B_i \left[V_{ix}^2(t) - V_{ix}(t)\,\hat{V}_{ix}^B(t)\cos\left(\delta\theta_i(t)\right) \right] \tag{5.3}$$

where, $B_i = 1/(\omega_0 L_i)$, is the nominal admittance of the coupling inductor L_i. The total reactive power $Q_i(t)$ of the $i-th$ unit is also included as the sum of the single-phase reactive powers previously defined. This model is used to limit the power contribution of DG_i within the DMPC formulation.

$$Q_i(t) = \sum_x Q_{ix}(t) \qquad x = \{a, b, c\} \tag{5.4}$$

5.3.4 Phase voltage unbalance rate index

As discussed in the introduction section, imbalance sharing methods should be designed to achieve simultaneously the imbalance sharing and the regulation of the voltage at the output of the DG units. Currently, only a few works have explored this topic [33, 39]. In this sense, the proposed predictive controller addresses this issue by using the phase voltage unbalance rate index (PVUR) (5.5) to quantify the unbalance at the $i-th$ DG's output [39].

$$\text{PVUR}_i(t) = \frac{1}{V_i(t)} \max_{x=\{a,b,c\}} \{|V_{ix}(t)| - V_i(t)\} \tag{5.5}$$

This index is regulated in each DG unit to meet IEEE standard 1547-2018 [40], where a maximum voltage imbalance of 5% is allowed. In (5.5), $|V_{ix}(t)|$ and $V_i(t)$ are the per-phases voltage magnitudes and the average voltage magnitude among the phases at t, defined in (5.1) and (5.2), respectively.

5.4 Distributed MPC formulation for imbalance sharing

The main objective of the proposed DMPC is to share imbalances through a single-phase approach between the DGs that comprise the MG whilst the unbalanced voltage at the converters' output is regulated below the maximum allowed PVUR to meet the IEEE power quality standard [40]. A consensus in the three-phase active power is also sought in this strategy. Furthermore, instead of restoring the average frequency and the average voltage to their

nominal values, a more flexible objective is proposed. These variables are kept within predefined bands and only restored when they are outside their band, and this is achieved through the use of soft constraints. Note that by regulating the MG average voltage, it is possible to have good reactive power-sharing, as the voltage nodes can have different voltage levels, which are close to the MG average voltage.

5.4.1   Cost function

The cost function of the proposed DMPC comprises ten weighted terms and is presented in (5.6).

$$
\begin{aligned}
J_i(k) = &\sum_{j=1,j\neq i}^{N} \sum_{m=1}^{N_y} \lambda_{1i} a_{ij}(k) \left(\frac{3Q_{ia}(k+m)}{|S_{i\,max}|} - \frac{3Q_{ja}(k+m-\hat{\tau}_{ij})}{|S_{j\,max}|} \right)^2 \\
&+ \sum_{j=1,j\neq i}^{N} \sum_{m=1}^{N_y} \lambda_{2i} a_{ij}(k) \left(\frac{3Q_{ib}(k+m)}{|S_{i\,max}|} - \frac{3Q_{jb}(k+m-\hat{\tau}_{ij})}{|S_{j\,max}|} \right)^2 \\
&+ \sum_{j=1,j\neq i}^{N} \sum_{m=1}^{N_y} \lambda_{3i} a_{ij}(k) \left(\frac{3Q_{ic}(k+m)}{|S_{i\,max}|} - \frac{3Q_{jc}(k+m-\hat{\tau}_{ij})}{|S_{j\,max}|} \right)^2 \\
&+ \sum_{j=1,j\neq i}^{N} \sum_{m=1}^{N_y} \lambda_{4i} a_{ij}(k) \left(\frac{P_i(k+m)}{|S_{i\,max}|} - \frac{P_j(k+m-\hat{\tau}_{ij})}{|S_{j\,max}|} \right)^2 \qquad (5.6) \\
&+ \sum_{m=1}^{N_y} \left[\lambda_{5i}(\omega_{aux,i}(k+m))^2 + \lambda_{6i}(V_{aux,i}(k+m))^2 \right] \\
&+ \sum_{m=1}^{N_u} \left[\lambda_{7i}(\Delta V_{s,ia}(k+m-1))^2 + \lambda_{7i}(\Delta V_{s,ib}(k+m-1))^2 \right] \\
&+ \sum_{m=1}^{N_u} \left[\lambda_{7i}(\Delta V_{s,ic}(k+m-1))^2 + \lambda_{8i}(\Delta \omega_{s,i}(k+m-1))^2 \right]
\end{aligned}
$$

The first to the third terms achieve a normalised consensus in the reactive power contribution in phases a, b and c, respectively, which are used to produce the sharing of imbalance. The fourth term seeks consensus for the the three-phase normalised active power. The fifth and sixth terms penalise the auxiliary variables $\omega_{aux,i}$, $V_{aux,i}$. These variables act as slack variables to keep both average voltage and average frequency within predefined bands while an unfeasible solution is avoided. Terms fifth and sixth work in conjunction with

the soft constraints (5.15a) and (5.15b), respectively. The seventh to ninth terms penalise any variations of the voltage control actions in each phase, and the tenth term penalises any variation of the frequency control action. The objectives of sharing reactive power per phase and restoring the average voltage are achieved with the control actions of the terms seven to nine, while the objectives of sharing active power and restoring frequency are achieved by the control action of tenth term. These control actions are applied in their respective droop controllers (see Fig. 5.1). The terms λ_{1i} to λ_{7i} are positive tuning parameters explained in Section 5.5.

By penalising the control action variations, the control effort is minimised, and the transient performance of the controller is improved. Note that all the consensus objectives consider the communication terms $a_{ij}(k)$ and the estimated time delay $\hat{\tau}_{ij}$, which is defined as one sample period at the secondary level. As the consensus objectives in each DG are optimised considering the predictions from communicated neighbouring DGs, the regulation is global for the entire MG.

5.4.2   Predictive models and constraints

The optimisation problem incorporates the dynamic models presented in Section 5.3, which are included as equality constraints based on (3.6)-(3.8), (5.1)-(5.4), and inequality constraints based on (5.5). All these models are discretised and generalised for the prediction horizon (N_y) and a sequence of control actions for the control horizon (N_u) is calculated through a numerical optimisation problem. The discretisation is carried out through the forward Euler method, where $k = nT_{sec}, n \in \mathbb{Z}^+$, and T_{sec} is the sample time of the controller. Then, they are generalised for $k + m$ steps ahead, where $m \in \mathbb{Z}^+$. Furthermore, the incremental operator (3.9) is applied in models (3.6) and (5.1) to express the optimisation problem as a function of the variation of the frequency control action and the per-phase voltage control actions $\vartriangle\omega_{s,i}$ and $\vartriangle V_{s,ix}$ with

$x=\{a,b,c\}$, respectively. The non-linear power transfer models (3.8), (5.3), and the PVUR (5.5) model are linearised via a Taylor expansion around the measured/estimated point $\{\omega_i(k), \hat{\omega}_i^B(k), V_i(k), V_{ix}(k), \hat{V}_i^B(k), \hat{V}_{ix}^B(k), \delta\theta_i(k), P_i(k), Q_{ix}(k)\}$ with $x=\{a,b,c\}$ before their discretisation.

The predictive models of the $\omega - P$ (3.6) and $Q_{ix} - V_{ix}$ (5.1) droop controllers, are presented in (5.7a) and (5.7b), respectively.

$$\omega_i(k+m)=\omega_i(k+m-1)+M_{p\omega,i}[P_i(k+m)-P_i(k+m-1)]+\Delta\omega_{s,i}(k+m-1) \qquad \text{(5.7a)}$$

$$V_{ix}(k+m)=V_{ix}(k+m-1)+M_{qv,i}[Q_{ix}(k+m)-Q_{ix}(k+m-1)]+\Delta V_{s,ix}(k+m-1)$$
$$\text{(5.7b)}$$

The predictive model of the average voltage, described previously in (5.2), is presented in (5.8).

$$V_i(k+m) = \frac{1}{3}\sum_x V_{ix}(k+m) \qquad x=\{a,b,c\} \qquad \text{(5.8)}$$

The predictive model of the phase angle difference, described previously in (3.7), is presented in (5.9).

$$\delta\theta_i(k+m) = \delta\theta_i(k+m-1) + T_{sec}\left[\omega_i(k+m) - \hat{\omega}_i^B(k)\right] \qquad \text{(5.9)}$$

The predictive models of the three-phase active power, described previously in (3.8), and the per-phase reactive power, described previously in (5.3), are presented in (5.10a) and (5.10b), respectively.

$$P_i(k+m)=P_i(k)+[V_i(k+m)-V_i(k)]B_i\hat{V}_i^B(k)\sin(\delta\theta_i(k))$$
$$+[\delta\theta_i(k+m)-\delta\theta_i(k)]B_iV_i(k)\hat{V}_i^B(k)\cos(\delta\theta_i(k)) \qquad \text{(5.10a)}$$

$$Q_{ix}(k+m)=Q_{ix}(k)+[V_{ix}(k+m)-V_{ix}(k)]B_i\left[2V_{ix}(k)-\hat{V}_{ix}^B(k)\cos(\delta\theta_i(k))\right]$$
$$+[\delta\theta_i(k+m)-\delta\theta_i(k)]B_iV_{ix}(k)\hat{V}_{ix}^B(k)\sin(\delta\theta_i(k)) \qquad \text{(5.10b)}$$

The predictive model of the three-phase reactive power, described previously

in (5.4), is presented in model (5.11).

$$Q_i(k+m) = \sum_x Q_{ix}(k+m) \qquad x=\{a,b,c\} \tag{5.11}$$

As the *max* operator for (5.5) cannot be included directly in the DMPC formulation, all the possible cases of the operator are included through a set of linear inequality constraints (see equations (5.12a), (5.12b), (5.12c)); thus, the PVUR at the DG's output is regulated in the solution to comply with standard IEEE 1547-2018 [40]. Note that although the coefficients produced in the linearisation are updated each sample time, they are constant during the optimisation and not computed within the controller.

$$\mathcal{K}_{iaa}(k)[V_{ia}(k+m)-V_{ia}(k)]+\mathcal{K}_{iab}(k)[V_{ib}(k+m)-V_{ib}(k)]$$
$$+\mathcal{K}_{iac}(k)[V_{ic}(k+m)-V_{ic}(k)]+\mathcal{F}_{ia}(k){\leq}PVUR^*(k) \tag{5.12a}$$

$$\mathcal{K}_{iba}(k)[V_{ia}(k+m)-V_{ia}(k)]+\mathcal{K}_{ibb}(k)[V_{ib}(k+m)-V_{ib}(k)]$$
$$+\mathcal{K}_{ibc}(k)[V_{ic}(k+m)-V_{ic}(k)]+\mathcal{F}_{ib}(k){\leq}PVUR^*(k) \tag{5.12b}$$

$$\mathcal{K}_{ica}(k)[V_{ia}(k+m)-V_{ia}(k)]+\mathcal{K}_{icb}(k)[V_{ib}(k+m)-V_{ib}(k)]$$
$$+\mathcal{K}_{icc}(k)[V_{ic}(k+m)-V_{ic}(k)]+\mathcal{F}_{ic}(k){\leq}PVUR^*(k) \tag{5.12c}$$

The coefficients of (5.12a) at time k produced in the linearisation process are expressed in (5.13). The coefficients of (5.12b) and (5.12c) have a similar structure to the coefficients of (5.12a), and are detailed in Appendix C.

$$\mathcal{F}_{ia}(k)=\left[\frac{3V_{ia}(k)-[V_{ia}(k)+V_{ib}(k)+V_{ic}(k)]}{[V_{ia}(k)+V_{ib}(k)+V_{ic}(k)]}\right] \tag{5.13a}$$

$$\mathcal{K}_{iaa}(k)=\left[\frac{[3][V_{ib}(k)+V_{ic}(k)]}{[V_{ia}(k)+V_{ib}(k)+V_{ic}(k)]^2}\right] \tag{5.13b}$$

$$\mathcal{K}_{iab}(k)=\left[\frac{[-3V_{ia}(k)]}{[V_{ia}(k)+V_{ib}(k)+V_{ic}(k)]^2}\right] \tag{5.13c}$$

$$\mathcal{K}_{iac}(k) = \left[\frac{[-3V_{ia}(k)]}{[V_{ia}(k) + V_{ib}(k) + V_{ic}(k)]^2} \right] \tag{5.13d}$$

The following operational constraints are also included in the optimisation. The models (5.14a) and (5.14b) compute local approximations of average frequency and MG average voltage based on the predictions of frequency and voltage at the connection bus of DG_i and the predictions of frequency and voltage at their respective connection buses of the communicating neighbouring DGs, respectively. These models consider the communication terms $a_{ij}(k)$ and the estimated time delay $\hat{\tau}_{ij}$, i.e. only the information received through the communication network is used.

$$\overline{\omega}_i(k+m) = \frac{\omega_i(k+m) + \sum\limits_{j=1}^{N} a_{ij}(k)\omega_j(k+m-\hat{\tau}_{ij})}{1 + \sum\limits_{j=1}^{N} a_{ij}(k)} \tag{5.14a}$$

$$\overline{V}_i(k+m) = \frac{V_i(k+m) + \sum\limits_{j=1}^{N} a_{ij}(k)V_j(k+m-\hat{\tau}_{ij})}{1 + \sum\limits_{j=1}^{N} a_{ij}(k)} \tag{5.14b}$$

The soft constraints (5.15a) and (5.15b) work in conjunction with the previous defined models and the auxiliary variables $\omega_{aux,i}$, $V_{aux,i}$ of the objective function (5.6) to achieve the objective to keep both average voltage and average frequency within predefined bands while an unfeasible solution is avoided.

$$\overline{\omega}_{min} \leq \overline{\omega}_i(k+m) + \omega_{aux,i}(k+m) \leq \overline{\omega}_{max} \tag{5.15a}$$

$$\overline{V}_{min} \leq \overline{V}_i(k+m) + V_{aux,i}(k+m) \leq \overline{V}_{max} \tag{5.15b}$$

As these auxiliary variables are penalised in the cost function, see (5.6), they will temporally relax the average frequency and average voltage inequality

constraints, allowing these variables to take values outside their predefined band for a short time. The optimisation problem is relaxed by applying these constraints, and a feasible solution is guaranteed [47], as long as the demanded power is within the physical capacity of the MG.

The maximum apparent power capacity of DG_i is also included through the triangular linearised constraint (5.16) to limit the solution within the physical capacity of DG_i (see Appendix C for the detailed procedure to obtain this model).

$$
\begin{aligned}
|P_i\left(k\right)| + |Q_i\left(k\right)| + \operatorname{sign}\left(P_i\left(k\right)\right)\left[P_i\left(k+m\right) - P_i\left(k\right)\right] \\
+ \operatorname{sign}\left(Q_i\left(k\right)\right)\left[Q_i\left(k+m\right) - Q_i\left(k\right)\right] \leq S_{\max}
\end{aligned}
\tag{5.16}
$$

The proposed DMPC controller has a quadratic cost function, linear equality constraints and linear inequality constraints. Therefore, the optimisation problem is convex and can be synthesised in a canonical quadratic programming (QP) formulation. The optimisation vector of the QP problem, $\mathbb{X}_i$ in (5.17), comprises the predicted variables $\mathbb{X}_{p,i}$ and the control decisions $\mathbb{X}_{\Delta,i}$.

$$
\mathbb{X}_i = \{\mathbb{X}_{p,i}, \mathbb{X}_{\Delta,i}\}
\tag{5.17}
$$

The predicted variables are presented in (5.18) with $x=\{a,b,c\}$. These prediction variables are shared through the communication network to achieve the consensus objectives.

$$
\begin{aligned}
\mathbb{X}_{p,i} = [\omega_i\left(k+m\right), \delta\theta_i\left(k+m\right), V_i\left(k+m\right), V_{ix}\left(k+m\right), \\
\omega_{aux,i}\left(k+m\right), V_{aux,i}\left(k+m\right), P_i\left(k+m\right), \\
Q_i\left(k+m\right), Q_{ix}\left(k+m\right), \bar{\omega}_i\left(k+m\right), \bar{V}_i\left(k+m\right)]_{m=1}^{N_y}
\end{aligned}
\tag{5.18}
$$

The predicted control decisions are presented in (5.19) with $x=\{a,b,c\}$. Then, only the first control decisions of $_{\Delta}V_{s,ix}$ for phases $x=\{a,b,c\}$ and $_{\Delta}\omega_{s,i}$ pass through integrators and are applied to the system (see Fig. 5.1), and the optimisation problem is repeated at each sample time with updated measures

(rolling horizon) [45].

$$\mathbb{X}_{\Delta,i} = [_\Delta V_{s,ix}(k+m-1), {}_\Delta \omega_{s,i}(k+m-1)]_{m=1}^{N_u} \tag{5.19}$$

The QP problem is solved using the QPKWIK Matlab built-in algorithm, which is a stable variation of the classic active-set method [137]. Moreover, the methodology to solve the DMPC scheme is similar to the one described in Algorithm 1. This algorithm details all the necessary steps to obtain a cooperative solution among the DGs that form the MG. Given that the cost function represented in (5.6) is convex and QP is used to solve the optimisation problem, the controller will find the optimum of the objective function at each sample time [47].

5.5   Microgrid setup and simulation results

The MG simulator implemented to test the performance of the DMPC scheme is shown in Fig. 5.3. It comprises four power electronic DG units with different power ratings, different coupling inductances and transmission lines with different impedances, which are represented in Table 5.1. The MG electrical parameters are presented in Table 5.2.
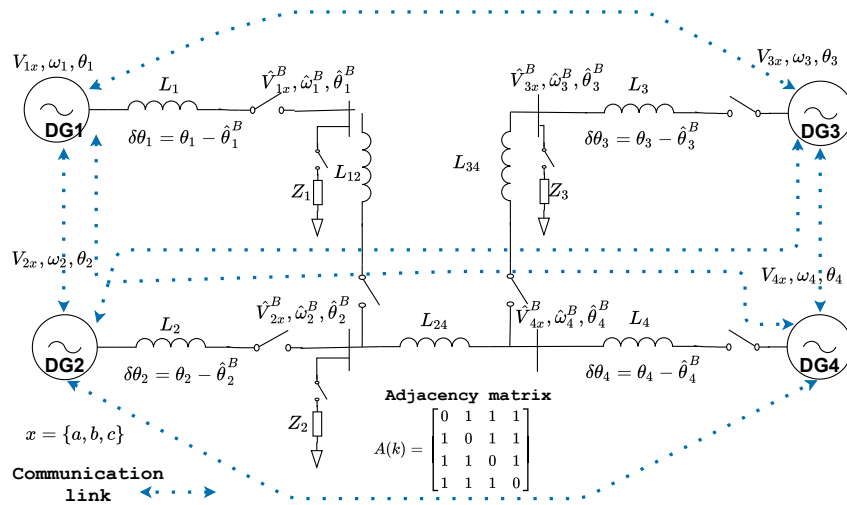
Figure 5.3: *Implemented MG simulator*

Table 5.1: MG electrical parameters

Description	Parameter	DG_1	DG_2	DG_3	DG_4
Power capacity	S_{imax} [KVA]	12.5	11.25	10	8.75
Coupling inductances	L_i [mH]	2.5	2.75	3	3.25
$P-\omega$ Droop slope	$M_{p\omega,i}$ [rad/sW]	$1.6 \cdot 10^{-4}$	$1.44 \cdot 10^{-4}$	$1.28 \cdot 10^{-4}$	$1.12 \cdot 10^{-4}$
$Q-V$ Droop slope	$M_{qv,i}$ [V/VAR]	$3.2 \cdot 10^{-3}$	$2.88 \cdot 10^{-3}$	$2.56 \cdot 10^{-3}$	$2.24 \cdot 10^{-3}$

Table 5.2: MG parameters and loads

Description	Parameter	Value
Primary level sample period	T_{prim}[s]	$1/(16 \cdot 10^3)$
Nominal frequency	ω_0 $[rad/s]$	$2\pi \cdot 50$
Nominal voltage (peak)	V_0 [V]	220
Droop controller cutoff frequency	ω_c $[rad/s]$	10π
Unbalanced load 1 (Z1)	Positive sequence current [A]	69.23
	Negative sequence current [A]	23.76
Unbalanced load 2 (Z2)	Positive sequence current [A]	27.81
	Negative sequence current [A]	1.58
Unbalanced load 3 (Z3)	Positive sequence current [A]	26.8
	Negative sequence current [A]	1.05

The MG electrical model is built with the PLECS blockset®, whereas the primary and secondary controllers are implemented in Matlab/Simulink® environment. Each DG unit possesses at the primary level a three-phase active power - frequency droop controller, per phase reactive power - voltage droop controllers, and self-tuning voltage and current PR controllers in the abc reference frame [26] (see the bottom of Fig. 5.1). The following simplifications were considered in the simulator since their high-bandwidth dynamics are much faster than that of the studied controllers, and they are not relevant on the time-scale of the proposed controllers:

- The DGs are simulated as regulable voltage sources.

- The modulation techniques (PWM, SVM) of the converters are not considered.

- The switching of the switching devices is not considered.

Table 5.3 presents the DMPC design parameters and the weighting factors. The parameters were chosen aiming to reduce the computational effort. This is because the computational burden is directly affected by the sample time, and prediction and control horizons [47]. The sample time was selected considering the frequency and active power open loop rise time ($T_r = 0.7s$) as $T_{sec} = 0.7/14 = 0.05s$ [86]. The prediction and control horizons were selected as 10 samples because with these values the controller always finds a solution within the sample time, and the traffic over the communication network is reduced. The frequency and average voltage are limited to a band of 1% and 5% with respect to their nominal values (ω_0 and V_0), respectively, as recommended in [40]. The PVUR limit ($PVUR^*$ in equations (5.12a), (5.12b), (5.12c)) was selected as 4% to meet the converter's output voltage quality standard (below 5%) [40]. These limits are fixed for all the test-scenarios; however, these can be modified, as long as they are within the recommendations of the IEEE standard.

Table 5.3: Controller parameters and weights

Description	Parameter	Value
Controller sample time	T_{sec} [s]	0.05
Estimated communication delay	$\hat{\tau}_{ij}$ [s]	0.05
Prediction horizon	N_y	10
Control horizon	N_u	10
Average voltage predefined band	$[V_{max}, V_{min}]\,[V]$	[231,209]
Frequency predefined band	$[\omega_{max}, \omega_{min}]\,[rad/s]$	$[101\pi, 99\pi]$
Maximum PVUR limit	$PVUR^*[\%]$	4
Phase a - Reactive power consensus	$\lambda_{1i}\,[(\frac{VA}{VAR})^2]$	9.5
Phase b - Reactive power consensus	$\lambda_{2i}\,[(\frac{VA}{VAR})^2]$	8.0
Phase c - Reactive power consensus	$\lambda_{3i}\,[(\frac{VA}{VAR})^2]$	1.7
Active power consensus	$\lambda_{4i}\,[(\frac{VA}{W})^2]$	2.1
Average frequency regulation	$\lambda_{5i}\,[(\frac{s}{rad})^2]$	$3.8 \cdot 10^2$
Average voltage regulation	$\lambda_{6i}\,[(\frac{1}{V})^2]$	5.0
Per phase voltage control actions	$\lambda_{7i}\,[(\frac{1}{V})^2]$	3.0
Frequency control action	$\lambda_{8i}\,[(\frac{s}{rad})^2]$	$5.0 \cdot 10^1$

The weighting factors were tuned following the guidelines in [89], i.e., looking for a trade-off between the control objectives and, if needed giving more importance to one objective compared to the rest of the objectives. The load changes scenario was used to tune the controller. Note that this scenario does not consider failures such as communication delays/failures and topology changes. However, the results show that the proposed controller achieves good performance even when these issues occur in the MG. First, the weights related to the frequency control action variation and the per-phase voltage control actions variations were established (λ_{7i} and λ_{8i}) for avoiding undesired behaviours in the DGs. Then, as frequency and voltage regulations are the main tasks of the secondary control level, the weights associated with these objectives were fixed (λ_{5i} and λ_{6i}). Later, the weights related with the per-phase reactive power consensus were established (λ_{1i}, λ_{2i} and λ_{3i}). Finally, the weight associated with active power consensus was established (λ_{4i}).

It is worth highlighting that these weighting factors will not affect the steady-

state solution of the controller. Indeed they are only related to the convergence speed of the objectives. Note that the control actions will be zero after the objectives have been met when the DGs are in steady-state. At this point, the cost function will take the value of zero. Moreover, as no constraints are associated with the control actions, the desired objectives will always be achieved. Additionally, because soft constraints are incorporated, the controller's feasibility and convergence are ensured.   The main notion is that if a feasible solution can be established and the prediction horizon (Ny) is large enough to cover the transient of the output variables, the cost function is monotonically decreasing and can be understood as a Lyapunov function, which would provide stability [47, 85].   Moreover, it can also be shown that the problem will be feasible in the next iteration. Therefore, considering that the optimisation problem is always feasible and its convergence is guaranteed, it is possible to state that the controller will remain stable.

Three case-scenarios test the performance of the DMPC scheme. The first scenario consists of connecting unbalanced loads at different nodes. The second scenario tests the controller when there are both a short and a large constant time-delay over the communication network. Finally, the last scenario tests the controller when two failures occur in conjunction, i.e. communication link failures and a DG is disconnected/reconnected from/to the MG. The communication network for the first two tests is represented by the adjacency matrix $A(k)$ (see Fig. 5.3), which remains constant for the whole test. Only in the last scenario is the adjacency matrix changed according to the events of the test. These three test scenarios were selected because these are the most common phenomena that a controller at the secondary level confronts [49, 135]. A distributed controller must perform well against communication issues, such as communication delays and failures. In addition, the possibility of disconnecting and reconnecting DGs to the MG without changes in the programming of the controllers is essential.

5.5.1   *Scenario I* (base case) - Unbalanced load changes

This test verifies the performance of the DMPC on the MG when there are several unbalanced load impacts at different nodes. The MG starts with Z1 connected and the primary control enabled, i.e. droop controllers, and PR controllers enabled. Note that without the DMPC both per phase normalised reactive power and three-phase normalised active power are shared unevenly (see Fig. 5.4 and Fig. 5.5 before 10 s). This is because the DGs have different power ratings and different droop slopes. At $t = 10s$, the predictive controllers are enabled, so the power consensus objectives are achieved in less than 7 seconds.

As discussed in the introduction section, to share the imbalance, it is necessary to induce small imbalances in the output voltage of the DGs. Therefore, the maximum unbalanced voltage allowed in the MG must be regulated to avoid power quality issues. This regulation is achieved by the inequality constraints (5.12a), (5.12b), (5.12c), which limit the maximum allowed PVUR in the voltage at DG's output. In this test, the maximum allowed PVUR in each DG is set to 4%. Fig. 5.6 shows that the closest DG to the load impact reaches the PVUR limit; however, it is never surpassed. At $t = 30s$, both Z2 and Z3 are connected; thus, the MG is subject to its total load.

This event takes the average frequency outside its band, and the DMPC restores this variable inside the band immediately, as shown in Fig. 5.7a at $t = 30s$. This approach makes flexible the behaviour of the frequency and average voltage by restoring them only when it is strictly necessary, instead of restoring these variables to their nominal values at each sample time, as reported in previous approaches. Finally, at $t = 50s$, Z3 is disconnected. During all the load perturbations the controller presents a smooth response and all the objectives are achieved without large overshoots and with settling times below 7 seconds. Furthermore, none of the constraints are violated.

Note that regardless of the approach used (regulate to fixed values or reg-
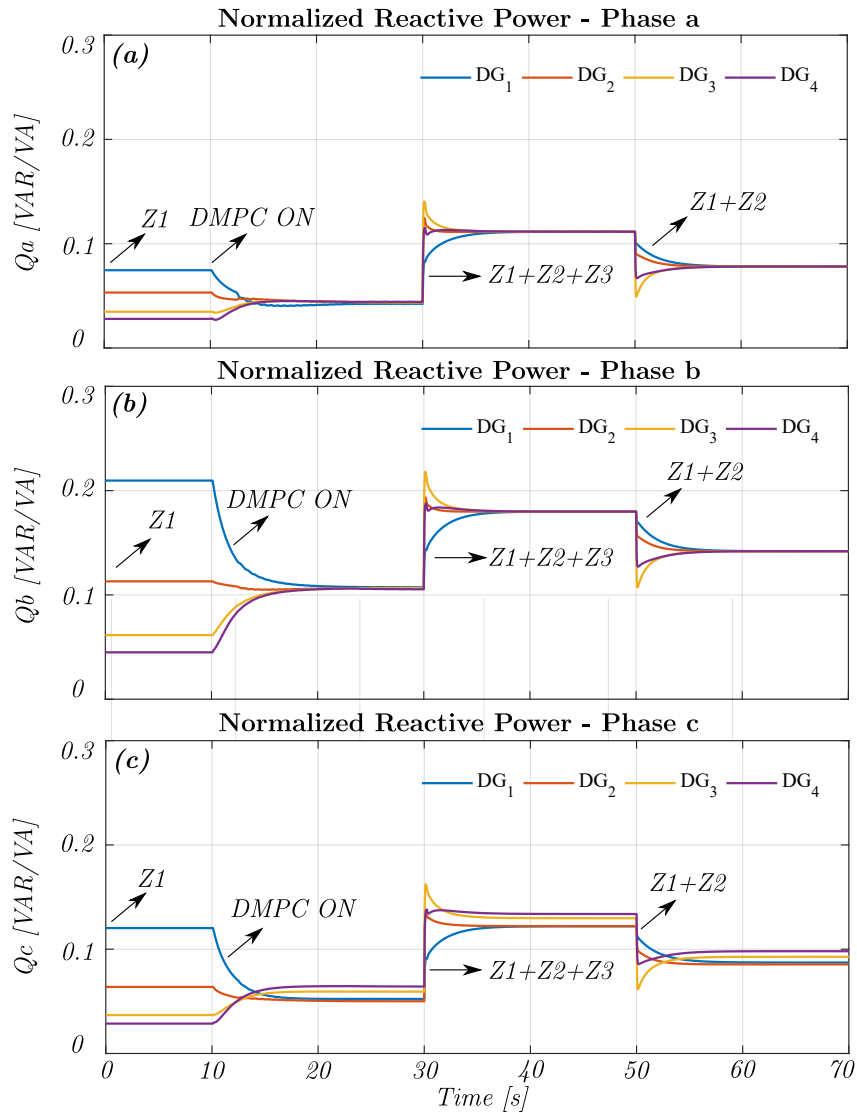
Figure 5.4: *Base Case a) Normalised reactive power consensus - Phase a for load changes, b) Normalised reactive power consensus - Phase b for load changes, c) Normalised reactive power consensus - Phase c for load changes*
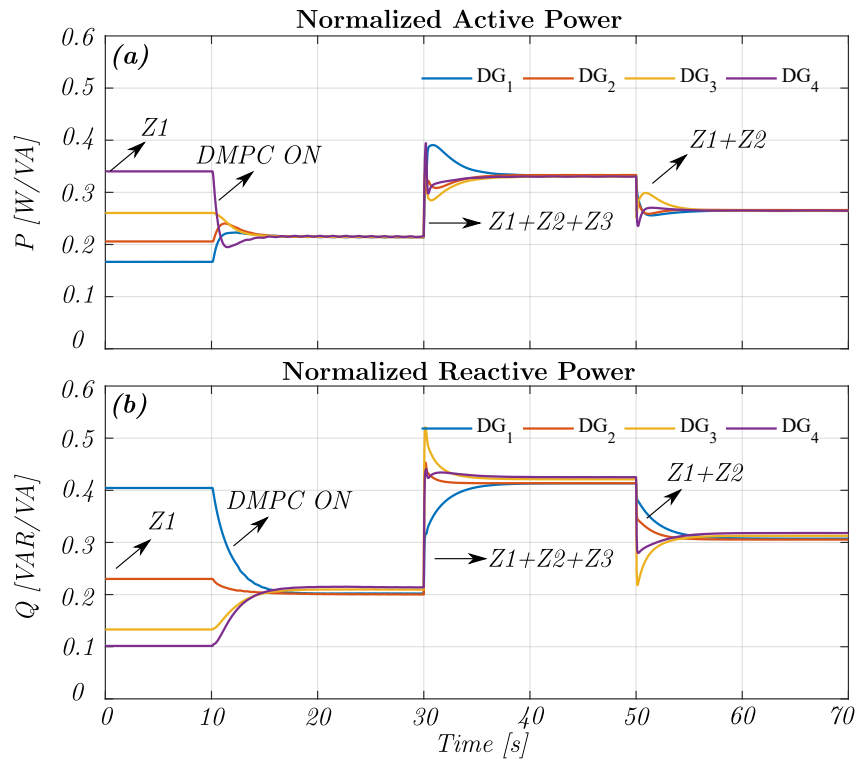
Figure 5.5: *a) Three phase normalised active power consensus for load changes - Base Case, b) Three-phase normalised reactive power consensus for load changes - Base Case*
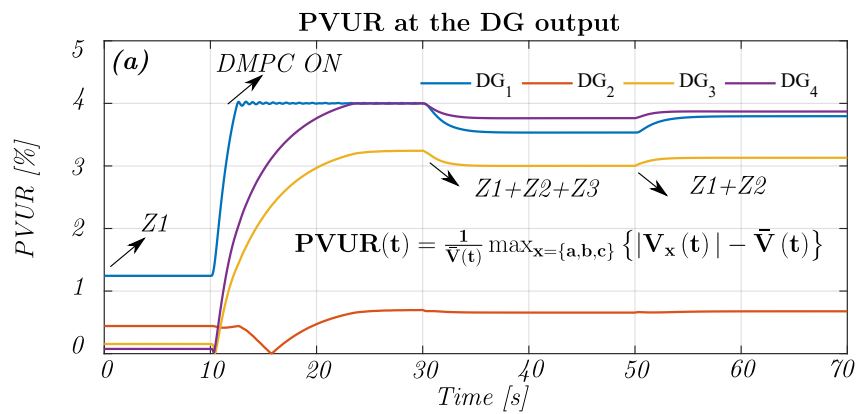
Figure 5.6: *PVUR index of the voltage at the DGs output for load changes - Base Case.*
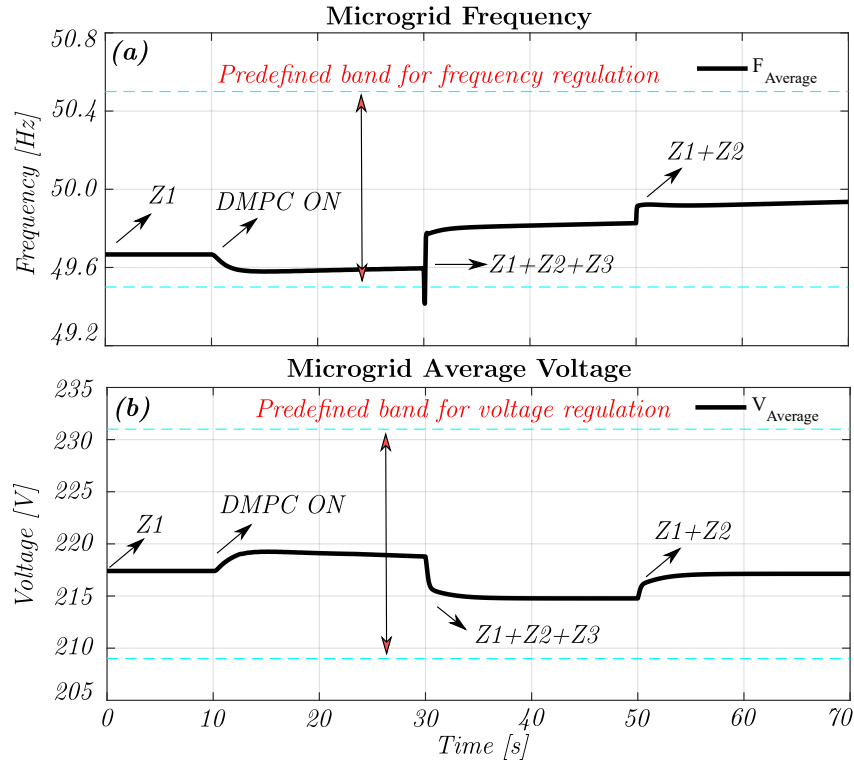
Figure 5.7: *a) Frequency regulation for load changes - Base Case, b) Average voltage regulation for load changes - Base Case. The dashed cyan lines represent the predefined band limits for both variables.*

ulate to a band), temporal violations will always occur. These are due to external physical events, such as connection/disconnection of loads or connection/disconnection of generation units, and are not related to the control system. In this sense, our proposed DMPC control system ensures quick recovery from those temporary violations following the guidelines established by the IEEE 1547-2018 standard [40].

5.5.2 *Scenario II* - Communication delays

This scenario verifies the performance of the controllers when there is a constant delay (τ_{ij}) over the entire communication network, whilst the estimated delay $(\hat{\tau}_{ij})$ is kept constant at one sample. Two cases are considered: a) small time-delay $(\tau_{ij}=0.25s)$ and b) large time-delay $(\tau_{ij} = 1s)$. Note that the worst-case scenario represents a 20-sample delay, which is two times larger than the prediction horizon (N_y). A delay of one second is considered to be a large delay (see [16, 17]); such a delay may be due to weather conditions or line of

sight requirements in rural/remote areas [135]. For this test, the same load changes considered in *scenario I* are applied.
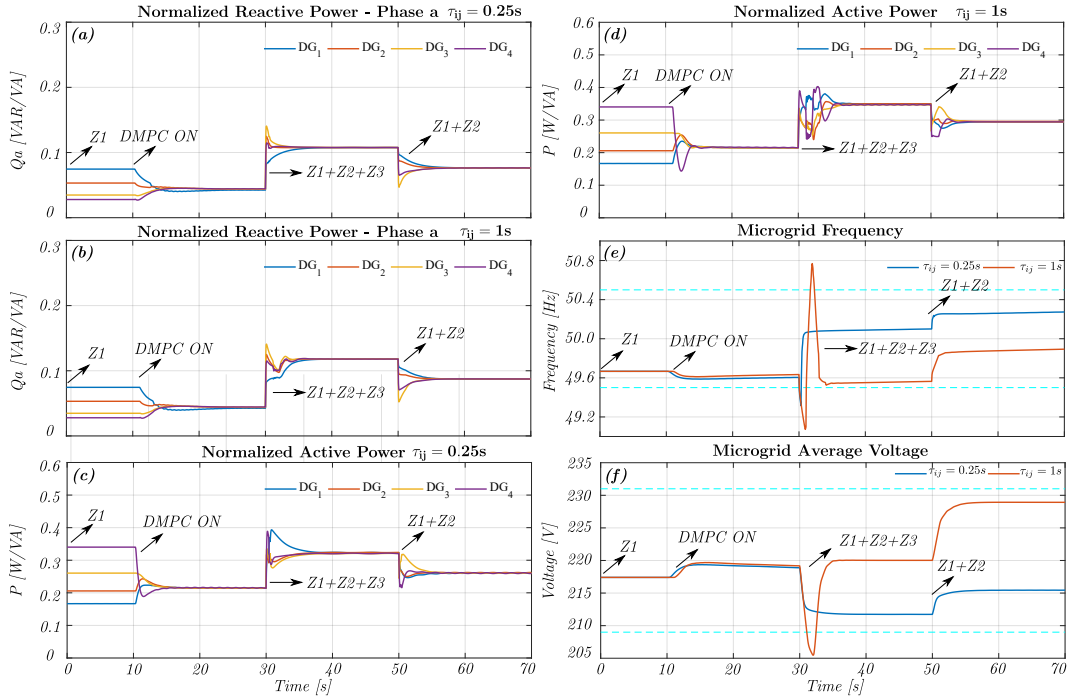
Figure 5.8: *Communication delay test: a) Normalised reactive power consensus - Phase a for $\tau_{ij} = 0.25s$, b) Normalised reactive power consensus - Phase a for $\tau_{ij} = 1s$, c) Three-phase normalised active power consensus for $\tau_{ij} = 0.25s$, d) Three-phase normalised active power consensus for $\tau_{ij} = 1s$, e) Frequency regulation for $\tau_{ij} = 0.25s$ and $\tau_{ij} = 1s$, f) Average voltage regulation for $\tau_{ij} = 0.25s$ and $\tau_{ij} = 1s$. The dashed cyan lines represent the predefined band limits for both latter variables.*

Fig. 5.8 shows the test results. Fig. 5.8a shows the reactive power in phase a for a delay of 0.25s, while Fig. 5.8b shows the same information for a delay of 1s. The rest of the phases are omitted as they present the same behaviour. Fig. 5.8c and Fig. 5.8d present the results for the active power sharing for a delay of 0.25s and 1s, respectively. Fig. 5.8e and Fig. 5.8f present the results for the average frequency regulation and average voltage regulation for both delays. The results show that the DMPC is robust against communication delays, and the delay affects the overshoot and the settling time of the consensus variables: the single phase reactive power is slightly affected when two unbalanced loads are connected simultaneously at different points in the MG at $t = 30s$, and the active power consensus is the variable most affected by

delays.

The more the delay the larger the overshoot and the settling time. It is observed that although the frequency and average voltage are taken outside the defined limits, the proposed controller is capable of regulating these variables within their predefined bands. This is due to the inequality constraints (5.15a) and (5.15b) that allow temporary violations. Therefore, the DMPC presents a good performance against communication delays even when the delay is two times the prediction/control horizons. This is because the rolling horizon scheme provides robustness against delays in the shared information by correcting the control action sequences [46].

5.5.3   *Scenario III* - Combined communication link failures and robustness in the presence of changes in microgrid structure

This test presents the behaviour of the predictive controllers when two of the most demanding scenarios are present in the MG at the same time. The test starts with the controllers enabled and Z1 connected. A communication failure is forced at $t = 10s$ between the communication channels of DG1-DG3 and DG2-DG4, so the MG continues operating with four communication channels, and the MG adjacency matrix is modified (see $A(k)$ in Fig. 5.9a at $t = 10s$). The control algorithm automatically identifies the failure and and changes the consensus (5.6) and average (5.14a), (5.14b) calculations . At $t = 30s$ an unscheduled failure occurs, i.e. DG4 is disconnected from both the electrical system and the communication network. The MG continues operating with the remaining connected DGs until $t = 50s$, when Z2 is connected. At $t = 70s$, after a synchronisation routine, DG4 is reconnected to the MG. Note that when DG4 is disconnected there is only one communication path among the remaining DGs, which is the worst communication scenario for distributed controllers [133] (see $A(k)$ in Fig. 5.9a at $t = 30s$).
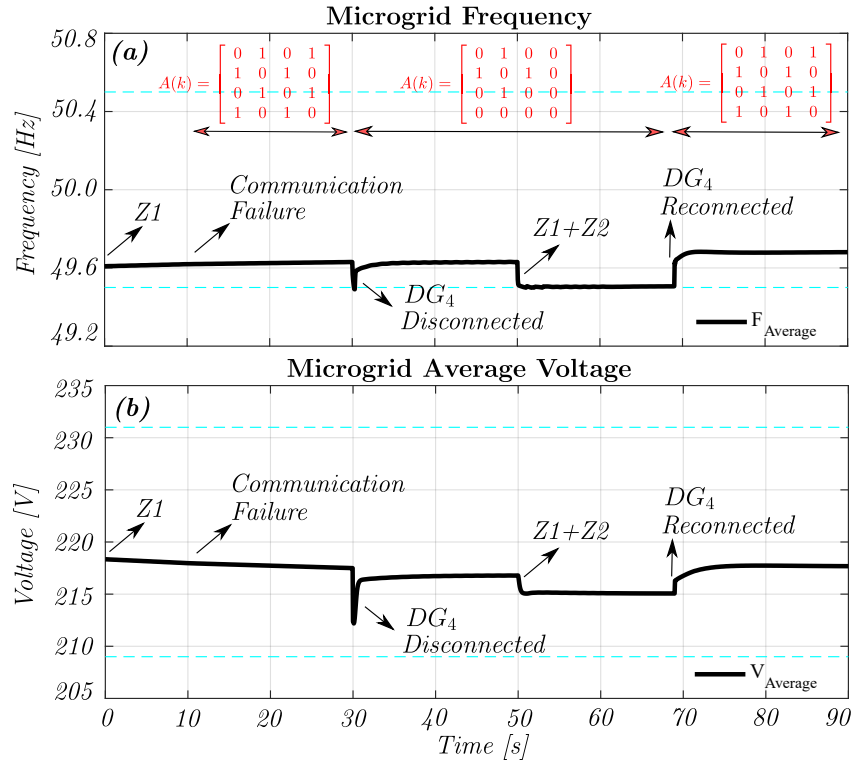
Figure 5.9: *Communication failure and robustness in the presence of changes in microgrid structure test. a) Frequency regulation, b) Average voltage regulation. The dashed cyan lines represent the predefined band limits for both variables.*

Fig. 5.9 and Fig. 5.10 show the test results. When the communication failure occurs ($t = 10s$), the predictive controllers do not suffer noticeable deterioration; only the frequency and voltage present a slight variation, as shown in Fig. 5.9. Furthermore, the controller performance is not affected by both phenomena, and the remaining operating DGs achieve the consensus objectives, even when both failures are present at the same time. Nevertheless, the transient response is different, both overshoot and settling time are increased slightly. This is because the adjacency matrix is not complete, and the consensus objectives depend on the known information of the neighbouring DGs. Note that when DG4 is reconnected (see Fig. 5.10 at $t = 70s$), this DG unit achieves the consensus objectives in a higher time. The time response of the proposed DMPC scheme depends on the density of the adjacency matrix A. This implies that the dynamic response is slow when A is sparse (most of the elements of A are zero, meaning few communication channels), whereas the dynamic response is fast when the density of A is high (most of the elements
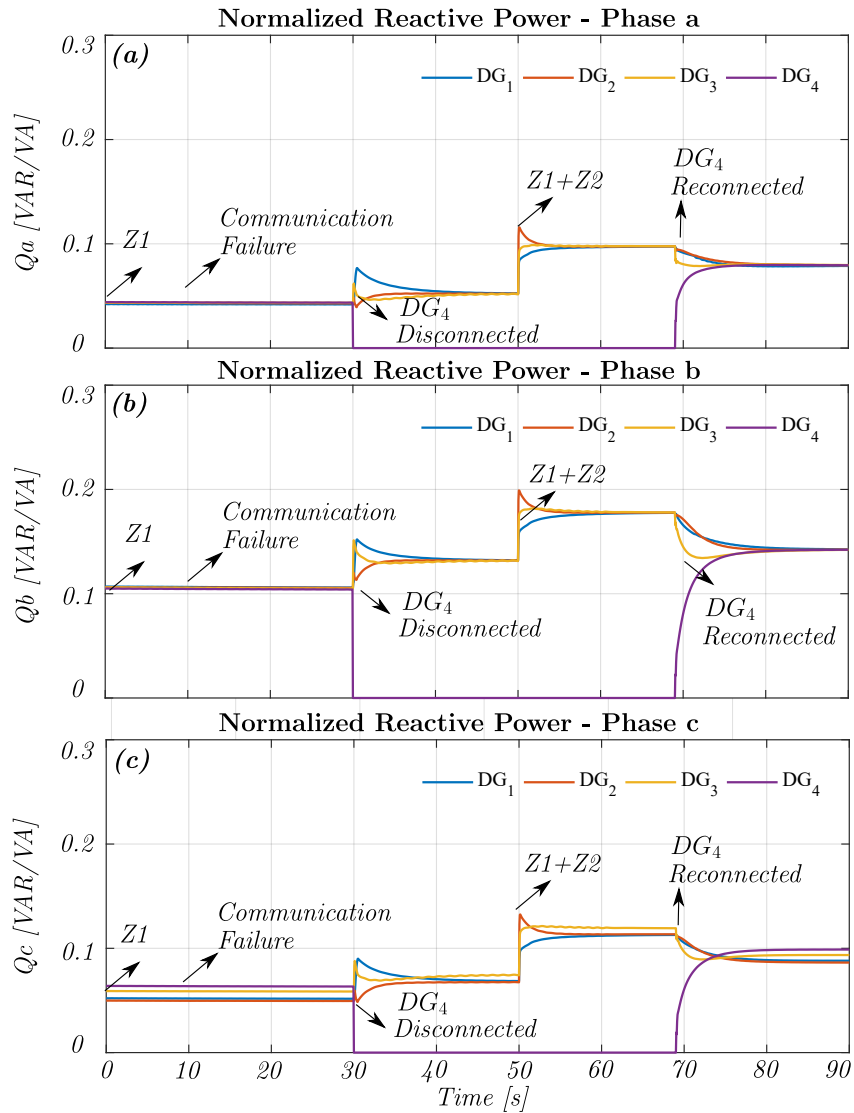
Figure 5.10: *Communication failure and robustness in the presence of changes in microgrid structure test. a) Normalised reactive power consensus - Phase a, b) Normalised reactive power consensus - Phase b, c) Normalised reactive power consensus - Phase c*

of A are one, meaning more communication channels). Furthermore, it has been reported that the convergence time is not related directly to the number of DGs that form the MG, and the convergence time will not be affected as long as the new DGs are properly communicated [42]. Indeed, if more well-communicated DGs are added, the converge speed will be improved [42].

5.6   Real-time simulation validation

The proposed DMPC scheme has been implemented and validated via real-time simulation to illustrate the physical simulation's fidelity. For this purpose, the real-time (RT) platform OP4510 OPAL-RT power grid digital simulator was used. This widely used FPGA-based platform allows real-time simulation validation, as it assigns an independent processor's core for control tasks and another core for system simulation tasks. The OPAL-RT platform is shown in Fig. 5.11. The MG simulator with four DGs of Fig. 5.3 was implemented in the OPAL platform. The DGs implemented in the OPAL include the DMPC controllers along with the primary and droop controllers (see Section 5.2 for a detailed explanation).

To corroborate the results obtained in the simulation section, the test presented in Section Section 5.5.3 was selected for the real-time simulation validation because this is the most demanding test, as it combines the failure of two communication links and the disconnection and reconnection of a DG (to see the events that occur in this test see Section Section 5.5.3).

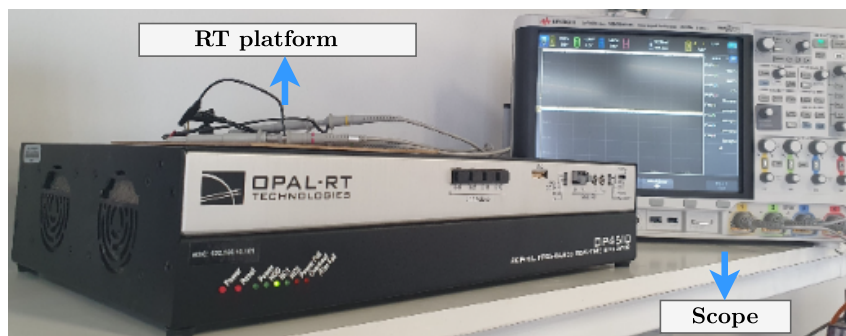**Figure 5.11:** *OPAL-RT platform for real-time simulation validation*
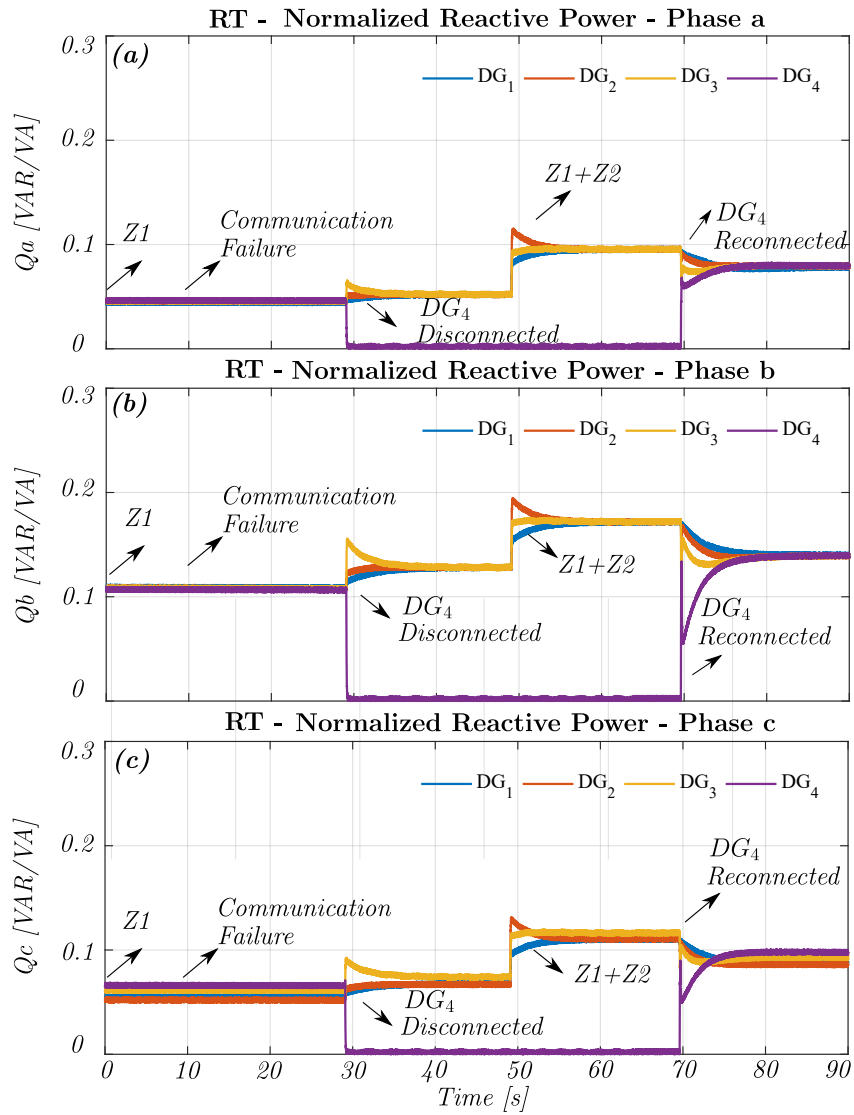
Figure 5.12: *RT - Communication failure and robustness in the presence of changes in microgrid structure test. a) Normalised reactive power consensus - Phase a, b) Normalised reactive power consensus - Phase b, c) Normalised reactive power consensus - Phase c*

The real-time simulation results are consistent with the simulations. For example, Fig. 5.12 shows the single-phase reactive powers in the OPAL platform. When comparing this figure with the one obtained by simulations (Fig. 5.10), it can be seen that they are similar.

Furthermore, this section presents waveforms that cannot be obtained from simulations. For instance, Fig. 5.13 shows the single-phase currents in the natural reference frame at the connection points of DG4 and DG3 (see Fig. 5.3) when DG4 is reconnected at around $t = 70s$. Fig. 5.13a shows the single-phase currents of DG4 during the reconnection of DG4, together with the voltage on one phase. When the DMPC on DG4 is enabled, a good dynamic response without overshoots is appreciated. On the other hand, Fig. 5.13b shows the current injected by DG3 during the reconnection of DG4. Note that in this image, after reconnecting DG4, the current of DG3 decreases since DG4 takes part of the MG load.
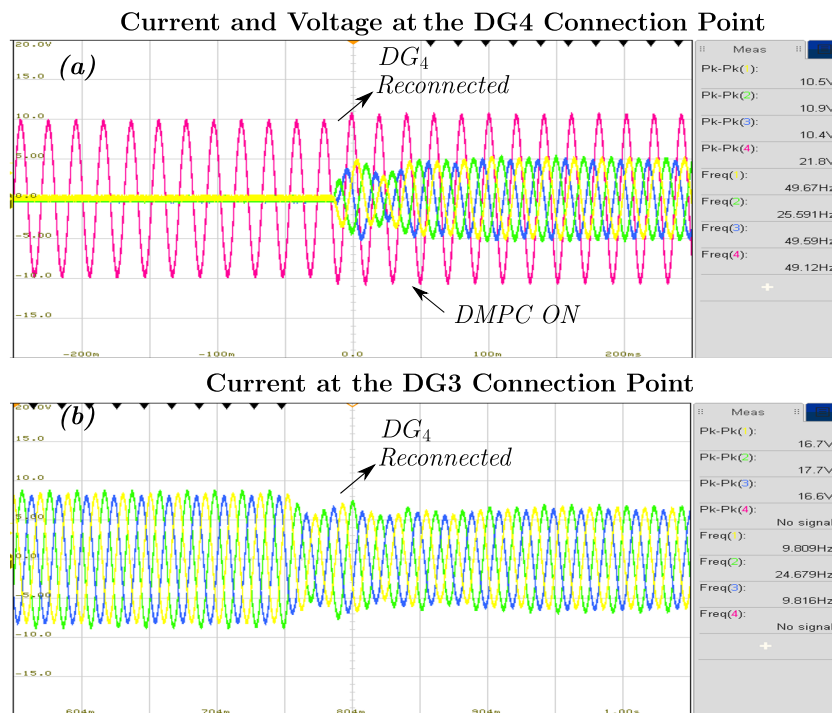
Figure 5.13: *RT - Communication failure and robustness in the presence of changes in microgrid structure test. a) Current and voltage at the DG4 connection point, b) Current at the DG3 connection point, Yellow: Ia, Green: Ib, Blue:Ic, Pink:Va - (20 A/Div, 100 V/Div).*

5.7 Scalability and comparison with a DAPI-based controller

In this section, the scalability of the proposed DMPC and a comparison study with the reported technique in [39] (based on the widely used virtual impedance method) are provided. To test both scenarios an MG simulator with eight DGs was implemented (see Fig. 5.14), as four new generators were added, i.e. DG_5, DG_6, DG_7 and DG_8.
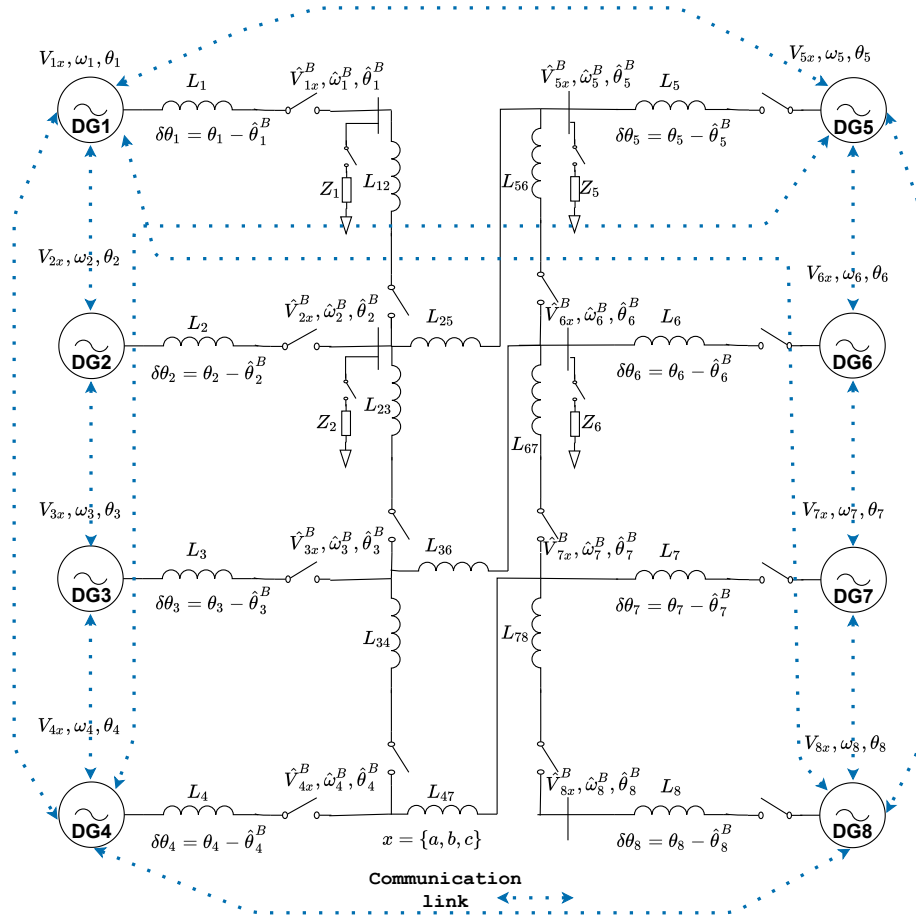
Figure 5.14: *Implemented MG simulator for scalability and comparison scenarios*

These generators have the same droop slopes, power capacities, and coupling inductors of DG_1, DG_2, DG_3 and DG_4, respectively. Furthermore, the same controller and weighting parameters presented in Table 5.3 are configured in the new generators, and a reduced number of communication links is used for the information sharing (see the blue dashed lines in Fig. 5.14). In the same

fashion, the transmission lines were duplicated (see Section 5.5). Note that loads Z_5 and Z_6 were added with the same values of Z_1 and Z_2, respectively (see Table 5.2).

5.7.1   Scalability

Scalability is crucial for a distributed control strategy, and its dynamic behaviour is directly affected by the communication topology of its DGs (agents) and not necessarily related to the number of DGs [42]. Moreover, its behaviour can be analysed through the eigenvalues of the Laplacian matrix L, which is defined as $L = D - A$. Where A is the adjacency matrix (defined in Section 3.4.1), and D is a diagonal matrix formed by the sum of the elements in each row of the adjacency matrix A, i.e., $D = diag\sum_{j=1}^{N} a_{ij}$. The Laplacian matrix L is symmetric for *undirected* graphs, and its eigenvalues are nonnegative real [42]. In particular, the control strategy convergence speed depends on the Laplacian second eigenvalue, which is known as the Fiedler Eigenvalue [42].

The following test evaluates the proposal's scalability. The test starts with two loads connected and five DGs operating with their DMPCs enabled. Then, DG_8, DG_7 and DG_6 are connected (after a synchronisation routine) to the microgrid at around $t = 10s$, $t = 40s$ and $t = 70s$, respectively. The remaining two loads are added at $t = 100s$. In order for the control algorithm to work an initial configuration is needed when a new DG is introduced for the first time to the MG, as is the case of the majority of distributed consensus techniques. All operating DGs need to know their neighbouring power capacities (S_{jmax}), and the number of DGs that form the MG (N).

This does not compromise the robustness in the presence of changes in microgrid structure capability of our proposal, as DGs can be disconnected or reconnected at any time. Then, the DMPC algorithm automatically updates the consensus terms on (5.6) and (5.14) in all operating DGs to solve the optimisation problem. Note that thanks to the distributed structure of the

controller, the number of predicted variables is fixed. Therefore, the computational burden does not increase when new DGs are introduced into the MG. This is of high importance for the scalability of control techniques at the secondary control level.

The performance of the controller is depicted in Fig. 5.15 and Fig. 5.16, where it is observed that due to the reduced density of the adjacency matrix A, the new DGs achieve the consensus objectives in a higher settling time (around 5 seconds) with a smooth transitory response, and the average voltage and frequency are kept within the predefined operating band in all the events in this test.

The optimisation time for the DMPC scheme is presented in Fig. 5.17. It is observed that all predictive controllers find a solution at around 0.01 seconds, which is well below the sample time (0.05 seconds). It should be noted that due to the distributed structure of the predictive scheme, the number of optimisation variables is fixed (see (5.18) and (5.19)). Fig. 5.17 shows that the time required to obtain a solution does not increase when DG_8, DG_7, and DG_6 are connected to the MG at $t = 10s$, $t = 50s$ and $t = 70s$, respectively. These tests were performed on a 9th generation Intel Core i7 3.6GHz computer with 32GB of RAM.
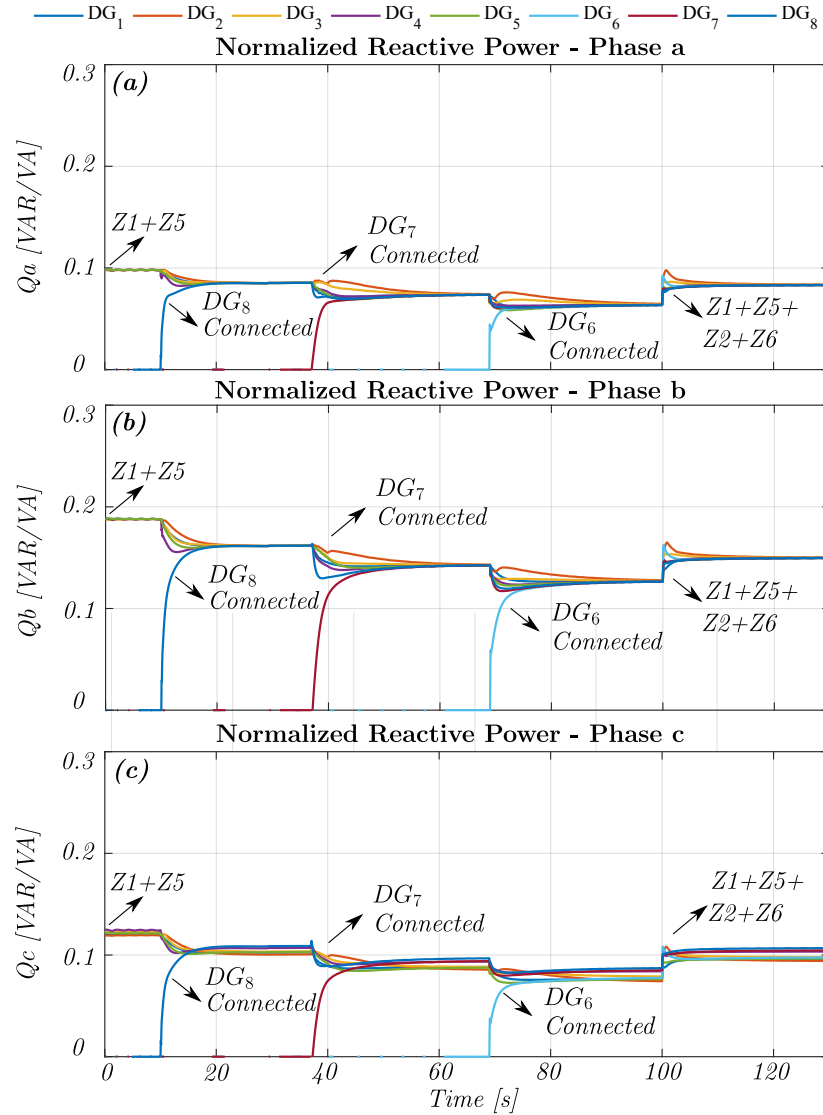
Figure 5.15: *Scalability robustness in the presence of changes in microgrid structure test. a) Normalised reactive power consensus - Phase a, b) Normalised reactive power consensus - Phase b, c) Normalised reactive power consensus - Phase c*
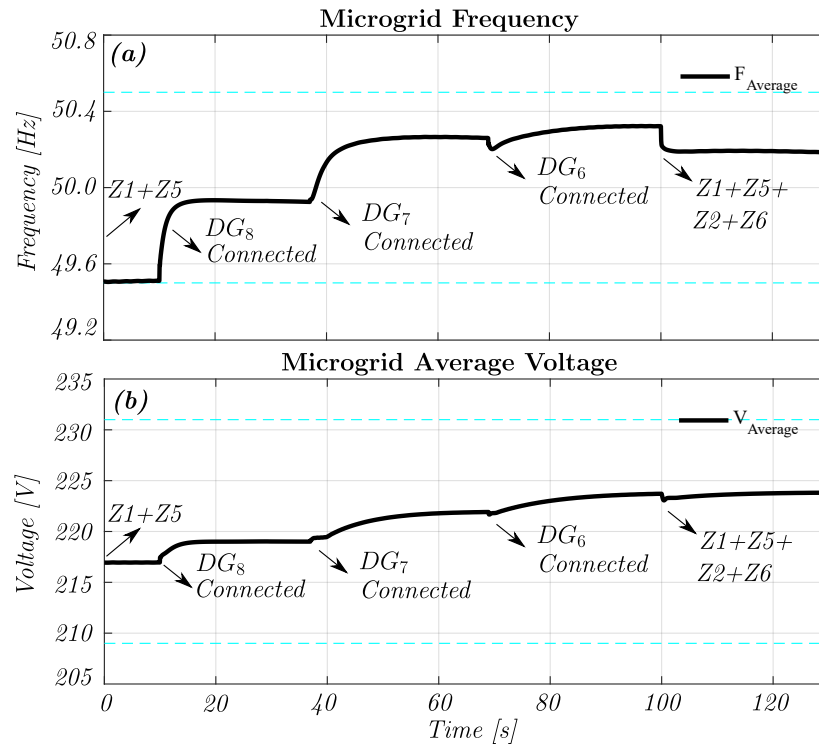
Figure 5.16: *Scalability robustness in the presence of changes in microgrid structure test. a) Frequency regulation, b) Average voltage regulation. The dashed cyan lines represent the predefined band limits for both variables.*
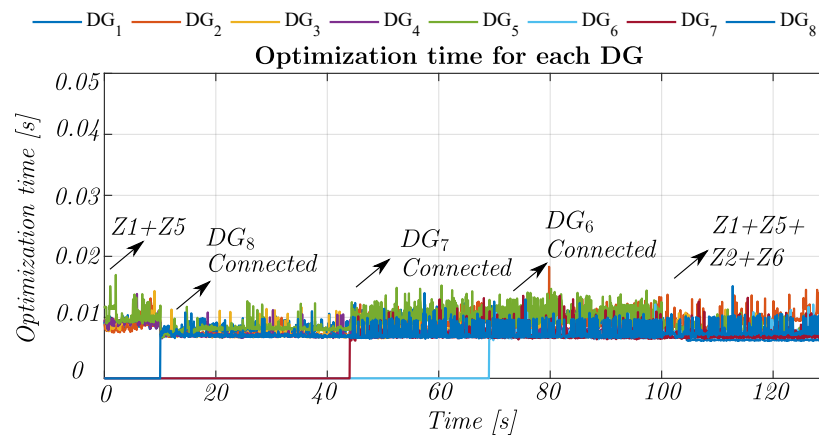
Figure 5.17: *Optimisation time for the scalability test*

5.7.2   Comparison with a distributed consensus-based controller for imbalance sharing

A comparison between our proposal and the work of [39] is presented. This comparison is suitable because both control techniques include consensus objectives to improve imbalance sharing in a distributed fashion, regulate the PVUR of the DGs' output voltage and use an adjacency matrix to represent their communication topology. The work of [39] is based on the concept of virtual impedance and, the imbalance sharing is achieved via a consensus in the three-phase unbalanced power defined by the Conservative Power Theory (CPT) [26]. In the following tests, both control strategies have a PVUR limit of 4%.
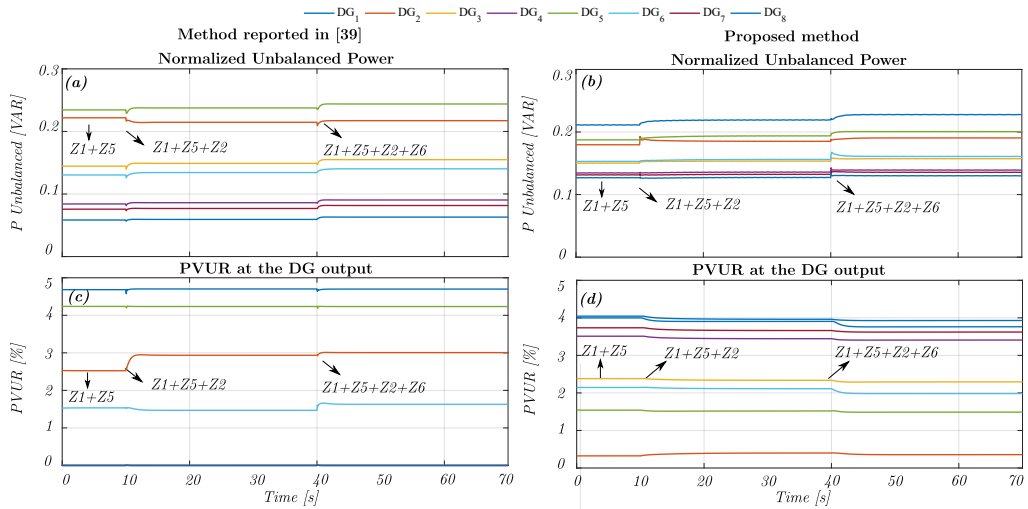
Figure 5.18: *Comparison between the proposed DMPC scheme and a DAPI-based method. a)-b) Unbalanced Power for the two methods compared, c)-d) PVUR index of the voltage at the DGs output for the two methods compared.*

The behaviour of the unbalanced power sharing and PVUR at the DGs' output voltage for [39] in the presence of load changes are presented on the left side of Fig. 5.18. It is observed that although this technique improves the sharing of unbalanced power, a high PVUR at the DGs output voltage is present, which is outside of the desired limit. This is because the DG units that are far from where the loads are connected, do not increase their PVUR. Furthermore, the single-phase reactive powers' behaviour for [39] is presented on the left side of
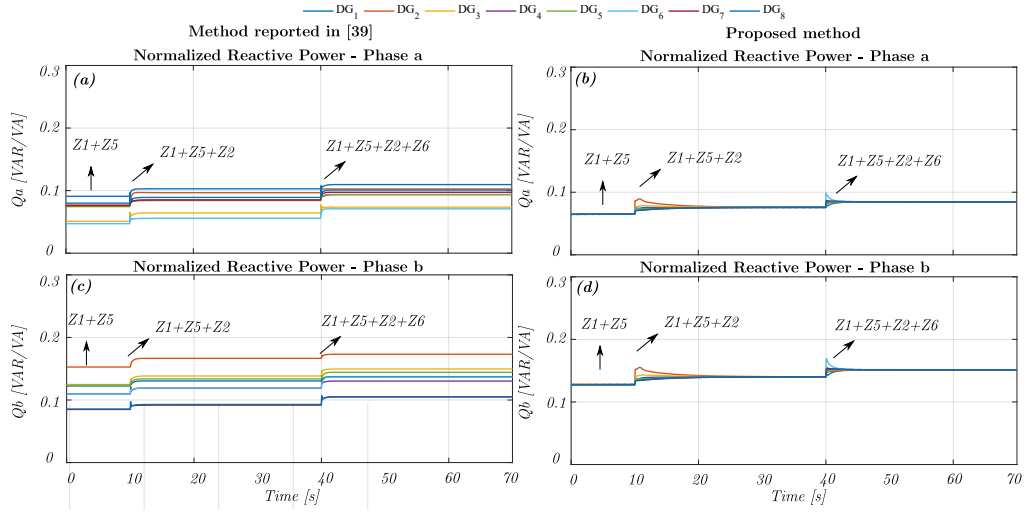
Figure 5.19: *Comparison between the proposed DMPC scheme and a DAPI-based method. a)-b) Normalised reactive power in the phase a for the two methods compared, c)-d) Normalised reactive power in the phase b for the two methods compared.*

Fig. 5.19. Phase c is omitted as it presents the same behaviour.

These results demonstrate that methods based on virtual impedance and defined in the sequence components domain, where the consensus is defined only considering magnitudes and not sequence phase angles, do not guarantee good sharing in the phases (i.e., phase a to phase c). On the other hand, the proposed strategy's performance is presented on the right side of Fig. 5.18 and Fig. 5.19. It is observed that this technique has better performance for unbalanced power sharing with a reduced PVUR that is always below the established limit (4%). Furthermore, the reactive power in the phases is shared properly. Another advantage of the proposed technique is its resilience under communication delays. This is verified by applying a constant delay of one second ($\tau_{ij} = 1s$) on the entire communication network and testing the performance of both strategies. The results for [39] are presented on the left side of Fig. 5.20, whilst the results of our proposal are depicted on the right side. Phase c is omitted as it presents the same behaviour. It is observed that [39] is highly affected under large delays by presenting oscillations in its behaviour when the MG load condition changes. Whereas, the proposed DMPC is slightly affected in the transitory response; nevertheless, the consensus objectives are achieved regardless of the delay. This is because the rolling horizon property and the

delay estimation of the DMPC scheme correct the control actions sequences [46], making the controller stable in the presence of the delays. On the other hand, the consensus technique of [39] does not consider the existence of delays.
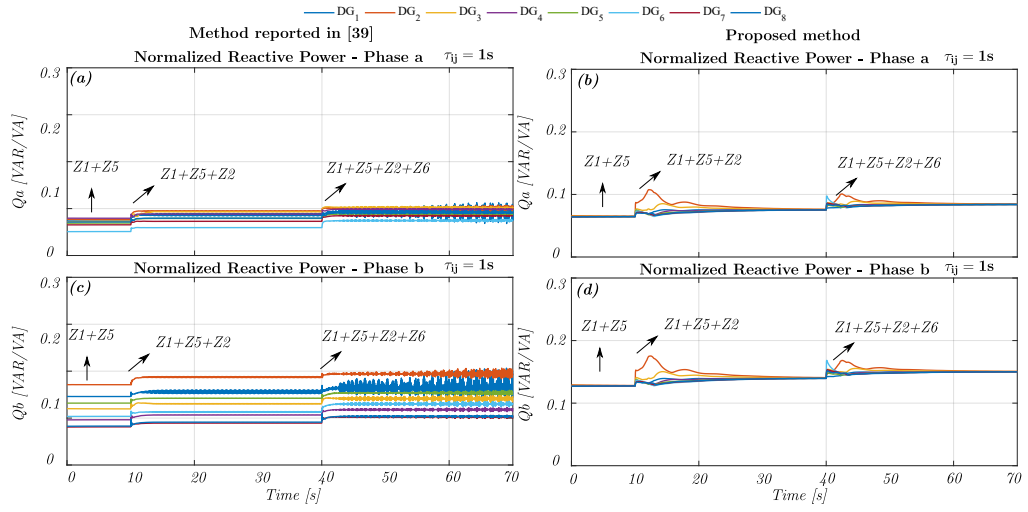
Figure 5.20: *Comparison between the proposed DMPC scheme and a DAPI-based method for $\tau_{ij} = 1s$. a)-b) Normalised reactive power in the phase a for the two methods compared, c)-d) Normalised reactive power in the phase b for the two methods compared.*

To further verify the effect of delays on both control strategies, their control actions are presented in Fig. 5.21. It is observed that this large delay of 1 second considerably affects the voltage control action of [39] (see Fig. 5.21c), which explains the oscillations of Fig. 5.20. On the other hand, the control actions for the proposed strategy are only slightly affected by the delay, as shown on the right-hand side of Fig. 5.21.
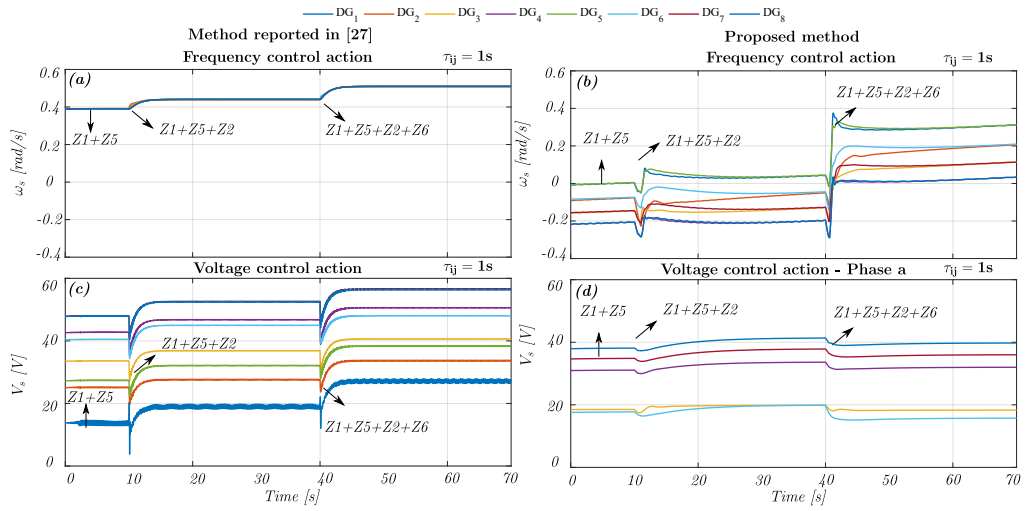
Figure 5.21: *Comparison between the proposed DMPC scheme and a DAPI-based method for $\tau_{ij} = 1s$. a)-b) Frequency control action for the two methods compared, c)-d) Voltage control action for the two methods compared.*

5.8 Discussion

This Chapter presented a novel distributed predictive control strategy to cope with per-phase power imbalance sharing and active power sharing in *ac* isolated MGs. The proposed DMPC scheme is able to achieve all the consensus control objectives simultaneously, while the imposed physical constraints are respected. The dynamic performance of the controller was evaluated and discussed under three of the most demanding test scenarios. Simulation and real-time simulation results verify the good performance of the rolling horizon scheme for communication network issues, PVUR limit restrictions and the disconnection and reconnection of DGs. Furthermore, the proposal's scalability and a comparison study with the usual consensus technique based on the virtual impedance method were evaluated. In summary, the results demonstrated the main advantages of the proposed strategy, which are:

- Per-phase reactive power is shared proportionally among DGs when a load is connected to the MG and when a DG is disconnected from and reconnected to the H-MG.

- The frequency and voltage are restored within secure bands in steady-state under all the analysed cases.

- The DMPC scheme operates appropriately with a reduced communication network, where DGs are communicated only with neighbouring DGs. Moreover, global objectives are achieved through information sharing.

- DGs can easily be connected to or disconnected from the MG, and the control structure, demonstrating the robustness in the presence of changes in microgrid structure of the proposed strategy.

- The superior behaviour of the DMPC scheme against usual DAPI-based controllers is demonstrated under communication issues.

This strategy was validated through real-time simulation and simulation tests in the journal paper:

A. Navas-Fonseca, C. Burgos, J. S. Gómez, F. Donoso, L. Tarisciotti, D. Sáez, R. Cárdenas D., and M. Sumner, "Distributed Predictive Control for Imbalance Sharing in *ac* Microgrids," in IEEE Transactions on Smart Grid, vol. 13, no. 1, pp. 20-37, Jan. 2022, doi:

10.1109/TSG.2021.3108677, [**Q1-IF 8.960 - published**].

Chapter 6

Conclusions and final remarks

Microgrids are positioning themselves as the key enablers for integrating distributed generation and energy storage systems. Nevertheless, new and more sophisticated control systems must be developed to harness their benefits. Distributed model predictive control (DMPC) is one of the leading approaches to managing microgrids (MGs). In this context, the main objective of this PhD thesis was to propose distributed predictive cooperative strategies for secondary control in MGs. These strategies combined the benefits of distributed control and model predictive control, giving a better overall performance of the MG.

The results show that DMPC provides the flexibility to achieve the main task of the secondary control level (restoring frequency and voltage) along with complementary objectives within the same formulation. These complementary objectives can be minimisation of operational cost or phase imbalance sharing. The proposed DMPC schemes include detailed models of the dynamics of the generators (and interlinking converters) including equality constraints and physical limits as inequality constraints. In addition, the rolling horizon property of the proposed DMPCs provides robustness against communication delays. These characteristics allow the proposed DMPC schemes to perform better than traditional controllers. The main findings of this PhD thesis are highlighted as:

For balanced *ac* MGs

- It is demonstrated that DMPC can minimise the MG's operating cost and restore the frequency to its nominal value over a similar time scale. The response of the controller is enhanced by including power rating limits, local dynamic models of the DGs, and a model of the communication network model. In addition, the controller does not need knowledge of the MG topology.

- Extensive experimental tests validate the performance of the proposed control scheme against sudden load changes, communication delays, communication failures, as well as disconnection and reconnection of DGs.

For hybrid *ac/dc* MGs

- It was shown that the frequency, ac voltage and dc voltage on hybrid ac/dc MGs can be restored to within secure bands. This strategy gives flexibility to the operation of MGs where frequency and voltages are restored only when they are outside predefined bands. This is different to most approaches proposed in the literature, which restore these variables to nominal values at each sample time.

- The proposed control strategy regulates the frequency of all *ac* DGs (a global variable). By contrast, since the voltage is not a global variable, the proposed control scheme regulates the average ac voltage and dc voltage, allowing different voltages in the voltage buses of the MG and employing accurate reactive power control.

- Since the proposed strategy is implemented in each DG or ILC, the computational burden required for the predictive controllers is reduced and does not increase when more DGs or ILCs are added to the MG. This is because the number of optimisation variables is fixed. In addition, consensus objectives are achieved through information sharing and coordination between DGs and ILCs. The controllers operate with the usual

measurements at the primary level, and no additional measurements are required.

- Extensive simulation studies verify the performance of the proposed control scheme against sudden *ac* and *dc* load changes, communication delays, communication failures, as well as disconnection and reconnection of *ac* DGs, *dc* DGs and ILCs. A detailed comparison study was carried out in terms of performance under communication delays.

For unbalanced *ac* MGs

- Phase imbalance sharing between DGs is controlled through the control of single-phase reactive power. The proposed distributed model predictive control scheme does not require virtual impedance loops or the inclusion of additional power converters for managing single-phase reactive power between distributed generators. In fact, with the proposed technique, the sharing of imbalance is performed directly in terms of single-phase reactive power and without adding extra power converters into the microgrid.

- As part of sharing imbalance through the single-phase reactive power, the DMPC bounds the unbalanced voltage at the DGs' output, fulfilling the recommendation of the IEEE standard 1547-2018 [40]. Moreover, power rating limits are also considered in the formulation.

- Extensive real-time simulation and simulation studies verify the performance of the proposed control schemes against sudden load changes, communication delays, communication failures, as well as disconnection and reconnection of DGs. Tests to show he controller's scalability and a detailed comparative performance study under communication delays were also carried out.

In summary, it is verified that currently distributed predictive control is one of the most promising strategies for MG management, as they allow the achieve-

ment of global objectives through information sharing. Moreover, they allow the pursuit of more flexible objectives using soft constraints. They also allow modelling and the use of limits in states and inputs within the formulation. All the proposed distributed predictive strategies are easy to scale, and do not increase the computational burden when more agents are added; this is because the number of predicted variables is fixed.

6.1 Future work

A few areas that could form the basis of future research are detailed in the following.

- A direct future path could be the design of a controller that combines economic dispatch and imbalance sharing in hybrid *ac/dc* MGs. Also, energy storage systems and specific renewable energy services should be considered in the formulation.

- The proposed control strategy could be extended to consider congestion management of the distribution line currents. The losses on the ILCs and the losses on the distribution lines could also be considered in the formulation.

- A current hot research topic is the study of the effects of cyber-attacks on distributed controllers. A common cyber-attack is known as the false data injection attack (FDIA). FDIAs can appear in sensors, communication links, and actuators. Therefore, a direct extension of the proposed DMPC schemes would be to incorporate new detection methods and counteract mechanisms to tackle cyber-attacks.

- Different tuning methodologies for the weighting parameters could be explored. For instance, heuristic algorithms, such as particle swarm optimisation (PSO) or genetic algorithms (GA), could be used.

- An open research topic is the study of theoretical stability on distributed model predictive control. Concepts like terminal costs and terminal invariant sets could be incorporated into the formulation.

6.2 Publications

6.2.1 Journal papers

[1] **A. Navas-Fonseca**, J. S. Gomez, J. Llanos, E. Rute, D. Saez, and M. Sumner, "Distributed Predictive Control Strategy for Frequency Restoration of Microgrids Considering Optimal Dispatch," in IEEE Transactions on Smart Grid, vol. 12, no. 4, pp. 2748-2759, July 2021, doi: 10.1109/TSG.2021.3053092 **(Q1, impact factor: 8.960)**.

[2] **A. Navas-Fonseca**, C. Burgos-Mellado, J. S. Gómez, F. Donoso, L. Tarisciotti, D. Sáez, R. Cárdenas D., and M. Sumner, "Distributed Predictive Control for Imbalance Sharing in AC Microgrids," in IEEE Transactions on Smart Grid, vol. 13, no. 1, pp. 20-37, Jan. 2022, doi: 10.1109/TSG.2021.3108677 **(Q1, impact factor: 8.960)**.

[3] **A. Navas-Fonseca**, C. Burgos-Mellado, J. S. Gómez, E. Espina, J. Llanos, D. Sáez, M. Sumner, and D. E. Olivares, "Distributed predictive secondary control with soft constraints for optimal dispatch in hybrid AC/DC microgrids," in IEEE Transactions on Smart Grid, 2022 **(under review, Q1, impact factor: 8.960)**.

[4] E. Rute, **A. Navas-Fonseca**, J. S. Gómez, E. Espina, C. Burgos-Mellado, D. Sáez, M. Sumner and Diego Muñoz-Carpintero, "Distributed Predictive Control for Secondary Level in Hybrid ac/dc Microgrids," in Journal of Emerging and Selected Topics in Power Electronics, doi: 10.1109/JESTPE.2022.3157979 **(Q1, impact factor: 4.472)**.

[5] M. Martinez-Gomez, **A. Navas-Fonseca**, M. E. Orchard, S. Bozhko, C. Burgos-Mellado and R. Cardenas, "Multi-Objective Finite-Time Control

for the Interlinking Converter on Hybrid AC/DC Microgrids," in IEEE Access, vol. 9, pp. 116183-116193, 2021, doi: 10.1109/ACCESS.2021.3105649 **(Q1, impact factor: 3.367)**.

6.2.2 Conference papers

[1] **A. Navas-Fonseca**, C. Burgos, E. Espina, E. Rute, D. Saez, and M. Sumner, "Distributed Predictive Secondary Control for Voltage Restoration and Economic Dispatch of Generation for DC Microgrids," 2021 IEEE Fourth International Conference on DC Microgrids (ICDCM), 2021, pp. 1-6, doi: 10.1109/ICDCM50975.2021.9504612.

[2] **A. Navas-Fonseca**, C. Burgos-Mellado, J. Gomez, J. Llanos, E. Espina, D Saez, and M. Sumner, "Distributed Predictive Control using Frequency and Voltage Soft Constraints in AC Microgrids including Economic Dispatch of Generation," 2021 47th Annual Conference of the IEEE Industrial Electronics Society (IECON), Toronto, Canada, 2021.

[3] E. Espina, **A. Navas-Fonseca**, J. S. Gómez, R. Cárdenas D, "Experimental Performance Evaluation of a Distributed Secondary Control Strategy for Hybrid ac/dc-Microgrids in the event of Communication Loss/Delay", 2021 IEEE, 23rd European Conference on Power Electronics and Applications.

[4] R. Bustos, L. Marin, **A. Navas-Fonseca**, D. Saez, "Demand Side Management based on Fuzzy Prediction Intervals for Microgrids," 2022 IEEE World Congress on Computational Intelligence (WCCI), [accepted for publication].

[5] M. Martinez-Gomez, R. Cardenas D., **A. Navas-Fonseca**, and E. Rute, "A Multi-Objective Distributed Finite-Time Optimal Dispatch of Hybrid Microgrids," IECON 2020 The 46th Annual Conference of the IEEE Industrial Electronics Society, 2020, pp. 3755-3760, doi: 10.1109/IECON-43393.2020.9254375.

[6] E. Espina, C. Burgos-Mellado, J. S. Gómez, J. Llanos, E. Rute, **A. Navas-Fonseca**, M. Martínez, R. Cárdenas, and D. Sáez, "Experimental Hybrid AC/DC-Microgrid Prototype for Laboratory Research," 2020 22nd European Conference on Power Electronics and Applications (EPE'20 ECCE Europe), 2020, pp. 1-9, doi: 10.23919/EPE20ECCE-Europe43536.2020.9215751.

[7] T. Roje, **A. Navas-Fonseca**, M. Urrutia, P. Mendoza-Araya and G. Jiménez-Estévez, "Advanced lead-acid battery models for the state-of-charge estimation in an isolated microgrid," 2019 IEEE CHILEAN Conference on Electrical, Electronics Engineering, Information and Communication Technologies (CHILECON), 2019, pp. 1-6, doi: 10.1109/CHILE-CON47746.2019.8987985.

References

[1] "What were the outcomes of COP26?" [Online]. Available: https://commonslibrary.parliament.uk/what-were-the-outcomes-of-cop26/

[2] "UK targets power from 100% renewable sources by 2035 — S&P Global Commodity Insights." [Online]. Available: https://www.spglobal.com/commodityinsights/en/market-insights/latest-news/energy-transition/100421-uk-targets-power-from-100-renewable-sources-by-2035

[3] "2022 comienza en Chile con la fotovoltaica generando el 20% de la electricidad - ACERA - AG." [Online]. Available: https://acera.cl/2022-comienza-en-chile-con-la-fotovoltaica-generando-el-20-de-\la-electricidad/

[4] "86% de los MW que entrarán a Chile este año son renovables." [Online]. Available: https://www.revistaei.cl/2022/05/05/un-86-de-los-mw-que-entraran-a-operar-en-chile-este-ano-provienen-de\-energia-solar-o-eolica/

[5] Department of Energy office of Electricity Delivery and Energy Reliability, "Summary report : 2012 DOE microgrid workshop," U.S. Dep. Energy, Tech. Rep., Jul. 2012.

[6] D. E. Olivares, A. Mehrizi-Sani, A. H. Etemadi, C. A. Cañizares, R. Iravani, M. Kazerani, A. H. Hajimiragha, O. Gomis-Bellmunt, M. Saeedifard, R. Palma-Behnke, G. A. Jiménez-Estévez, and N. D. Hatziargyriou, "Trends in microgrid control," *IEEE Trans. Smart Grid*, vol. 5, no. 4, pp. 1905–1919, Jul. 2014.

[7] R. Lasseter, "Microgrids," in *2002 IEEE Power Engineering Society Winter Meeting. Conference Proceedings (Cat. No.02CH37309)*, vol. 1, 2002, pp. 305–308 vol.1.

[8] E. Espina, J. Llanos, C. Burgos-Mellado, R. Cárdenas-Dobson, M. Martínez-Gómez, and D. Sáez, "Distributed control strategies for microgrids: An overview," *IEEE Access*, vol. 8, pp. 193 412–193 448, 2020.

[9] K. Ahmed, M. Seyedmahmoudian, S. Mekhilef, N. M. Mubarak, and A. Stojcevski, "A review on primary and secondary controls of inverter-interfaced microgrid," *Journal of Modern Power Systems and Clean Energy*, vol. 9, no. 5, pp. 969–985, Sep. 2021.

[10] S. K. Sahoo, A. K. Sinha, and N. K. Kishore, "Control Techniques in AC, DC, and Hybrid AC–DC Microgrid: A Review," *IEEE J. Emerg. Sel. Top. Power Electron.*, vol. 6, no. 2, pp. 738–759, Jun. 2018.

[11] T. Dragicevic, X. Lu, J. C. Vásquez, and J. M. Guerrero, "DC microgrids - Part I: A review of control strategies and stabilization techniques," *IEEE Trans. Power Electron.*, vol. 31, no. 7, pp. 4876–4891, Sep. 2016.

[12] F. Nejabatkhah and Y. W. Li, "Overview of Power Management Strategies of Hybrid AC/DC Microgrid," *IEEE Trans. Power Electron.*, vol. 30, no. 12, pp. 7072–7089, Dec. 2015.

[13] C. D. Burgos Mellado, "Control strategies for improving power quality and PLL stability evaluation in microgrids (PhD thesis)," Ph.D. dissertation, University of Nottingham, 2019.

[14] E. Nasr-Azadani, C. A. Canizares, D. E. Olivares, and K. Bhattacharya, "Stability analysis of unbalanced distribution systems with synchronous machine and DFIG based distributed generators," *IEEE Transactions on Smart Grid*, vol. 5, no. 5, pp. 2326–2338, Sep. 2014.

[15] J. M. Guerrero, J. C. Vásquez, J. Matas, L. G. de Vicuňa, and M. Castilla, "Hierarchical control of droop-controlled ac and dc microgrids–a general approach toward standardization," *IEEE Trans. Ind. Electron.*, vol. 58, no. 1, pp. 158–172, Aug. 2011.

[16] J. Llanos, D. E. Olivares, J. W. Simpson-Porco, M. Kazerani, and D. Saez, "A novel distributed control strategy for optimal dispatch of isolated microgrids considering congestion," *IEEE Trans. Smart Grid*, vol. 10, no. 6, pp. 6595–6606, Nov. 2019.

[17] G. Chen and Z. Guo, "Distributed secondary and optimal active power sharing control for islanded microgrids with communication delays," *IEEE Trans. Smart Grid*, vol. 10, no. 2, pp. 2002–2014, Mar. 2017.

[18] M. Zaery, P. Wang, W. Wang, and D. Xu, "Distributed Global Economical Load Sharing for a Cluster of DC Microgrids," *IEEE Trans. Power Syst.*, vol. 35, no. 5, pp. 3410–3420, Sep. 2020.

[19] R. Babazadeh-Dizaji and M. Hamzeh, "Distributed Hierarchical Control for Optimal Power Dispatch in Multiple DC Microgrids," *IEEE Syst. J.*, vol. 14, no. 1, pp. 1015–1023, Mar. 2020.

[20] A. Navas-Fonseca, J. S. Gomez, J. Llanos, E. Rute, D. Saez, and M. Sumner, "Distributed Predictive Control Strategy for Frequency Restoration of Microgrids Considering Optimal Dispatch," *IEEE Trans. Smart Grid*, vol. 12, no. 4, pp. 2748–2759, Jul. 2021.

[21] W. Feng, J. Yang, Z. Liu, H. Wang, M. Su, and X. Zhang, "A unified distributed control scheme on cost optimization for hybrid ac/dc microgrid," in *2018 IEEE 4th South. Power Electron. Conf. (SPEC)*, Dec. 2018, pp. 1–6.

[22] Z. Li, Z. Cheng, J. Si, and S. Li, "Distributed event-triggered hierarchical control to improve economic operation of hybrid ac/dc microgrids," *IEEE Trans. Power Syst*, pp. 1–1, 2021.

[23] C. Burgos-Mellado, J. Llanos, E. Espina, D. Saez, R. Cárdenas, M. Sumner, and A. Watson, "Single-phase consensus-based control for regulating voltage and sharing unbalanced currents in 3-wire isolated ac microgrids," *IEEE Access*, vol. 8, pp. 164 882–164 898, Sep. 2020.

[24] A. S. Vijay, S. Doolla, and M. C. Chandorkar, "Unbalance mitigation strategies in microgrids," *IET Power Electron.*, vol. 13, no. 9, pp. 1687–1710, Jul. 2020.

[25] V. Gali, N. Gupta, and R. Gupta, "Mitigation of power quality problems using shunt active power filters: A comprehensive review," in *2017 12th IEEE Conference on Industrial Electronics and Applications (ICIEA)*. IEEE, Jun. 2017, pp. 1100–1105.

[26] C. Burgos-Mellado, C. Hernández-Carimán, R. Cárdenas, D. Sáez, M. Sumner, A. Costabeber, and H. K. Morales Paredes, "Experimental evaluation of a cpt-based four-leg active power compensator for distributed generation," *IEEE Trans. Emerg. Sel. Topics Power Electron.*, vol. 5, no. 2, pp. 747–759, Nov. 2017.

[27] A. Mortezaei, M. G. Simões, M. Savaghebi, J. M. Guerrero, and A. Al-Durra, "Cooperative control of multi-master–slave islanded microgrid with power quality enhancement based on conservative power theory," *IEEE transactions on smart grid*, vol. 9, no. 4, pp. 2964–2975, Jul. 2016.

[28] H. M. Munir, R. Ghannam, H. Li, T. Younas, N. A. Golilarz, M. Hassan, and A. Siddique, "Control of distributed generators and direct harmonic voltage controlled active power filters for accurate current sharing and power quality improvement in islanded microgrids," *Inventions*, vol. 4, no. 2, p. 27, May 2019.

[29] D. I. Brandao, T. Caldognetto, F. P. Marafão, M. G. Simões, J. A. Pomilio, and P. Tenti, "Centralized control of distributed single-phase inverters arbitrarily connected to three-phase four-wire microgrids," *IEEE Transactions on Smart Grid*, vol. 8, no. 1, pp. 437–446, Jan. 2016.

[30] X. Zhou, F. Tang, P. C. Loh, X. Jin, and W. Cao, "Four-leg converters with improved common current sharing and selective voltage-quality enhancement for islanded microgrids," *IEEE Trans. Power Deliv.*, vol. 31, no. 2, pp. 522–531, Jun. 2016.

[31] B. Liu, Z. Liu, J. Liu, R. An, H. Zheng, and Y. Shi, "An adaptive virtual impedance control scheme based on small-ac-signal injection for unbalanced and harmonic power sharing in islanded microgrids," *IEEE Transactions on Power Electronics*, vol. 34, no. 12, pp. 12 333–12 355, Dec. 2019.

[32] Y. Karimi, H. Oraee, and J. M. Guerrero, "Decentralized method for load sharing and power management in a hybrid single/three-phase-islanded microgrid consisting of hybrid source pv/battery units," *IEEE Transactions on Power Electronics*, vol. 32, no. 8, pp. 6135–6144, Aug. 2016.

[33] C. Burgos-Mellado, R. Cardenas, D. Saez, A. Costabeber, and M. Sumner, "A control algorithm based on the conservative power theory for cooperative sharing of imbalances in four-wire systems," *IEEE Trans. Power Electron.*, vol. 34, no. 6, pp. 5325–5339, Sep. 2019.

[34] L. Meng, F. Tang, M. Savaghebi, J. C. Vásquez, and J. M. Guerrero, "Tertiary control of voltage unbalance compensation for optimal power quality in islanded microgrids," *IEEE Trans. on Energy Conversion*, vol. 29, no. 4, pp. 802–815, Jul. 2014.

[35] M. Savaghebi, A. Jalilian, J. C. Vásquez, and J. M. Guerrero, "Secondary control for voltage quality enhancement in microgrids," *IEEE Trans. Smart Grid*, vol. 3, no. 4, pp. 1893–1902, Jul. 2012.

[36] D. I. Brandao, L. S. Araujo, A. M. S. Alonso, G. L. dos Reis, E. V. Liberado, and F. P. Marafão, "Coordinated control of distributed three-and single-phase inverters connected to three-phase three-wire microgrids," *IEEE Trans. Emerg. Sel. Topics Power Electron.*, pp. 1–1, 2019.

[37] L. Meng, X. Zhao, F. Tang, M. Savaghebi, T. Dragicevic, J. C. Vásquez, and J. M. Guerrero, "Distributed voltage unbalance compensation in islanded microgrids by using a dynamic consensus algorithm," *IEEE Trans. Power Electron.*, vol. 31, no. 1, pp. 827–838, Jan. 2016.

[38] J. Zhou, S. Kim, H. Zhang, Q. Sun, and R. Han, "Consensus-based distributed control for accurate reactive, harmonic, and imbalance power sharing in microgrids," *IEEE Trans. Smart Grid*, vol. 9, no. 4, pp. 2453–2467, Jul. 2018.

[39] C. Burgos-Mellado, J. J. Llanos, R. Cardenas, D. Saez, D. E. Olivares, M. Sumner, and A. Costabeber, "Distributed control strategy based on a consensus algorithm and on the conservative power theory for imbalance and harmonic sharing in 4-wire microgrids," *IEEE Trans. Smart Grid*, vol. 11, no. 2, pp. 1604–1619, Mar. 2020.

[40] IEEE Standard Association, *IEEE Std. 1547-2018. Standard for interconnection and interoperability of distributed energy resources with associated electric power systems interfaces.* IEEE, 2018.

[41] Y. Khayat, Q. Shafiee, R. Heydari, M. Naderi, T. Dragičević, J. W. Simpson-Porco, F. Dörfler, M. Fathi, F. Blaabjerg, J. M. Guerrero, and H. Bevrani, "On the secondary control architectures of ac microgrids: An overview," *IEEE Trans. Power Electron.*, vol. 35, no. 6, pp. 6482–6500, Jun. 2020.

[42] F. L. Lewis, H. Zhang, K. Hengster-Movric, and A. Das, *Cooperative Control of Multi-Agent Systems*, ser. Communications and Control

Engineering. London: Springer London, 2014. [Online]. Available: http://link.springer.com/10.1007/978-1-4471-5574-4

[43] E. Espina, R. Cardenas-Dobson, J. W. Simpson-Porco, D. Saez, and M. Kazerani, "A Consensus-Based Secondary Control Strategy for Hybrid AC/DC Microgrids with Experimental Validation," *IEEE Trans. Power Electron.*, vol. 36, no. 5, pp. 5971–5984, May 2021.

[44] Q. Shafiee, V. Nasirian, J. C. Vasquez, J. M. Guerrero, and A. Davoudi, "A multi-functional fully distributed control framework for ac microgrids," *IEEE Trans. Smart Grid*, vol. 9, no. 4, pp. 3247–3258, Jul. 2018.

[45] C. Bordons, F. Garcia-Torres, and M. A. Ridao, *Model predictive control of microgrids*, 1st ed., ser. Advances in Industrial Control. Springer International Publishing, 2020.

[46] J. Hu, Y. Shan, J. M. Guerrero, A. Ioinovici, K. W. Chan, and J. Rodriguez, "Model predictive control of microgrids – an overview," *Renew. Sust. Energ. Rev.*, vol. 136, p. 110422, Feb. 2021.

[47] E. F. Camacho and C. Bordons, "Constrained model predictive control," in *Model Predictive Control*, 2nd ed., ser. Advanced Textbooks in Control and Signal Processing. London: Springer London, 2007.

[48] O. Babayomi, Z. Zhang, T. Dragicevic, R. Heydari, Y. Li, C. Garcia, J. Rodriguez, and R. Kennel, "Advances and opportunities in the model predictive control of microgrids: Part II–Secondary and tertiary layers," *Int. J. Electr. Power Energy Syst.*, vol. 134, p. 107339, Jan. 2022.

[49] J. S. Gomez, D. Saez, J. W. Simpson-Porco, and R. Cardenas, "Distributed predictive control for frequency and voltage regulation in microgrids," *IEEE Trans. Smart Grid*, vol. 11, no. 2, pp. 1319–1329, Mar. 2020.

[50] Q. Sun, J. Zhou, J. M. Guerrero, and H. Zhang, "Hybrid three-phase/single-phase microgrid architecture with power management capabilities," *IEEE Trans. Power Electron.*, vol. 30, no. 10, pp. 5964–5977, Oct. 2015.

[51] S. A. Raza and J. Jiang, "Intra-and inter-phase power management and control of a residential microgrid at the distribution level," *IEEE Trans. Smart Grid*, vol. 10, no. 6, pp. 6839–6848, Nov. 2019.

[52] D. I. Brandao, W. M. Ferreira, A. M. S. Alonso, E. Tedeschi, and F. P. Marafão, "Optimal multiobjective control of low-voltage ac microgrids: Power flow regulation and compensation of reactive power and unbalance," *IEEE Trans. Smart Grid*, vol. 11, no. 2, pp. 1239–1252, Mar. 2020.

[53] E. Espina, R. Cárdenas-Dobson, M. B. Espinoza, C. Burgos-Mellado, and D. Saez, "Cooperative regulation of imbalances in three-phase four-wire microgrids using single-phase droop control and secondary control

algorithms," *IEEE Trans. Power Electron.*, vol. 35, no. 2, pp. 1978–1992, Feb. 2020.

[54] J. Vásquez, J. Guerrero, M. Savaghebi, E. G. Carrasco, and R. Teodorescu, "Modeling, analysis, and design of stationary reference frame droop controlled parallel three-phase voltage source inverters," *IEEE Trans. Ind. Electron.*, vol. 60, pp. 1271–1280, Apr. 2013.

[55] S. Parhizi, H. Lotfi, A. Khodaei, and S. Bahramirad, "State of the art in research on microgrids: A review," *IEEE Access*, vol. 3, pp. 890–925, Jun. 2015.

[56] G. S. Rawat and Sathans, "Survey on DC microgrid architecture, power quality issues and control strategies," in *2018 2nd Int. Conf. Inven. Syst. Control*, no. Icisc.   IEEE, Jan. 2018, pp. 500–505.

[57] A. Bidram and A. Davoudi, "Hierarchical structure of microgrids control system," *IEEE Trans. Smart Grid*, vol. 3, no. 4, pp. 1963–1976, Dec. 2012.

[58] F. Dörfler, J. W. Simpson-Porco, and F. Bullo, "Breaking the hierarchy: Distributed control and economic optimality in microgrids," *IEEE Trans. Control Netw. Syst.*, vol. 3, no. 3, pp. 241–253, Sep. 2016.

[59] Z. Li, Z. Cheng, J. Liang, J. Si, L. Dong, and S. Li, "Distributed event-triggered secondary control for economic dispatch and frequency restoration control of droop-controlled AC microgrids," *IEEE Trans. Sustain. Energy*, vol. 11, no. 3, pp. 1938–1950, Jul. 2020.

[60] X. Feng, A. Shekhar, F. Yang, R. E. Hebner, and P. Bauer, "Comparison of hierarchical control and distributed control for microgrid," *Electr. Power Components Syst.*, vol. 45, no. 10, pp. 1043–1056, Jul. 2017.

[61] T. Dragičević, X. Lu, J. C. Vasquez, and J. M. Guerrero, "Dc microgrids—part i: A review of control strategies and stabilization techniques," *IEEE Transactions on Power Electronics*, vol. 31, no. 7, pp. 4876–4891, Jul 2016.

[62] Q. Shafiee, T. Dragičević, J. C. Vasquez, and J. M. Guerrero, "Hierarchical control for multiple dc-microgrids clusters," *IEEE Transactions on Energy Conversion*, vol. 29, no. 4, pp. 922–933, Dec 2014.

[63] M. Ben Said-Romdhane, M. W. Naouar, I. S. Belkhodja, and E. Monmasson, "An Improved LCL Filter Design in Order to Ensure Stability without Damping and Despite Large Grid Impedance Variations," *Energies 2017, Vol. 10, Page 336*, vol. 10, no. 3, p. 336, Mar. 2017.

[64] Y.-J. Kim and H. Kim, "Optimal design of LCL filter in grid-connected inverters," *IET Power Electron.*, vol. 12, no. 7, pp. 1774–1782, Jun. 2019.

[65] J. Hu, J. M. Guerrero, and S. Islam, *Model predictive control for microgrids from power electronic converters to energy management*, ser. IET energy engineering series 199.   London: The Institution of Engineering and Technology, 2021.

[66] A. Mehrizi-Sani and R. Iravani, "Secondary control for microgrids using potential functions : Modeling issues," in *Conference on Power Systems*, 2009.

[67] J. W. Simpson-Porco, Q. Shafiee, F. Dorfler, J. C. Vasquez, J. M. Guerrero, and F. Bullo, "Secondary frequency and voltage control of islanded microgrids via distributed averaging," *IEEE Trans. Ind. Electron.*, vol. 62, no. 11, pp. 7025–7038, Nov. 2015.

[68] A. Parisio, C. Wiezorek, T. Kyntäjä, J. Elo, K. Strunz, and K. H. Johansson, "Cooperative MPC-based energy management for networked microgrids," *IEEE Trans. Smart Grid*, vol. 8, no. 6, pp. 3066–3074, Aug. 2017.

[69] D. E. Olivares, C. A. Cañizares, and M. Kazerani, "A centralized energy management system for isolated microgrids," *IEEE Transactions on Smart Grid*, vol. 5, no. 4, pp. 1864–1875, July 2014.

[70] D. E. Olivares, C. A. Canizares, and M. Kazerani, "A centralized optimal energy management system for microgrids," in *2011 IEEE Power and Energy Society General Meeting*, July 2011, pp. 1–6.

[71] O. Cartagena, S. Parra, D. Muñoz-Carpintero, L. G. Marín, and D. Sáez, "Review on fuzzy and neural prediction interval modelling for nonlinear dynamical systems," *IEEE Access*, vol. 9, pp. 23 357–23 384, 2021.

[72] B. V. Solanki, A. Raghurajan, K. Bhattacharya, and C. A. Cañizares, "Including smart loads for optimal demand response in integrated energy management systems for isolated microgrids," *IEEE Transactions on Smart Grid*, vol. 8, no. 4, pp. 1739–1748, Jul. 2017.

[73] B. V. Solanki, K. Bhattacharya, and C. A. Cañizares, "A sustainable energy management system for isolated microgrids," *IEEE Transactions on Sustainable Energy*, vol. 8, no. 4, pp. 1507–1517, Oct 2017.

[74] B. V. Solanki, C. A. Cañizares, and K. Bhattacharya, "Practical energy management systems for isolated microgrids," *IEEE Transactions on Smart Grid*, pp. 1–1, Sep. 2018.

[75] I. A. Sajjad, G. Chicco, and R. Napoli, "Effect of aggregation level and sampling time on load variation profile — a statistical analysis," in *MELECON 2014 - 2014 17th IEEE Mediterranean Electrotechnical Conference*, Apr 2014, pp. 208–212.

[76] M. Shahbazi and A. Khorsandi, "Power Electronic Converters in Microgrid Applications," *Microgrid: Advanced Control Methods and Renewable Energy System Integration*, pp. 281–309, jan 2017.

[77] P. C. Loh, D. Li, Y. K. Chai, and F. Blaabjerg, "Autonomous operation of hybrid microgrid with ac and dc subgrids," *IEEE Trans. Power Electron.*, vol. 28, no. 5, pp. 2214–2223, May 2013.

[78] H. J. Yoo, T. T. Nguyen, and H. M. Kim, "Consensus-based distributed coordination control of hybrid AC/DC microgrids," *IEEE Trans. Sustain. Energy*, vol. 11, no. 2, pp. 629–639, Apr. 2020.

[79] J.-W. Chang, G.-S. Lee, S.-I. Moon, and P.-I. Hwang, "A novel distributed control method for interlinking converters in an islanded hybrid ac/dc microgrid," *IEEE Trans. Smart Grid*, vol. 12, no. 5, pp. 3765–3779, Sep. 2021.

[80] G. A. Papafotiou, G. D. Demetriades, and V. G. Agelidis, "Technology readiness assessment of model predictive control in medium-and high-voltage power electronics," *IEEE Trans. Ind. Electron.*, vol. 63, no. 9, pp. 5807–5815, Jan. 2016.

[81] A. Andersson and T. Thiringer, "Assessment of an improved finite control set model predictive current controller for automotive propulsion applications," *IEEE Trans. Ind. Electron.*, vol. 67, no. 1, pp. 91–100, Feb. 2019.

[82] F. Mehmood, B. Khan, S. M. Ali, and J. A. Rossiter, "Distributed model predictive based secondary control for economic production and frequency regulation of MG," *IET Control Theory Appl.*, vol. 13, no. 17, pp. 2948–2958, Nov. 2019.

[83] L. Liang, Y. Hou, and D. J. Hill, "Design guidelines for MPC-based frequency regulation for islanded microgrids with storage, voltage, and ramping constraints," *IET Renew. Power Gener.*, vol. 11, no. 8, pp. 1200–1210, Jul. 2017.

[84] Y. Du, J. Wu, S. Li, C. Long, and S. Onori, "Coordinated energy dispatch of autonomous microgrids with distributed MPC optimization," *IEEE Trans. Ind. Informat.*, vol. 15, no. 9, pp. 5289–5298, Feb. 2019.

[85] J. Rossiter, *A First Course in Predictive Control*. CRC Press, 2018. [Online]. Available: https://books.google.cl/books?id=q30StAEACAAJ

[86] K. J. Åström and B. Wittenmark, *Adaptive Control*. Addison-Wesley, 1989.

[87] Z. Guo, S. Li, and Y. Zheng, "Feedback linearization based distributed model predictive control for secondary control of islanded microgrid," *Asian J. Control*, vol. 22, no. 1, pp. 460–473, Jan. 2020.

[88] C. Ahumada, R. Cárdenas, D. Sáez, and J. M. Guerrero, "Secondary Control Strategies for Frequency Restoration in Islanded Microgrids With Consideration of Communication Delays," *IEEE Transactions on Smart Grid*, vol. 7, no. 3, pp. 1430–1441, May 2016.

[89] J. Rossiter, *Model-Based Predictive Control: A Practical Approach (Control Series)*, 1st ed. CRC Press, 2017.

[90] R. Holiš and V. Bobál, "Model predictive control of time-delay systems with measurable disturbance compensation," in *2015 20th International Conference on Process Control (PC)*, 2015, pp. 209–214.

[91] G. Lou, W. Gu, Y. Xu, M. Cheng, and W. Liu, "Distributed mpc-based secondary voltage control scheme for autonomous droop-controlled microgrids," *IEEE Trans. Sustain. Energy*, vol. 8, no. 2, pp. 792–804, Apr. 2017.

[92] K. Liu, T. Liu, Z. Tang, and D. J. Hill, "Distributed MPC-based frequency control in networked microgrids with voltage constraints," *IEEE Trans. Smart Grid*, vol. 10, no. 6, pp. 6343–6354, Nov. 2019.

[93] Z. Guo, H. Jiang, Y. Zheng, and S. Li, "Distributed model predictive control for efficient operation of islanded microgrid," in *2017 Chinese Automation Congress (CAC)*. Institute of Electrical and Electronics Engineers Inc., Oct. 2017, pp. 6253–6258.

[94] R. Reginatto and R. A. Ramos, "On electrical power evaluation in dq coordinates under sinusoidal unbalanced conditions," *IET Gener. Transm. Distrib.*, vol. 8, no. 5, pp. 976–982, May 2014.

[95] S. V. Viscido, J. K. Parrish, and D. Grünbaum, "The effect of population size and number of influential neighbors on the emergent properties of fish schools," *Ecol. Modell.*, vol. 183, no. 2, pp. 347 – 363, Apr. 2005.

[96] F. Guo, C. Wen, J. Mao, and Y. Song, "Distributed secondary voltage and frequency restoration control of droop-controlled inverter-based microgrids," *IEEE Trans. Ind. Electron.*, vol. 62, no. 7, pp. 4355–4364, Jul. 2015.

[97] B. Wei, Y. Gui, S. Trujillo, J. M. Guerrero, and J. C. Vásquez, "Distributed average integral secondary control for modular ups systems-based microgrids," *IEEE Trans. Power Electron.*, vol. 34, no. 7, pp. 6922–6936, Jul. 2019.

[98] Y. Han, K. Zhang, H. Li, E. A. A. Coelho, and J. M. Guerrero, "Mas-based distributed coordinated control and optimization in microgrid and microgrid clusters: A comprehensive overview," *IEEE Trans. Power Electron.*, vol. 33, no. 8, pp. 6488–6508, Aug. 2018.

[99] G. Chen and Z. Guo, "Distributed secondary and optimal active power sharing control for islanded microgrids with communication delays," *IEEE Trans. Smart Grid*, vol. 10, no. 2, pp. 2002–2014, Mar. 2019.

[100] C. Li, J. C. Vasquez, and J. M. Guerrero, "Convergence analysis of distributed control for operation cost minimization of droop controlled DC microgrid based on multiagent," in *Conference Proceedings - IEEE Applied Power Electronics Conference and Exposition - APEC*, vol. 2016-May. Institute of Electrical and Electronics Engineers Inc., may 2016, pp. 3459–3464.

[101] G. Chen and Z. Zhao, "Delay Effects on Consensus-Based Distributed Economic Dispatch Algorithm in Microgrid," *IEEE Transactions on Power Systems*, vol. 33, no. 1, pp. 602–612, may 2017.

[102] T. Zhao and Z. Ding, "Distributed agent consensus-based optimal resource management for microgrids," *IEEE Transactions on Sustainable Energy*, vol. 9, no. 1, pp. 443–452, Jan 2018.

[103] Z. Wang, W. Wu, and B. Zhang, "A fully distributed power dispatch method for fast frequency recovery and minimal generation cost in autonomous microgrids," *IEEE Transactions on Smart Grid*, vol. 7, no. 1, pp. 19–31, Jan 2016.

[104] Y. Xu and Z. Li, "Distributed optimal resource management based on the consensus algorithm in a microgrid," *IEEE Transactions on Industrial Electronics*, vol. 62, no. 4, pp. 2584–2592, Apr 2015.

[105] X. He, J. Yu, T. Huang, and C. Li, "Distributed power management for dynamic economic dispatch in the multimicrogrids environment," *IEEE Transactions on Control Systems Technology*, vol. 27, no. 4, pp. 1651–1658, Jul 2019.

[106] C. Li, X. Yu, T. Huang, and X. He, "Distributed optimal consensus over resource allocation network and its application to dynamical economic dispatch," *IEEE Transactions on Neural Networks and Learning Systems*, vol. 29, no. 6, pp. 2407–2418, Jun 2018.

[107] B. Huang, L. Liu, Y. Li, and H. Zhang, "Distributed optimal energy management for microgrids in the presence of time-varying communication delays," *IEEE Access*, vol. 7, pp. 83 702–83 712, Jun. 2019.

[108] P. Lü, J. Zhao, J. Yao, and S. Yang, "A decentralized approach for frequency control and economic dispatch in smart grids," *IEEE Journal on Emerging and Selected Topics in Circuits and Systems*, vol. 7, no. 3, pp. 447–458, Sep. 2017.

[109] M. Hamdi, M. Chaoui, L. Idoumghar, and A. Kachouri, "Coordinated consensus for smart grid economic environmental power dispatch with dynamic communication network," *IET Generation, Transmission Distribution*, vol. 12, no. 11, pp. 2603–2613, Jun 2018.

[110] H. Xing, Z. Lin, M. Fu, and B. F. Hobbs, "Distributed algorithm for dynamic economic power dispatch with energy storage in smart grids," *IET Control Theory Applications*, vol. 11, no. 11, pp. 1813–1821, Jul 2017.

[111] A. Gabash and P. Li, "Active-reactive optimal power flow in distribution networks with embedded generation and battery storage," *IEEE Transactions on Power Systems*, vol. 27, no. 4, pp. 2026–2035, 2012.

[112] Y. Zhao, M. Irving, and Y. Song, "A cost allocation and pricing method for reactive power service in the new deregulated electricity market environment," in *2005 IEEE/PES Transmission Distribution Conference Exposition: Asia and Pacific*, 2005, pp. 1–6.

[113] S. M. Sadek, W. A. Omran, M. A. M. Hassan, and H. E. A. Talaat, "Data driven stochastic energy management for isolated microgrids based on generative adversarial networks considering reactive power capabilities of distributed energy resources and reactive power costs," *IEEE Access*, vol. 9, pp. 5397–5411, 2021.

[114] M. M. Gomez, C. Burgos Mellado, and R. C. Dobson, "Distributed control for a cost-based droop-free microgrid," in *2020 IEEE 21st Workshop on Control and Modeling for Power Electronics (COMPEL)*, 2020, pp. 1–7.

[115] I. Khan, Z. Li, Y. Xu, and W. Gu, "Distributed control algorithm for optimal reactive power control in power grids," *International Journal of Electrical Power & Energy Systems*, vol. 83, pp. 505–513, 2016.

[116] V. Nasirian, F. L. Lewis, and A. Davoudi, "Distributed optimal dispatch for DC distribution networks," in *2015 IEEE 1st Int. Conf. Direct Curr. Microgrids, ICDCM 2015*. Institute of Electrical and Electronics Engineers Inc., Jul. 2015, pp. 97–101.

[117] S. Moayedi and A. Davoudi, "Unifying Distributed Dynamic Optimization and Control of Islanded DC Microgrids," in *IEEE Trans. Power Electron.*, vol. 32, no. 3. Institute of Electrical and Electronics Engineers Inc., Mar. 2017, pp. 2329–2346.

[118] J. Hu, J. Duan, H. Ma, and M.-Y. Chow, "Distributed adaptive droop control for optimal power dispatch in dc microgrid," *IEEE Transactions on Industrial Electronics*, vol. 65, no. 1, pp. 778–789, 2018.

[119] H. Han, H. Wang, Y. Sun, J. Yang, and Z. Liu, "Distributed control scheme on cost optimisation under communication delays for DC microgrids," *IET Gener. Transm. Distrib.*, vol. 11, no. 17, pp. 4193–4201, Nov 2017.

[120] A. Hussain, V.-H. Bui, and H.-M. Kim, "Robust optimal operation of ac/dc hybrid microgrids under market price uncertainties," *IEEE Access*, vol. 6, pp. 2654–2667, 2018.

[121] A. Maulik and D. Das, "Optimal power dispatch considering load and renewable generation uncertainties in an AC–DC hybrid microgrid," *IET Gener. Transm. Distrib.*, vol. 13, no. 7, pp. 1164–1176, apr 2019.

[122] P. Buduma, M. K. Das, S. Mishra, and G. Panda, "Robust power management and control for hybrid ac-dc microgrid," in *2020 3rd International Conference on Energy, Power and Environment: Towards Clean Energy Technologies*, 2021, pp. 1–6.

[123] K. Zhang, M. Su, Y. Sun, P. Wu, Z. Luo, and H. Han, "A novel distributed control for hybrid ac/dc microgrid with consideration of power limit," in *2021 IEEE 12th Energy Conversion Congress Exposition - Asia (ECCE-Asia)*, 2021, pp. 1856–1859.

[124] P. Lin, C. Jin, J. Xiao, X. Li, D. Shi, Y. Tang, and P. Wang, "A distributed control architecture for global system economic operation in autonomous hybrid ac/dc microgrids," *IEEE Transactions on Smart Grid*, vol. 10, no. 3, pp. 2603–2617, 2019.

[125] P. Yang, M. Yu, Q. Wu, P. Wang, Y. Xia, and W. Wei, "Decentralized economic operation control for hybrid ac/dc microgrid," *IEEE Transactions on Sustainable Energy*, vol. 11, no. 3, pp. 1898–1910, 2020.

[126] Z. Zhao, J. Zhang, B. Yan, R. Cheng, C. S. Lai, L. Huang, Q. Guan, and L. L. Lai, "Decentralized Finite Control Set Model Predictive Control Strategy of Microgrids for Unbalanced and Harmonic Power Management," *IEEE Access*, vol. 8, pp. 202 298–202 311, Oct. 2020.

[127] J. Liu, Y. Miura, and T. Ise, "Cost-Function-Based Microgrid Decentralized Control of Unbalance and Harmonics for Simultaneous Bus Voltage Compensation and Current Sharing," *IEEE Trans. Power Electron.*, vol. 34, no. 8, pp. 7397–7410, Aug. 2019.

[128] S. R. Mohapatra and V. Agarwal, "Model Predictive Control for Flexible Reduction of Active Power Oscillation in Grid-Tied Multilevel Inverters under Unbalanced and Distorted Microgrid Conditions," *IEEE Trans. Ind. Appl.*, vol. 56, no. 2, pp. 1107–1115, Mar. 2020.

[129] M. Yazdanian and A. Mehrizi-Sani, "Distributed control techniques in microgrids," *IEEE Trans. Smart Grid*, vol. 5, no. 6, pp. 2901–2909, Nov. 2014.

[130] S. Boyd and L. Vandenberghe, *Convex optimization*. USA: Cambridge University Press, 2004.

[131] P. Kundur, *Power system stability and control*. McGraw-Hill, 1994, vol. 7.

[132] A. E. Leon and J. A. Solsona, "Design of reduced-order nonlinear observers for energy conversion applications," *IET Control Theory Appl.*, vol. 4, no. 5, pp. 724–734, May 2010.

[133] F. Bullo, *Lectures on network systems*, 1st ed. Kindle Direct Publishing, 2020, with contributions by J. Cortes, F. Dorfler, and S. Martinez. [Online]. Available: http://motion.me.ucsb.edu/book-lns

[134] W. Ren, R. W. Beard, and E. M. Atkins, "Information consensus in multivehicle cooperative control," *IEEE Control Syst.*, vol. 27, no. 2, pp. 71–82, Jul. 2007.

[135] I. Serban, S. Cespedes, C. Marinescu, C. A. Azurdia-Meza, J. S. Gomez, and D. Saez Hueichapan, "Communication requirements in microgrids: A practical survey," *IEEE Access*, vol. 8, pp. 47 694–47 712, Mar. 2020.

[136] Z. Wang, S. Mei, F. Liu, P. Yi, and M. Cao, "Asynchronous Distributed Power Control of Multi-Microgrid Systems Based on the Operator Splitting Approach," *arXiv*, Oct 2018.

[137] C. Schmid and L. T. Biegler, "Quadratic programming methods for reduced hessian sqp," *Comput. Chem. Eng.*, vol. 18, no. 9, pp. 817–832, Sep. 1994.

[138] Y. jun Zhang and Z. Ren, "Optimal reactive power dispatch considering costs of adjusting the control devices," *IEEE Trans. Power Syst*, vol. 20, no. 3, pp. 1349–1356, Aug. 2005.

[139] J. Solsona and A. Leon, "Design of reduced-order nonlinear observers for energy conversion applications," *IET Control Theory Appl.*, vol. 4, no. 5, pp. 724–734, Jul. 2010.

Appendix A

# Design of a reduced order nonlinear observer to estimate the voltage after a coupling inductance

In this appendix, we provide an explanation of the application of the reduced-order non-linear observer proposed in [139] to estimate the voltage $(\hat{V}_i^B)$ after the coupling inductance (L_i). For a complete description of the demonstration of the observer, the reader is encouraged to read the aforementioned work. Consider a class of nonlinear system given by

$$\dot{\mathbf{x}} = \mathbf{F}\left(\mathbf{x}_a, \mathbf{u}\right)\mathbf{x} + \mathbf{g}\left(\mathbf{x}_a, \mathbf{u}\right) \tag{A.1}$$

where $\mathbf{x} \in \mathbb{R}^{n \times 1}$ is the state vector and $\mathbf{u} \in \mathbb{R}^{m \times 1}$ is the input vector, with $\mathbf{F} \in \mathbb{R}^{n \times n}$ and $\mathbf{g} \in \mathbb{R}^{n \times 1}$. The state vector can be partionated as $\mathbf{x} = \left[\mathbf{x}_a\ \mathbf{x}_b\right]^T$, where $\mathbf{x}_a \in \mathbb{R}^{n_a \times 1}$ contains measurable variables and $\mathbf{x}_b \in \mathbb{R}^{n_b \times 1}$ contains non-measurable variables. The representation of (A.1) can be rewritten as follows.

$$\begin{bmatrix} \dot{\mathbf{x}}_a \\ \dot{\mathbf{x}}_b \end{bmatrix} = \begin{bmatrix} \mathbf{N}\left(\mathbf{x}_a, \mathbf{u}\right) & \mathbf{M}\left(\mathbf{x}_a, \mathbf{u}\right) \\ \mathbf{R}\left(\mathbf{x}_a, \mathbf{u}\right) & \mathbf{S}\left(\mathbf{x}_a, \mathbf{u}\right) \end{bmatrix} \begin{bmatrix} \mathbf{x}_a \\ \mathbf{x}_b \end{bmatrix} + \begin{bmatrix} \mathbf{g}_a\left(\mathbf{x}_a, \mathbf{u}\right) \\ \mathbf{g}_b\left(\mathbf{x}_a, \mathbf{u}\right) \end{bmatrix} \tag{A.2}$$

The previously described non-linear observer of reduced-order is used to estimate the voltage $(\hat{V}_i^B)$ after the coupling inductance (L_i), as shown at the bottom of Fig. A.1. The observer works in the $\alpha - \beta$ framework. Considering $\hat{V}_{\alpha,i}^B = V_m sin(\theta_i)$ and $\hat{V}_{\beta,i}^B = V_m cos(\theta_i)$, where V_m depends on the $abc - \alpha\beta$ transformation used. Equation (A.3), which represents the estimated states, is obtained deriving both expressions. Where ω_o is the nominal frequency.
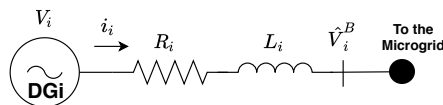
Figure A.1: *Electrical output circuit*

$$\hat{\dot{V}}_{\alpha,i}^B = V_m\omega_o cos(\theta_i) = \omega_o \hat{V}_{\beta,i}^B$$
$$\hat{\dot{V}}_{\beta,i}^B = -V_m\omega_o sin(\theta_i) = -\omega_o \hat{V}_{\alpha,i}^B$$

(A.3)

Equation (A.4), which represents the measured estates, is obtained applying the Kirchhoff's voltage law to the circuit of Fig. A.1. Where R_i represents the cable resistance, and is assumed as $R_i = 0.01\Omega$.

$$L_i\dot{i}_{\alpha,i} = -Ri_{\alpha,i} + V_{\alpha,i} - \hat{V}\alpha, i^B$$
$$L_i\dot{i}_{\beta,i} = -Ri_{\beta,i} + V_{\beta,i} - \hat{V}\beta, i^B$$

(A.4)

The measured states (x_a) and estimated states (x_b) are presented in Equation (A.5). These are obtained expressing (A.3) and (A.4) in the required form of the observer (A.2). Where its inputs are the measured values of the output voltage V_i and the output current i_i (both at the output of the LCL filter, before L_i, and in the $\alpha - \beta$ framework).

$$\underbrace{\begin{bmatrix} \dot{i}_{\alpha,i} \\ \dot{i}_{\beta,i} \end{bmatrix}}_{\dot{x}_a} = \underbrace{\begin{bmatrix} -\frac{R_i}{L_i} & 0 \\ 0 & -\frac{R_i}{L_i} \end{bmatrix}}_{N} \underbrace{\begin{bmatrix} i_{\alpha,i} \\ i_{\beta,i} \end{bmatrix}}_{x_a} + \underbrace{\begin{bmatrix} -\frac{1}{L_i} & 0 \\ 0 & -\frac{1}{L_i} \end{bmatrix}}_{M} \underbrace{\begin{bmatrix} \hat{V}_{\alpha,i}^B \\ \hat{V}_{\beta,i}^B \end{bmatrix}}_{x_b} + \underbrace{\begin{bmatrix} \frac{V_{\alpha,i}}{L_i} \\ \frac{V_{\beta,i}}{L_i} \end{bmatrix}}_{g_a}$$

$$\underbrace{\begin{bmatrix} \hat{\dot{V}}_{\alpha,i}^B \\ \hat{\dot{V}}_{\beta,i}^B \end{bmatrix}}_{\dot{x}_b} = \underbrace{\begin{bmatrix} 0 & 0 \\ 0 & 0 \end{bmatrix}}_{R} \underbrace{\begin{bmatrix} i_{\alpha,i} \\ i_{\beta,i} \end{bmatrix}}_{x_a} + \underbrace{\begin{bmatrix} 0 & \omega_o \\ -\omega_o & 0 \end{bmatrix}}_{S} \underbrace{\begin{bmatrix} \hat{V}_{\alpha,i}^B \\ \hat{V}_{\beta,i}^B \end{bmatrix}}_{x_b} + \underbrace{\begin{bmatrix} 0 \\ 0 \end{bmatrix}}_{g_b}$$

(A.5)

The structure of the observer is presented in (A.6).

$$\dot{\xi} = A_r(\xi + Gw) + B_r$$
$$\hat{\mathbf{x}}_b = \xi + Gw$$

(A.6)

Where $\mathbf{w}$ is a transformation that depends on the measured variables to obtain a linear dynamic of the error.

$$\mathbf{w} = \mathbf{T}(\mathbf{x_a}) = \begin{bmatrix} \omega_1 \\ \omega_2 \end{bmatrix} = \begin{bmatrix} -L_i(i_{\alpha,i} + \frac{\omega_o i_{\beta,i}}{gv}) \\ -L_i(i_{\beta,i} - \frac{\omega_o i_{\alpha,i}}{gv}) \end{bmatrix}$$

(A.7)

The estimation error dynamic $\mathbf{A}_r$ (A.8) is obtained through pole placement so that the observer is able to follow the phase of the estimated voltages, and it is faster than the secondary controller. Finally, the gains gv were placed at -31500, and $\mathbf{B}_r$ is represented in (A.9).

$$\mathbf{A}_r = -\mathbf{G} = \begin{bmatrix} -gv & 0 \\ 0 & -gv \end{bmatrix}$$

(A.8)

$$\mathbf{B}_r = \mathbf{R}\mathbf{x}_a + \mathbf{g}_b - \mathbf{G}\frac{\partial \mathbf{T}}{\partial \mathbf{x}_a}(\mathbf{N}\mathbf{x}_a + \mathbf{g}_a)$$

(A.9)

Appendix B

Derivation of predictive linear models used as equality constraints in *ac* DGs

B.1 Continuous time model for equality constraints

The set of equations (3.6)-(3.8) and (5.1)-(5.4) is rewritten as (B.1). As it was mentioned, (B.1) characterises frequency and voltage droop controllers, phase angle deviation and, the active/reactive power transferred from the i-th DG to the microgrid.

$$\omega_i(t) = \omega_0 + M_{p\omega,i}P_i(t) + \omega_{s,i}(t) \tag{B.1a}$$

$$\delta\theta_i(t) = \theta_i(t) - \hat{\theta}_i^B(t) = \int_0^t \left[\omega_i(\tau) - \hat{\omega}_i^B(\tau)\right]d\tau \tag{B.1b}$$

$$P_i(t) = B_i V_i(t)\hat{V}_i^B(t)\sin(\delta\theta_i(t)) \tag{B.1c}$$

$$V_i(t) = \frac{1}{3}(V_{ia}(t) + V_{ib}(t) + V_{ic}(t)) \tag{B.1d}$$

$$V_{ia}(t) = V_0 + M_{qv,i}Q_{ia}(t) + V_{s,ia}(t) \tag{B.1e}$$

$$V_{ib}(t) = V_0 + M_{qv,i}Q_{ib}(t) + V_{s,ib}(t) \tag{B.1f}$$

$$V_{ic}(t) = V_0 + M_{qv,i}Q_{ic}(t) + V_{s,ic}(t) \tag{B.1g}$$

$$Q_i(t) = Q_{ia}(t) + Q_{ib}(t) + Q_{ic}(t) \tag{B.1h}$$

$$Q_{ia}(t) = B_i \left[V_{ia}(t)^2 - V_{ia}(t) \hat{V}_{ia}^B(t) \cos(\delta\theta_i(t)) \right] \tag{B.1i}$$

$$Q_{ib}(t) = B_i \left[V_{ib}(t)^2 - V_{ib}(t) \hat{V}_{ib}^B(t) \cos(\delta\theta_i(t)) \right] \tag{B.1j}$$

$$Q_{ic}(t) = B_i \left[V_{ic}(t)^2 - V_{ic}(t) \hat{V}_{ic}^B(t) \cos(\delta\theta_i(t)) \right] \tag{B.1k}$$

Proof. **Balanced Case**

Assumption 1 *A balanced microgrid satisfies:*

$$V_{ia}(t) = V_{ib}(t) = V_{ic}(t) = V_{ix}(t) \ ; \ V_{s,ia}(t) = V_{s,ib}(t) = V_{s,ic}(t) = V_{s,ix}(t) \ ;$$
$$\hat{V}_{ia}^B(t) = \hat{V}_{ib}^B(t) = \hat{V}_{ic}^B(t) = \hat{V}_{ix}^B(t) \tag{B.2}$$

Therefore:
from (B.1h) to (B.1k)

$$Q_i(t) = B_i \left[V_{ia}(t)^2 - V_{ia}(t) \hat{V}_{ia}^B(t) \cos(\delta\theta_i(t)) \right] +$$
$$B_i \left[V_{ib}(t)^2 - V_{ib}(t) \hat{V}_{ib}^B(t) \cos(\delta\theta_i(t)) \right] +$$
$$B_i \left[V_{ic}(t)^2 - V_{ic}(t) \hat{V}_{ic}^B(t) \cos(\delta\theta_i(t)) \right] \tag{B.3}$$

$$Q_i(t) = 3B_i \left[V_{ix}(t)^2 - V_{ix}(t) \hat{V}_{ix}^B(t) \cos(\delta\theta_i(t)) \right] \tag{B.4}$$

from (B.1d) to (B.1g)

$$V_i(t) = \frac{1}{3} \left[V_0 + M_{qv,i} Q_{ia}(t) + V_{s,ia}(t) + V_0 + M_{qv,i} Q_{ib}(t) + V_{s,ib}(t) + V_0 \right] +$$
$$\frac{1}{3} \left[V_0 + M_{qv,i} Q_{ic}(t) + V_{s,ic}(t) \right] \tag{B.5}$$

$$V_i(t) = \frac{1}{3} \left[3V_0 + 3M_{qv,i} Q_{ix}(t) + 3V_{s,ix}(t) \right] = V_{ix}(t) \tag{B.6}$$

B.2 Model discretisation

This section details the discretisation of equations (B.1). We use the forward Euler method defined by (B.7). In this case, it is considered that $k = nT_{sec}, n \in \mathbb{Z}^+$, and T_{sec} is the sample time used at secondary control level.

$$T_{sec} \left. \frac{df(t)}{dt} \right|_{t=k} = [f(k+1) - f(k)] = \Delta f(k+1) \tag{B.7}$$

The discretisation process of each equation (model) is detailed as follows:

B.2.1 Droop equations

The linearisation process for the frequency droop equation (B.1a) is detailed as follows. The same procedure is applied to voltage droop equations (B.1e), (B.1f) and (B.1g)

From (B.1a), it is possible to rewrite $\omega_{s,i}(t)$ in function of $\Delta\omega_{s,i}(t)$.

$$\omega_i(t) = \omega_0 + M_{p\omega,i}P_i(t) + \omega_{s,i}(t) \tag{B.8}$$

$$\omega_i(t) = \omega_0 + M_{p\omega,i}P_i(t) + \frac{1}{T_{sec}}\int \Delta\omega_{s,i}(t)dt$$

Deriving both sides and applying forward Euler method:

$$\frac{d\omega_i(t)}{dt} = M_{p\omega,i}\frac{dP_i(t)}{dt} + \frac{1}{T_{sec}}\Delta\omega_{s,i}(t)$$

$$\left.\frac{d\omega_i(t)}{dt}\right|_{t=k} = M_{p\omega,i}\left.\frac{dP_i(t)}{dt}\right|_{t=k} + \frac{1}{T_{sec}}\Delta\omega_{s,i}(k)$$

$$\omega_i(k+1) - \omega_i(k) = M_{p\omega,i}\left[P_i(k+1) - P_i(k)\right] + \Delta\omega_{s,i}(k)$$

$$\omega_i(k+1) = \omega_i(k) + M_{p\omega,i}\left[P_i(k+1) - P_i(k)\right] + \Delta\omega_{s,i}(k) \tag{B.9}$$

$\square$

B.2.2 Phase angle equation

The linearisation process for the phase angle deviation model is shown from (B.10) to (B.12). Two procedures that reach the same result are detailed.

$$\delta\theta_i(t) = \theta_i(t) - \hat{\theta}_i^B(t) = \int_0^t \left[\omega_i(\tau) - \hat{\omega}_i^B(\tau)\right] d\tau \tag{B.10}$$

Procedure 1

$$\delta\theta_i(t) = \int_0^t \left[\omega_i(\tau) - \hat{\omega}_i^B(\tau)\right] d\tau$$

Deriving both sides and applying forward Euler method

$$\left.\frac{d\delta\theta_i(t)}{dt}\right|_{t=k} = \frac{d}{dt}\left[\int_0^t \left[\omega_i(\tau) - \hat{\omega}_i^B(\tau)\right] d\tau\right]_{t=k}$$

$$\delta\theta_i(k+1) - \delta\theta_i(k) = \int_0^{k+1} \left[\omega_i(\tau) - \hat{\omega}_i^B(\tau)\right] d\tau - \int_0^k \left[\omega_i(\tau) - \hat{\omega}_i^B(\tau)\right] d\tau$$

$$\delta\theta_i(k+1) - \delta\theta_i(k) = \int_k^{k+1} \left[\omega_i(\tau) - \hat{\omega}_i^B(\tau)\right] d\tau$$

$$\delta\theta_i(k+1) - \delta\theta_i(k) = T_{sec}[\omega_i(k) - \hat{\omega}_i^B(k)]$$

$$\delta\theta_i(k+1) = \delta\theta_i(k) + T_{sec}[\omega_i(k) - \hat{\omega}_i^B(k)] \tag{B.11}$$

$\square$

Procedure 2

Considering

$$\theta_i(t) = \int_0^t \omega_i(\tau), d\tau$$

Deriving both sides and applying forward Euler method

$$\left.\frac{d\theta_i(t)}{dt}\right|_{t=k} = \left.\frac{d}{dt}\left[\int_0^t \omega_i(\tau), d\tau\right]\right|_{t=k}$$

$$\theta_i(k+1) - \theta_i(k) = \int_0^{k+1} \omega_i(\tau)\,d\tau - \int_0^k \omega_i(\tau)\,d\tau$$

$$\theta_i(k+1) - \theta_i(k) = \int_k^{k+1} \omega_i(\tau)d\tau$$

$$\theta_i(k+1) - \theta_i(k) = T_{sec}\omega_i(k)$$

Then, from (A.1b)

$$\delta\theta_i(k+1) = \theta_i(k+1) - \hat{\theta}_i^B(k+1)$$

$$\delta\theta_i(k+1) = [\theta_i(k) + T_{sec}\omega_i(k)] - [\hat{\theta}_i^B(k) + T_{sec}\hat{\omega}_i^B(k)]$$

Re-ordering the terms

$$\delta\theta_i(k+1) = [\theta_i(k) - \hat{\theta}_i^B(k)] + [T_{sec}\omega_i(k) - T_{sec}\hat{\omega}_i^B(k)]$$

$$\delta\theta_i(k+1) = \delta\theta_i(k) + T_{sec}[\omega_i(k) - \hat{\omega}_i^B(k)] \tag{B.12}$$

$\square$

B.2.3 Power transfer equations

Due to power transfer equations (B.1c) and (B.1i)-(B.1k) are non-linear, these are linearised via a Taylor expansion around the measured/estimated point $p(k) = \{\omega_i(k), \hat{\omega}_i^B(k), V_i(k), V_{ix}(k), \hat{V}_i^B(k), \hat{V}_{ix}^B(k), \delta\theta_i(k), P_i(k), Q_i(k)\}$ with $x=\{a, b, c\}$. Then, the forward Euler discretisation is applied to the linearised equations. The same procedure is applied in equations (B.1c) and (B.1i)-(B.1k), but only the the procedure for (B.1c) is shown in the following.

$$P_i(t) = B_i V_i(t)\hat{V}_i^B(t)\sin\left(\delta\theta_i(t)\right) \tag{B.13}$$

Linearising

$$P_i(t) = P_i(k) + \left.\frac{\partial P_i(t)}{\partial V_i}\right|_{p(k)}[V_i(t) - V_i(k)] + \left.\frac{\partial P_i(t)}{\partial \hat{V}_i^B}\right|_{p(k)}[\hat{V}_i^B(t) - \hat{V}_i^B(k)] + \tag{B.14}$$

$$\left.\frac{\partial P_i(t)}{\partial \delta\theta}\right|_{p(k)}[\delta\theta_i(t) - \delta\theta_i(k)]$$

$$P_i(t) = P_i(k) + K_V[V_i(t) - V_i(k)] + K_{\hat{V}_i^B}[\hat{V}_i^B(t) - \hat{V}_i^B(k)] + K_{\delta\theta}[\delta\theta_i(t) - \delta\theta_i(k)]$$

where

$$K_V = B_i\hat{V}_i^B(k)\sin(\delta\theta_i(k))$$

$$K_{\hat{V}_i^B} = B_i V_i(k)\sin(\delta\theta_i(k))$$

$$K_{\delta\theta} = B_i V_i(k)\hat{V}_i^B(k)\cos(\delta\theta_i(k))$$

Deriving both sides and evaluating at $t = k$

$$\frac{P_i(t)}{dt} = \frac{P_i(k)}{dt}+K_V\frac{d}{dt}[V_i(t)-V_i(k)]+K_{\hat{V}_i^B}\frac{d}{dt}[\hat{V}_i^B(t)-\hat{V}_i^B(k)]+K_{\delta\theta}\frac{d}{dt}[\delta\theta_i(t)-\delta\theta_i(k)]$$

$$\left.\frac{dP_i(t)}{dt}\right|_{t=k} = K_V\left.\frac{dV_i(t)}{dt}\right|_{t=k} + K_{\hat{V}_i^B}\left.\frac{d\hat{V}_i^B(t)}{dt}\right|_{t=k} + K_{\delta\theta}\left.\frac{d\delta\theta_i(t)}{dt}\right|_{t=k}$$

$$P_i(k+1) - P_i(k) = K_V[V_i(k+1) - V_i(k)] + K_{\hat{V}_i^B}[\hat{V}_i^B(k+1) - \hat{V}_i^B(k)]+$$

$$\hspace{8cm}\text{(B.15)}$$

$$K_{\delta\theta}[\delta\theta_i(k+1) - \delta\theta_i(k)]$$

Assuming $\hat{V}_i^B$ is constant

$$\hat{V}_i^B(k+1) - \hat{V}_i^B(k) = 0$$

$$P_i(k+1) = P_i(k) + K_V[V_i(k+1) - V_i(k)] + K_{\delta\theta}[\delta\theta_i(k+1) - \delta\theta_i(k)]$$

Then

$$P_i(k+1) = P_i(k) + [B_i\hat{V}_i^B(k)\sin(\delta\theta_i(k))][V_i(k+1) - V_i(k)]+$$

$$[B_i V_i(k)\hat{V}_i^B(k)\cos(\delta\theta_i(k))][\delta\theta_i(k+1) - \delta\theta_i(k)] \hspace{1cm}\text{(B.16)}$$

$$\square$$

Therefore, the linear-discrete time model used to state the predictive model is summarised in (B.17).

$$\omega_i(k+1)=\omega_i(k)+M_{p\omega,i}[P_i(k+1)-P_i(k)]+\Delta\omega_{s,i}(k) \hspace{1cm}\text{(B.17a)}$$

$$\delta\theta_i(k+1)=\delta\theta_i(k)+T_{sec}\left[\omega_i(k+1)-\hat{\omega}_i^B(k)\right] \hspace{1cm}\text{(B.17b)}$$

$$P_i(k+1)=P_i(k)+[V_i(k+1)-V_i(k)]B_i\hat{V}_i^B(k)\sin(\delta\theta_i(k))+$$

$$[\delta\theta_i(k+1)-\delta\theta_i(k)]B_i V_i(k)\hat{V}_i^B(k)\cos(\delta\theta_i(k)) \hspace{1cm}\text{(B.17c)}$$

$$V_i(k+1)=\frac{1}{3}(V_{ia}(k+1)+V_{ib}(k+1)+V_{ic}(k+1)) \hspace{1cm}\text{(B.17d)}$$

$$V_{ia}(k+1)=V_{ia}(k)+M_{qv,i}[Q_{ia}(k+1)-Q_{ia}(k)]+\Delta V_{s,ia}(k) \hspace{1cm}\text{(B.17e)}$$

$$V_{ib}(k+1)=V_{ib}(k)+M_{qv,i}[Q_{ib}(k+1)-Q_{ib}(k)]+\Delta V_{s,ib}(k) \hspace{1cm}\text{(B.17f)}$$

$$V_{ic}(k+1)=V_{ic}(k)+M_{qv,i}[Q_{ic}(k+1)-Q_{ic}(k)]+\Delta V_{s,ic}(k) \hspace{1cm}\text{(B.17g)}$$

$$Q_i(k+1)=Q_{ia}(k+1)+Q_{ib}(k+1)+Q_{ic}(k+1) \hspace{1cm}\text{(B.17h)}$$

$$Q_{ia}(k+1)=Q_{ia}(k)+[V_{ia}(k+1)-V_{ia}(k)]B_i\left[2V_{ia}(k)-\hat{V}_{ia}^B(k)\cos(\delta\theta_i(k))\right]+$$

$$[\delta\theta_i(k+1)-\delta\theta_i(k)]B_i V_{ia}(k)\hat{V}_{ia}^B(k)\sin(\delta\theta_i(k)) \hspace{1cm}\text{(B.17i)}$$

$$Q_{ib}(k+1)=Q_{ib}(k)+[V_{ib}(k+1)-V_{ib}(k)]B_i\left[2V_{ib}(k)-\hat{V}^B_{ib}(k)\cos(\delta\theta_i(k))\right]+$$
$$[\delta\theta_i(k+1)-\delta\theta_i(k)]B_iV_{ib}(k)\hat{V}^B_{ib}(k)\sin(\delta\theta_i(k)) \tag{B.17j}$$

$$Q_{ic}(k+1)=Q_{ic}(k)+[V_{ic}(k+1)-V_{ic}(k)]B_i\left[2V_{ic}(k)-\hat{V}^B_{ic}(k)\cos(\delta\theta_i(k))\right]+$$
$$[\delta\theta_i(k+1)-\delta\theta_i(k)]B_iV_{ic}(k)\hat{V}^B_{ic}(k)\sin(\delta\theta_i(k)) \tag{B.17k}$$

B.3   Prediction model for equality constraints

From (B.17) it is possible to state the predictive model (B.18) to be used as a set of equality constraints in the optimisation problem. Note that the measured/estimated coefficients at $t = k$ are considered constant along the prediction horizon.

$$\omega_i(k+m)=\omega_i(k+m-1)+M_{p\omega,i}[P_i(k+m)-P_i(k+m-1)]+\!{}_{\Delta}\omega_{s,i}(k+m-1) \tag{B.18a}$$

$$\delta\theta_i(k+m)=\delta\theta_i(k+m-1)+T_{sec}\left[\omega_i(k+m)-\hat{\omega}^B_i(k)\right] \tag{B.18b}$$

$$P_i(k+m)=P_i(k)+[V_i(k+m)-V_i(k)]B_i\hat{V}^B_i(k)\sin(\delta\theta_i(k))+$$
$$[\delta\theta_i(k+m)-\delta\theta_i(k)]B_iV_i(k)\hat{V}^B_i(k)\cos(\delta\theta_i(k)) \tag{B.18c}$$

$$V_i(k+m)=\frac{1}{3}(V_{ia}(k+m)+V_{ib}(k+m)+V_{ic}(k+m)) \tag{B.18d}$$

$$V_{ia}(k+m)=V_{ia}(k+m-1)+M_{qv,i}[Q_{ia}(k+m)-Q_{ia}(k+m-1)]+\!{}_{\Delta}V_{s,ia}(k+m-1) \tag{B.18e}$$

$$V_{ib}(k+m)=V_{ib}(k+m-1)+M_{qv,i}[Q_{ib}(k+m)-Q_{ib}(k+m-1)]+\!{}_{\Delta}V_{s,ib}(k+m-1) \tag{B.18f}$$

$$V_{ic}(k+m)=V_{ic}(k+m-1)+M_{qv,i}[Q_{ic}(k+m)-Q_{ic}(k+m-1)]+\!{}_{\Delta}V_{s,ic}(k+m-1) \tag{B.18g}$$

$$Q_i(k+m)=Q_{ia}(k+m)+Q_{ib}(k+m)+Q_{ic}(k+m) \tag{B.18h}$$

$$Q_{ia}(k+m)=Q_{ia}(k)+[V_{ia}(k+m)-V_{ia}(k)]B_i\left[2V_{ia}(k)-\hat{V}^B_{ia}(k)\cos(\delta\theta_i(k))\right]+$$
$$[\delta\theta_i(k+m)-\delta\theta_i(k)]B_iV_{ia}(k)\hat{V}^B_{ia}(k)\sin(\delta\theta_i(k)) \tag{B.18i}$$

$$Q_{ib}(k+m)=Q_{ib}(k)+[V_{ib}(k+m)-V_{ib}(k)]B_i\left[2V_{ib}(k)-\hat{V}^B_{ib}(k)\cos(\delta\theta_i(k))\right]+$$
$$[\delta\theta_i(k+m)-\delta\theta_i(k)]B_iV_{ib}(k)\hat{V}^B_{ib}(k)\sin(\delta\theta_i(k)) \tag{B.18j}$$

$$Q_{ic}(k+m)=Q_{ic}(k)+[V_{ic}(k+m)-V_{ic}(k)]B_i\left[2V_{ic}(k)-\hat{V}^B_{ic}(k)\cos(\delta\theta_i(k))\right]+$$
$$[\delta\theta_i(k+m)-\delta\theta_i(k)]B_iV_{ic}(k)\hat{V}^B_{ic}(k)\sin(\delta\theta_i(k)) \tag{B.18k}$$

Appendix C

Derivation of predictive linear models used as inequality constraints in *ac* DGs

Inequality constraints are stated to bound the feasible solution space, considering operational requirements. This section presents the procedure to derive inequalities (5.12) and (5.16).

C.1 PVUR inequality

The phase voltage unbalance rate index (PVUR) is defined as (C.1) to quantify the voltage unbalance at the $i-$th DG's output, where $V_i(t)$ is defined as the average voltage magnitude among phases at t. It is required to preserve $PVUR_i(t)$ below to its maximum value $PVUR^*$. Thus, a linear approximation is required to include this model into the optimisation problem.

$$PVUR_i(t) = \frac{max\left\{[|V_{ia}(t)| - V_i(t)], [|V_{ib}(t)| - V_i(t)], [|V_{ic}(t)| - V_i(t)]\right\}}{V_i(t)} \quad \text{(C.1)}$$

$$PVUR_i(t) \leq PVUR^* \quad \text{(C.2)}$$

Considering that $V_{ix}(t) \geq 0$, from (C.1) and (C.2) a set of three inequalities (one per phase) can be stated:

$$\mathcal{F}_{ix}(V_{ia}(t), V_{ib}(t), V_{ic}(t)) = \frac{V_{ix}(t) - V_i(t)}{V_i(t)} \leq PVUR^* \; \forall x = a, b, c \quad \text{(C.3)}$$

Therefore, the linear approximation is defined as (C.4):

$$\mathcal{F}_{ix}(V_{ia}(t), V_{ib}(t), V_{ic}(t)) \approx \mathcal{F}_{ix}(V_{ia}(k), V_{ib}(k), V_{ic}(k)) +$$
$$\left[\frac{\partial \mathcal{F}_{ix}(V_{ia}(t), V_{ib}(t), V_{ic}(t))}{\partial V_{ia}(t)}\right]_{t=k} [V_{ia}(t) - V_{ia}(k)] +$$
$$\left[\frac{\partial \mathcal{F}_{ix}(V_{ia}(t), V_{ib}(t), V_{ic}(t))}{\partial V_{ib}(t)}\right]_{t=k} [V_{ib}(t) - V_{ib}(k)] +$$
$$\left[\frac{\partial \mathcal{F}_{ix}(V_{ia}(t), V_{ib}(t), V_{ic}(t))}{\partial V_{ic}(t)}\right]_{t=k} [V_{ic}(t) - V_{ic}(k)]$$

$$(C.4)$$

Solving for $x = a$, and considering $V_i(t) = \frac{V_{ia}(t) + V_{ib}(t) + V_{ic}(t)}{3}$ and $\frac{\partial V_i(t)}{\partial V_{ia}(t)} = \frac{\partial V_i(t)}{\partial V_{ib}(t)} = \frac{\partial V_i(t)}{\partial V_{ic}(t)} = \frac{1}{3}$

$$\left[\frac{\partial \mathcal{F}_{ia}(V_{ia}(t), V_{ib}(t), V_{ic}(t))}{\partial V_{ia}(t)}\right]_{t=k} = \frac{\partial}{\partial V_{ia}(t)}\left[\frac{V_{ia}(t) - V_i(t)}{V_i(t)}\right]_{t=k}$$
$$= \left[\frac{[1 - \frac{\partial V_i(t)}{\partial V_{ia}(t)}][V_i(t)] - [V_{ia}(t) - V_i(t)]\frac{\partial V_i(t)}{\partial V_{ia}(t)}}{V_i^2(t)}\right]_{t=k}$$
$$= \left[\frac{[V_i(t)] - [V_{ia}(t)]\frac{\partial V_i(t)}{\partial V_{ia}(t)}}{V_i^2(t)}\right]_{t=k}$$
$$= \left[\frac{[\frac{V_{ia}(t) + V_{ib}(t) + V_{ic}(t)}{3}] - [V_{ia}(t)]\frac{1}{3}}{[\frac{V_{ia}(t) + V_{ib}(t) + V_{ic}(t)}{3}]^2}\right]_{t=k}$$
$$= \left[\frac{[3][V_{ia}(t) + V_{ib}(t) + V_{ic}(t)] - [3V_{ia}(t)]}{[V_{ia}(t) + V_{ib}(t) + V_{ic}(t)]^2}\right]_{t=k}$$

$$\left[\frac{\partial \mathcal{F}_{ia}(V_{ia}(t), V_{ib}(t), V_{ic}(t))}{\partial V_{ia}(t)}\right]_{t=k} = \left[\frac{[3][V_{ib}(k) + V_{ic}(k)]}{[V_{ia}(k) + V_{ib}(k) + V_{ic}(k)]^2}\right] \qquad (C.5)$$

$$\left[\frac{\partial \mathcal{F}_{ix}(V_{ia}(t), V_{ib}(t), V_{ic}(t))}{\partial V_{ib}(t)}\right]_{t=k} = \frac{\partial}{\partial V_{ib}(t)}\left[\frac{V_{ia}(t) - V_i(t)}{V_i(t)}\right]_{t=k}$$
$$= \left[\frac{[-\frac{\partial V_i(t)}{\partial V_{ib}(t)}][V_i(t)] - [V_{ia}(t) - V_i(t)][\frac{\partial V_i(t)}{\partial V_{ib}(t)}]}{V_i^2(t)}\right]_{t=k}$$
$$= \left[\frac{-[V_{ia}(t)][\frac{1}{3}]}{V_i^2(t)}\right]_{t=k}$$
$$= \left[\frac{[-3V_{ia}(k)]}{[V_{ia}(k) + V_{ib}(k) + V_{ic}(k)]^2}\right] \qquad (C.6)$$

$$\left[\frac{\partial \mathcal{F}_{ix}(V_{ia}(t), V_{ib}(t), V_{ic}(t))}{\partial V_{ic}(t)}\right]_{t=k} = \frac{\partial}{\partial V_{ic}(t)}\left[\frac{V_{ia}(t) - V_i(t)}{V_i(t)}\right]_{t=k}$$

$$= \left[\frac{[-\frac{\partial V_i(t)}{\partial V_{ic}(t)}][V_i(t)] - [V_{ia}(t) - V_i(t)][\frac{\partial V_i(t)}{\partial V_{ic}(t)}]}{V_i^2(t)}\right]_{t=k}$$

$$= \left[\frac{-[V_{ia}(t)][\frac{1}{3}]}{V_i^2(t)}\right]_{t=k}$$

$$= \left[\frac{[-3V_{ia}(k)]}{[V_{ia}(k) + V_{ib}(k) + V_{ic}(k)]^2}\right] \tag{C.7}$$

Replacing in (C.4)

$$\mathcal{F}_{ia}(V_{ia}(t), V_{ib}(t), V_{ic}(t)) \approx \left[\frac{3V_{ia}(k) - [V_{ia}(k) + V_{ib}(k) + V_{ic}(k)]}{[V_{ia}(k) + V_{ib}(k) + V_{ic}(k)]}\right] +$$

$$\left[\frac{[3][V_{ib}(k) + V_{ic}(k)]}{[V_{ia}(k) + V_{ib}(k) + V_{ic}(k)]^2}\right][V_{ia}(t) - V_{ia}(k)] +$$

$$\left[\frac{[-3V_{ia}(k)]}{[V_{ia}(k) + V_{ib}(k) + V_{ic}(k)]^2}\right][V_{ib}(t) - V_{ib}(k)] +$$

$$\left[\frac{[-3V_{ia}(k)]}{[V_{ia}(k) + V_{ib}(k) + V_{ic}(k)]^2}\right][V_{ic}(t) - V_{ic}(k)]$$

Regarding inequations (C.3) for $x = a$, (C.8) has the linear representation defined by (C.9).

$$\frac{V_{ia}(t) - V_i(t)}{V_i(t)} \leq PVUR^* \tag{C.8}$$

$$\mathcal{F}_{ia}(k) + \mathcal{K}_{iaa}(k)\left[V_{ia}(t) - V_{ia}(k)\right] + \mathcal{K}_{iab}(k)\left[V_{ib}(t) - V_{ib}(k)\right] +$$
$$\mathcal{K}_{iac}(k)\left[V_{ic}(t) - V_{ic}(k)\right] \leq PVUR^* \tag{C.9}$$

where the coefficients produced in the linearisation are presented in (C.10).

$$\mathcal{F}_{ia}(k) = \left[\frac{3V_{ia}(k) - [V_{ia}(k) + V_{ib}(k) + V_{ic}(k)]}{[V_{ia}(k) + V_{ib}(k) + V_{ic}(k)]}\right]$$

$$\mathcal{K}_{iaa}(k) = \left[\frac{[3][V_{ib}(k) + V_{ic}(k)]}{[V_{ia}(k) + V_{ib}(k) + V_{ic}(k)]^2}\right]$$

$$\mathcal{K}_{iab}(k) = \left[\frac{[-3V_{ia}(k)]}{[V_{ia}(k) + V_{ib}(k) + V_{ic}(k)]^2}\right]$$

$$\mathcal{K}_{iac}(k) = \left[\frac{[-3V_{ia}(k)]}{[V_{ia}(k) + V_{ib}(k) + V_{ic}(k)]^2}\right] \tag{C.10}$$

Similarly, solving for $x = b$ and $x = c$:

$$\frac{V_{ib}(t) - V_i(t)}{V_i(t)} \leq PVUR^* \tag{C.11}$$

$$\frac{V_{ic}(t) - V_i(t)}{V_i(t)} \leq PVUR^* \tag{C.12}$$

Then

$$\mathcal{F}_{ib}(k) + \mathcal{K}_{iba}(k)\left[V_{ia}(t) - V_{ia}(k)\right] + \mathcal{K}_{ibb}(k)\left[V_{ib}(t) - V_{ib}(k)\right] + \\ \mathcal{K}_{ibc}(k)\left[V_{ic}(t) - V_{ic}(k)\right] \leq PVUR^* \tag{C.13}$$

$$\mathcal{F}_{ic}(k) + \mathcal{K}_{ica}(k)\left[V_{ia}(t) - V_{ia}(k)\right] + \mathcal{K}_{icb}(k)\left[V_{ib}(t) - V_{ib}(k)\right] + \\ \mathcal{K}_{icc}(k)\left[V_{ic}(t) - V_{ic}(k)\right] \leq PVUR^* \tag{C.14}$$

Where the coefficients produced in the linearisation for phase b and phase c are presented in (C.15) and (C.16), respectively.

$$\mathcal{F}_{ib}(k) = \left[\frac{3V_{ib}(k) - [V_{ia}(k) + V_{ib}(k) + V_{ic}(k)]}{[V_{ia}(k) + V_{ib}(k) + V_{ic}(k)]}\right]$$
$$\mathcal{K}_{iba}(k) = \left[\frac{[-3V_{ib}(k)]}{[V_{ia}(k) + V_{ib}(k) + V_{ic}(k)]^2}\right]$$
$$\mathcal{K}_{ibb}(k) = \left[\frac{[3][V_{ia}(k) + V_{ic}(k)]}{[V_{ia}(k) + V_{ib}(k) + V_{ic}(k)]^2}\right]$$
$$\mathcal{K}_{ibc}(k) = \left[\frac{[-3V_{ib}(k)]}{[V_{ia}(k) + V_{ib}(k) + V_{ic}(k)]^2}\right] \tag{C.15}$$

$$\mathcal{F}_{ic}(k) = \left[\frac{3V_{ic}(k) - [V_{ia}(k) + V_{ib}(k) + V_{ic}(k)]}{[V_{ia}(k) + V_{ib}(k) + V_{ic}(k)]}\right]$$
$$\mathcal{K}_{ica}(k) = \left[\frac{[-3V_{ic}(k)]}{[V_{ia}(k) + V_{ib}(k) + V_{ic}(k)]^2}\right]$$
$$\mathcal{K}_{icb}(k) = \left[\frac{[-3V_{ic}(k)]}{[V_{ia}(k) + V_{ib}(k) + V_{ic}(k)]^2}\right]$$
$$\mathcal{K}_{icc}(k) = \left[\frac{[3][V_{ia}(k) + V_{ib}(k)]}{[V_{ia}(k) + V_{ib}(k) + V_{ic}(k)]^2}\right]$$
$$\tag{C.16}$$

Therefore, the prediction model for PVUR inequality constraints is defined by (C.17), which is the same set of inequalities stated by (5.12). Note that the measured/estimated coefficients at $t = k$ are considered constant along the prediction horizon.

$$\mathcal{F}_{ia}(k) + \mathcal{K}_{iaa}(k)\left[V_{ia}(k+m) - V_{ia}(k)\right] + \mathcal{K}_{iab}(k)\left[V_{ib}(k+m) - V_{ib}(k)\right] + \\ \mathcal{K}_{iac}(k)\left[V_{ic}(k+m) - V_{ic}(k)\right] \leq PVUR^* \tag{C.17a}$$

$$\mathcal{F}_{ib}(k) + \mathcal{K}_{iba}(k)\left[V_{ia}(k+m) - V_{ia}(k)\right] + \mathcal{K}_{ibb}(k)\left[V_{ib}(k+m) - V_{ib}(k)\right] + \\ \mathcal{K}_{ibc}(k)\left[V_{ic}(k+m) - V_{ic}(k)\right] \leq PVUR^* \tag{C.17b}$$

$$\mathcal{F}_{ic}(k) + \mathcal{K}_{ica}(k)\left[V_{ia}(k+m) - V_{ia}(k)\right] + \mathcal{K}_{icb}(k)\left[V_{ib}(k+m) - V_{ib}(k)\right] + \\ \mathcal{K}_{icc}(k)\left[V_{ic}(k+m) - V_{ic}(k)\right] \leq PVUR^* \tag{C.17c}$$

C.2   Apparent power rating

Apparent power is used as a constraint to ensure that each DG operates within its physical limits, according to the inequality (C.18). As there is not a linear relationship among apparent, active and reactive powers, it is required to linearise and discretise (C.18).

$$|S_i(t)| = (P_i(t)^2 + Q_i(t)^2)^{1/2} < S_{\max} \tag{C.18}$$

Linearising $|S_i(t)|$ around the measured/estimated point
$p(k) = \{\omega_i(k), \hat{\omega}_i^B(k), V_i(k), V_{ix}(k), \hat{V}_i^B(k), \hat{V}_{ix}^B(k), \delta\theta_i(k), P_i(k), Q_i(k)\}$
with $x=\{a, b, c\}$:

$$
\begin{aligned}
|S_i(t)| \approx & (P_i(k)^2 + Q_i(k)^2)^{1/2} + \frac{\partial |S_i(t)|}{\partial P_i}(P_i(t) - P_i(k)) + \frac{\partial |S_i(t)|}{\partial Q_i}(Q_i(t) - Q_i(k)) \\
\approx & (P_i(k)^2 + Q_i(k)^2)^{1/2} + \frac{1}{2}(P_i(k)^2 + Q_i(k)^2)^{-1/2}(2P_i(k))(P_i(t) - P_i(k)) \\
& + \frac{1}{2}(P_i(k)^2 + Q_i(k)^2)^{-1/2}(2Q_i(k))(Q_i(t) - Q_i(k))
\end{aligned}
\tag{C.19}
$$

Note that (C.19) is not feasible when $P_i(k) = Q_i(k) = 0$; therefore, applying the triangular inequality, the polytopic inner approximation (C.20) is achieved. This approximation is feasible for any operation point.

$$(P_i(t)^2 + Q_i(t)^2)^{1/2} < |P_i(t)| + |Q_i(t)| = f(P_i, Q_i) \tag{C.20}$$

Note that if the right side of inequality (C.20) is less than S_{max}, the left side will also be. Therefore, linearising:

$$
\begin{aligned}
|P_i(t)| + |Q_i(t)| \approx & |P_i(k)| + |Q_i(k)| + \frac{\partial f(P_i, Q_i)}{\partial P_i}(P_i(t) - P_i(k)) + \\
& \frac{\partial f(P_i, Q_i)}{\partial Q_i}(Q_i(t) - Q_i(k)) \\
\approx & |P_i(k)| + |Q_i(k)| + \text{sign}(P_i(k))(P_i(t) - P_i(k)) + \\
& \text{sign}(Q_i(k))(Q_i(t) - Q_i(k))
\end{aligned}
\tag{C.21}
$$

In this case the discretisation can be directly derived. Then, extending along the prediction horizon (C.22) is obtained, which is the inequality (4.35) and (5.16). Note that the measured/estimated coefficients at $t = k$ are considered constant along the prediction horizon.

$$
\begin{aligned}
|P_i(k)| + |Q_i(k)| + \text{sign}(P_i(k))[P_i(k+m) - P_i(k)] \\
+ \text{sign}(Q_i(k))[Q_i(k+m) - Q_i(k)] < S_{max}
\end{aligned}
\tag{C.22}
$$

$$\square$$

Appendix D

Derivation of predictive linear models used as equality constraints in *dc* DGs

D.1 Continuous time model for equality constraints

Equations (4.15) and (4.16) are rewritten as (D.1). As it was mentioned, (D.1) characterises the voltage droop controller and the active power transferred from the $i-th$ *dc* DG to the microgrid.

$$V_i^{dc}(t){=}V_0^{dc}{+}M_{pv,i}P_i^{dc}(t){+}V_{s,i}^{dc}(t) \qquad \text{(D.1a)}$$

$$P_i^{dc}(t) = G_i V_i^{dc}(t)\Big(V_i^{dc}(t){-}\hat{V}_i^{dc,B}(t)\Big) \qquad \text{(D.1b)}$$

D.1.1 Droop equation

The linearisation process for the droop equation (D.1a) is described as follows. From (D.1a), it is possible to rewrite $V_{s,i}^{dc}(t)$ in function of $\vartriangle V_{s,i}^{dc}(t)$.

$$V_i^{dc}(t) = V_0^{dc} + M_{pv,i}P_i^{dc}(t) + V_{s,i}^{dc}(t) \qquad \text{(D.2)}$$

$$V_i^{dc}(t) = V_0^{dc} + M_{pv,i}P_i^{dc}(t) + \frac{1}{T_{sec}}\int \vartriangle V_{s,i}^{dc}(t)dt$$

Deriving both sides and applying the forward Euler method:

$$\frac{dV_i^{dc}(t)}{dt} = M_{pv,i}\frac{dP_i^{dc}(t)}{dt} + \frac{1}{T_{sec}}\vartriangle V_{s,i}^{dc}(t)$$

$$\left.\frac{dV_i^{dc}(t)}{dt}\right|_{t=k} = M_{pv,i}\left.\frac{dP_i^{dc}(t)}{dt}\right|_{t=k} + \frac{1}{T_{sec}}\vartriangle V_{s,i}^{dc}(k)$$

$$V_i^{dc}(k+1) - V_i^{dc}(k) = M_{pv,i}\left[P_i^{dc}(k+1) - P_i^{dc}(k)\right] + \vartriangle V_{s,i}^{dc}(k)$$

$$V_i^{dc}(k+1) = V_i^{dc}(k) + M_{pv,i}\left[P_i^{dc}(k+1) - P_i^{dc}(k)\right] + {}_\Delta V_{s,i}^{dc}(k) \qquad \text{(D.3)}$$

$\square$

D.1.2   Power transfer equation

Due to power transfer, equation (D.1b), is non-linear, this is linearised via a Taylor expansion around the measured/estimated point $p(k) = \{V_i^{dc}(k), \hat{V}_i^{dc,B}(k), P_i^{dc}(k)\}$. Then, the forward Euler discretisation is applied to the linearised equation.

$$P_i^{dc}(t) \;=\; V_i^{dc}(t)I_i^{dc}(t) \;=\; G_i V_i^{dc}(t)\left(V_i^{dc}(t) - \hat{V}_i^{dc,B}(t)\right) \qquad \text{(D.4)}$$

Linearising

$$P_i^{dc}(t) = P_i^{dc}(k) + \left.\frac{\partial P_i^{dc}(t)}{\partial V_i^{dc}}\right|_{p(k)} [V_i^{dc}(t) - V_i^{dc}(k)] + \left.\frac{\partial P_i^{dc}(t)}{\partial \hat{V}_i^{dc,B}}\right|_{p(k)} [\hat{V}_i^{dc,B}(t) - \hat{V}_i^{dc,B}(k)]$$

$$P_i^{dc}(t) = P_i^{dc}(k) + K_V[V_i^{dc}(t) - V_i^{dc}(k)] + K_{\hat{V}_i^{dc,B}}[\hat{V}_i^{dc,B}(t) - \hat{V}_i^{dc,B}(k)]$$

where

$$K_V = G_i\left[2V_i^{dc}(k) - \hat{V}_i^{dc,B}(k)\right]$$

$$K_{\hat{V}_i^{dc,B}} = -G_i V_i^{dc}(k)$$

Deriving both sides and evaluating at $t = k$

$$\frac{P_i^{dc}(t)}{dt} = \frac{P_i^{dc}(k)}{dt} + K_V \frac{d}{dt}[V_i^{dc}(t) - V_i^{dc}(k)] + K_{\hat{V}_i^{dc,B}}\frac{d}{dt}[\hat{V}_i^{dc,B}(t) - \hat{V}_i^{dc,B}(k)]$$

$$\left.\frac{dP_i^{dc}(t)}{dt}\right|_{t=k} = K_V \left.\frac{dV_i^{dc}(t)}{dt}\right|_{t=k} + K_{\hat{V}_i^{dc,B}}\left.\frac{d\hat{V}_i^{dc,B}(t)}{dt}\right|_{t=k}$$

$$P_i^{dc}(k+1) - P_i^{dc}(k) = K_V[V_i^{dc}(k+1) - V_i^{dc}(k)] + K_{\hat{V}_i^{dc,B}}[\hat{V}_i^{dc,B}(k+1) - \hat{V}_i^{dc,B}(k)]$$

Assuming $\hat{V}_i^{dc,B}$ is constant

$$\hat{V}_i^{dc,B}(k+1) - \hat{V}_i^{dc,B}(k) = 0$$

$$P_i^{dc}(k+1) = P_i^{dc}(k) + K_V[V_i^{dc}(k+1) - V_i^{dc}(k)]$$

Then

$$P_i^{dc}(k+1) = P_i^{dc}(k) + G_i[2V_i^{dc}(k) - \hat{V}_i^{dc,B}(k)][V_i^{dc}(k+1) - V_i^{dc}(k)] \qquad \text{(D.5)}$$

$\square$

D.2   Prediction model for equality constraints

From (D.3) and (D.5), it is possible to state the predictive models (D.6). These models are used as a set of equality constraints in the optimisation problem.

Note that the measured/estimated coefficients at $t = k$ are considered constant along the prediction horizon.

$$V_i^{dc}(k+m) = V_i^{dc}(k) + M_{pv,i}\left[P_i^{dc}(k+m) - P_i^{dc}(k)\right] + \Delta V_{s,i}^{dc}(k+m-1) \qquad \text{(D.6a)}$$

$$P_i^{dc}(k+m) = P_i^{dc}(k) + G_i[2V_i^{dc}(k) - \hat{V}_i^{dc,B}(k)][V_i^{dc}(k+m) - V_i^{dc}(k)] \qquad \text{(D.6b)}$$

Appendix E

IEEE Standard 1547-2018 for interconnection and interoperability of distributed energy resources with associated electric power systems interfaces

The criteria for connecting and operating distributed energy resources (DERs) with their related electric power system interfaces are laid forth in the IEEE Standard 1547-2018. It outlines specifications for the operation, testing, maintenance, performance, and safety aspects of the interconnection of DERs. Additionally, it contains standards and design criteria for general needs, responsiveness to abnormal situations, power quality, islanding, etc. These specifications are suitable for most installations and are universally required for the interconnection of DER, including synchronous machines, induction machines, or power inverters/converters. Furthermore, the criteria and requirements apply to all DER technologies interconnected power systems and microgrids at typical distribution voltages.

In this thesis, the IEEE standard 1547-2018 is used to define the bands in which frequency and voltage are regulated and limit the maximum PVUR when imbalances are present in the MG. Regulating the PVUR is an essential feature since the sharing of imbalance among the DG units can only be achieved by inducing small voltage imbalances at the DG units' output. Thus, the unbalanced voltage at the DG units' output must be regulated (according to some standard) to avoid power quality issues. For this reason, the PVUR index is introduced to quantify the level of imbalance in the voltage at the output of the DGs. The IEEE standard 1547-2018 establishes that the PVUR should not exceed 5% to guarantee that the MG is operating in normal conditions; therefore, we selected a PVUR limit of 4% to test the performance of the technique proposed in Chapter 5.

Moreover, the IEEE standard 1547-2018 for interconnection of distributed resources [40] recommends that the frequency should be within 1% of the MG nominal frequency ω_0 and that the voltage should be within 5% of the nominal value V_0. Furthermore, the IEEE standard 1547-2018 establishes that a DG can operate normally, i.e., contribute to the power-sharing, as long as the

frequency is $0.98 \leq f(p.u) \leq 1.02$ and the voltage is $0.88 \leq V(p.u) \leq 1.10$. If the frequency is outside that band, it should be restored within 299 seconds, and if the voltage is outside its band, it should be restored within 12 seconds. With these considerations, we selected the frequency band as 1% of the MG nominal frequency and the voltage band as 5% of the nominal value for the control strategies of Chapter 4 and Chapter 5.